REPORT NO.
EERC 2006-01

EARTHQUAKE ENGINEERING RESEARCH CENTER

VISCOUS HEATING OF FLUID DAMPERS UNDER WIND AND SEISMIC LOADING: EXPERIMENTAL STUDIES, MATHEMATICAL MODELING AND DESIGN FORMULAE

CAMERON BLACK
The University of California, Berkeley

NICOS MAKRIS
University of Patras, Greece
and
The University of California, Berkeley

Work conducted for the California Department of Transportation under Grant RTA-59A298

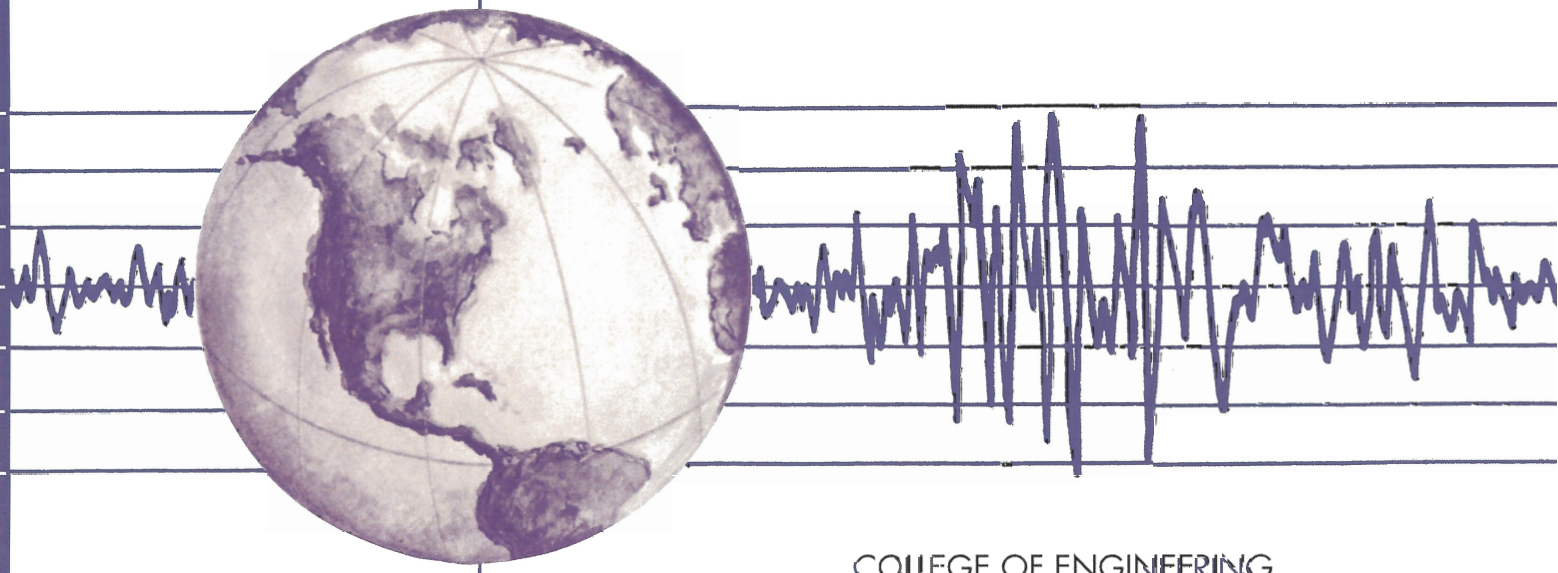

COLLEGE OF ENGINEERING
UNIVERSITY OF CALIFORNIA, BERKELEY

Viscous Heating of Fluid Dampers Under Wind and Seismic Loading: Experimental Studies, Mathematical Modeling and Design Formulae

by

Cameron Black
Ph.D. Candidate
Dept. of Civil and Environmental Engineering
The University of California, Berkeley

Nicos Makris
Professor of Structures and Applied Mechanics
Dept. of Civil Engineering
University of Patras, Greece
and
Research Engineer
Earthquake Engineering Research Center
The University of California, Berkeley

Work conducted for the California Department of
Transportation under Grant RTA-59A298

December 2005

Dept. of Civil and Environmental Engineering
The University of California, Berkeley

ABSTRACT

This report summarizes the results from a comprehensive experimental program that investigates the problem of viscous heating of fluid dampers under wind and seismic loading. Three fluid dampers of different size with corresponding force outputs of 3, 15 and 250 kips at maximum design velocities, have been instrumented and tested under various amplitudes and frequencies. Temperature histories at different locations along the damper casing and within the silicone fluid that undergoes the shearing action have been recorded. Together with the experimental results, this report presents an approximate energy balance formulation which simplifies the problem of viscous heating of fluid dampers to the solution of a one-dimensional energy equation.

Experimental data from testing the 250 kip damper under small-stroke motion (wind loading) shows that a single closed form solution of the linearized one-dimensional energy equation is capable of predicting the temperature rise at different locations along the damper with fidelity.

The recorded data under long-stroke motion (earthquake loading) suggest a two parameter law of cooling that allows the estimation of the internal temperature of the silicone oil once the external temperature on the damper casing is known. The presented cooling law is an extension of Newton's law of cooling. The report shows that for the medium (15 kip) and large (250 kip) dampers, the same values of the model parameters provide a good approximation of the cooling behavior. When the surface temperature of the damper is measured—a task easily accomplished in the field— the proposed two parameter cooling law leads to a simple closed form expression that provides a good estimate of the internal oil temperature of the silicone fluid after violent seismic shaking.

TABLE OF CONTENTS

LIST OF FIGURES

LIST OF TABLES

LIST OF SYMBOLS

A_p	area of piston head $[m^2]$
C	damping coefficient $[kg \ \ sec^2/m]$
C_p	heat capacity of silicone oil $[Joule/(kg°C)]$
d_p	diameter of piston head $[m]$
d_r	piston rod diameter $[m]$
$\delta(x)$	Dirac delta function
ε	thickness of damper housing $[m]$
h	combined heat transfer coefficient $[Joule/(sec \ \ m \ \ °C)]$
k	heat capacity of steel tube $[Joule/(sec \ \ m \ \ °C)]$
m	mass of the fluid that travels through the piston head $[kg]$
$p(x)$	heat source distribution
Δp	pressure drop across piston head $[(N/m^2)/m]$
$P(t)$	force on piston rod $[N]$
$q(t)$	radial heat
ρ	mass density of silicone oil $[kg/m^3]$
s	Laplace variable
t	time parameter $[sec]$
T_{air}	ambient air temperature $[°C]$
τ_{ik}	deviatoric stress $[N/m^2]$
θ_o	outside temperature $[°C]$
$\theta(x, t)$	internal temperature as a function of space and time $[°C]$
$\theta(t)$	internal temperature as a function of time $[°C]$
$u(t)$	piston displacement $[m]$
U_o	harmonic amplitude $[m]$
v_f	fluid velocity along the face of the piston head $[m/sec]$
v_j	components of fluid velocity $[m/sec]$
V_o	velocity amplitude $[m/sec]$
ω	harmonic frequency $[rad/sec]$

ACKNOWLEDGMENTS

Financial support for this study was provided by the California Department of Transportation under Grant RTA-59A298. Mr. Steven Yuen contributed in assembling the damper testing machine shown in Figures 3-19 and 3-20. Valuable technical assistance during the design and construction of the damper testing machine was provided by Mr. Don Clyde and Mr. Wes Neighbour at the Richmond Field Station, Structural Engineering Laboratory of The University of California, Berkeley. Additional help from Mr. David MacLam throughout testing is gratefully acknowledged. The valuable input and comments of Dr. Saad El-Azazy and Dr. Allaoua Kartoum from Caltrans are also appreciated.

1 INTRODUCTION

Fluid dampers which generate fluid flow through orifices or valves were originally developed for the shock isolation of military hardware. Currently, fluid dampers of similar technology have been implemented in civil structures to suppress earthquake and wind induced vibrations. In buildings, fluid dampers can be incorporated either within the skeleton of a structure (Miyamoto and Scholl 1997, ENR 2001) or in the isolation system for seismically isolated buildings (ENR 1995). The rapid success of fluid dampers in buildings, in association with the increasing need for safer bridges, has accelerated the implementation of large-capacity damping devices in bridges. The Vincent Thomas suspension bridge (Smyth et al. 2000), the Coronado Bridge and the 91/5 highway over-crossing (Delis et al. 1996, Zhang et al. 2004, Makris and Zhang 2004), all three in southern California, as well as the Rion-Antirion cable-stayed bridge (Papanikolas 2002) in Western Greece are examples of bridges that have been equipped with fluid dampers. Figure 1-1 (top) shows a view of four 250 kip dampers installed at the east abutment of the 91/5 over-crossing while Figure 1-1 (bottom) shows the Rion-Antirion bridge and one of four, 700 kip dampers which have been installed between each of the four piers and the suspended bridge deck.

When fluid dampers are installed within the skeleton of buildings to suppress earthquake or wind-induced vibrations the piston displacements and velocities are relatively small. In contrast, when the fluid dampers are incorporated either in the seismic isolation system of structures or between the towers/piers and the deck of bridges the piston displacements and velocities can be large.

Figure 1-1. View of the four, 250 kip dampers installed at the east abutment of the 91/5 over-crossing in Southern California (top); and a view of one of the four, 700 kip dampers (bottom-left) which have been installed in each of the four towers of the Rion-Antirion bridge (bottom-right) recently open to traffic in Western Greece.

Fluid dampers suppress structural vibrations by converting the kinetic energy of structures into heat. When the dampers undergo large and prolonged displacement histories, the temperature rise within the fluid of the damper might be appreciable to the extent that it may damage the end-seals and trigger failure of the damper.

This report presents a comprehensive experimental study on the problem of viscous heating of fluid dampers. Three fluid dampers of different size and corresponding force-output of 3 kip, 15 kip and 250 kip at their maximum design velocity, have been tested and temperature histories have been recorded at various locations of the damper housing and within the fluid of the damper. Figure 1-2 shows view of the three fluid dampers of interest mounted on their testing frames.

Experimental data under small-stroke motions from the 250 kip damper showed that a single closed-form expression derived from first principles is capable of predicting the temperature rise at different locations of the damper with remarkable fidelity.

The recorded time histories under long-stroke motions suggest a two parameter cooling law which is an extension of Newton's Law of cooling. The proposed two parameter cooling law allows for a dependable estimation of the internal temperature of the fluid that undergoes shearing action once the external temperature on the damper casing is known. Considering that the monitoring of the external temperature of the damper casing is a straight forward task, even when the damper is installed on a bridge or building structure, this study develops a valuable formula which estimates the internal fluid temperature of the damper during violent shaking.

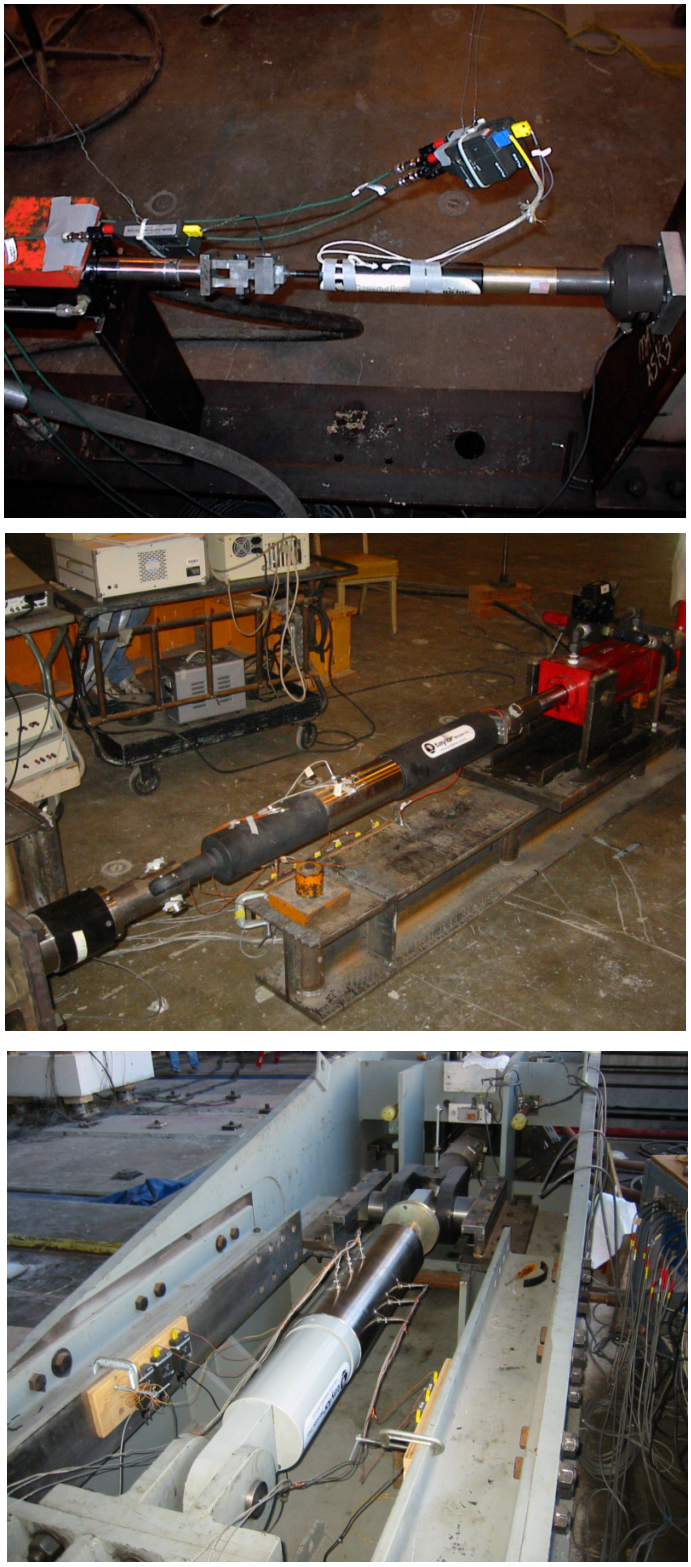

Figure 1-2. View of the three fluid dampers of interest in this study mounted on their testing frame. Top: 3 kip damper; center: 15 kip damper; and bottom: 250 kip damper.

2 THE HEAT TRANSFER EQUATION

Figure 2-1 (top) shows a schematic of a cross section of a typical double ended fluid damper used for vibration reduction in civil structures. As the piston head moves inside the damper cylinder, energy dissipates primarily due to friction between fluid particles and the piston head. This energy is converted into heat. The general three-dimensional equation of heat transfer through a fluid element is

$$\rho C_p\left(\frac{\partial \theta}{\partial t} + v_j \frac{\partial \theta}{\partial x_j}\right) = k_f \frac{\partial^2 \theta}{\partial x^2_j} + \tau_{ik} \frac{\partial v_i}{\partial x_k} \tag{2-1}$$

(Landau and Lifshitz 1987), in which $\theta(x_1, x_2, x_3, t)$ is the time-dependent temperature field, ρ is the fluid density, C_p is the heat capacity coefficient at constant pressure, k_f is the coefficient of thermal conductivity of the fluid, v_j are the components of the fluid velocity at a fixed position and τ_{ik} are the deviatoric stresses on the fluid element at this position.

Equation (2-1) is a nonlinear equation; however, when some terms are omitted, it can be solved analytically. For instance, Bird et al. (1960), Landau and Lifshtiz (1987) and Schlichting (1979), among others, have presented closed-form solutions of the steady-state version of Equation (2-1) ($\frac{\partial \theta}{\partial t} = 0$) for a variety of geometries and boundary conditions. Herein we are addressing a transient problem; therefore, the significance of the convected derivative term, $v_j \frac{\partial \theta}{\partial x_j}$, with respect to the time derivative term, $\frac{\partial \theta}{\partial t}$, must be evaluated. The significance of these two terms is compared

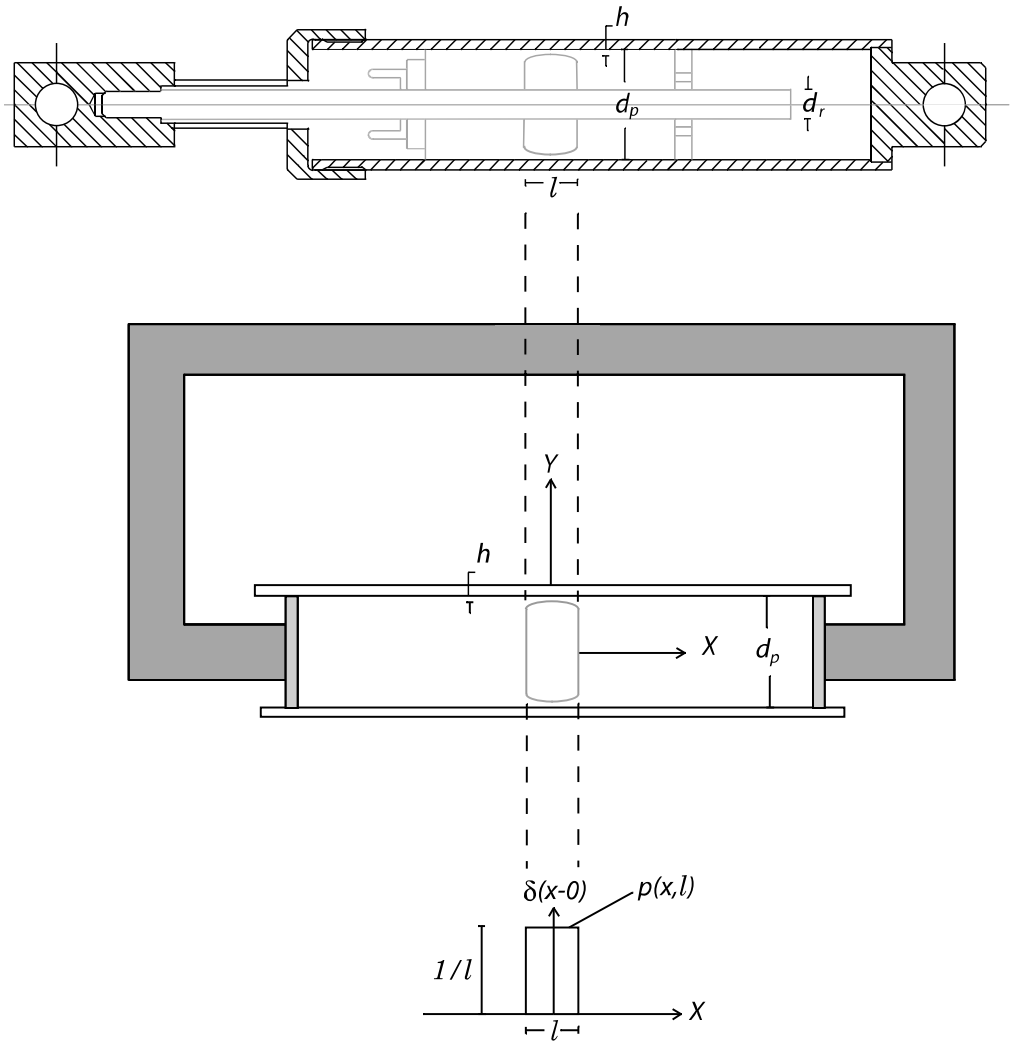

Figure 2-1. Top: Schematic of a typical fluid damper. Center: Virtual fluid damper. Bottom: Heat source distribution of piston head.

when Equation (2-1) describes the energy transfer in the neighborhood of a piston head undergoing harmonic motion.

The operator $v_j \frac{\partial \theta}{\partial x_j}$ denotes differentiation in the direction of the fluid velocity. Near the surface of the piston head, fluid velocities are nearly tangential (i.e., parallel to the face of the piston head). In the tangential direction, fluid velocities change appreciably only over distances of the order of the dimension of the piston head, d_p (for fluid dampers designed for wind and seismic applications, the width of the piston head, l, is of the same order of magnitude as d_p). Hence,

$$v_j \frac{\partial \theta}{\partial x_j} \sim \frac{v_f \theta}{d_p}, \tag{2-2}$$

where v_f is the fluid velocity along the face of the piston head. Under harmonic vibrations of frequency ω and amplitude U_o, the piston velocity is of the order of ωU_o. The fluid velocity along the surface of the piston head varies from a low value of the order ωU_o to its maximum value which is reached when fluid flows through the orifice. This maximum value of the fluid velocity can be estimated from volume conservation of the fluid (Schlichting 1979). Assuming an annular orifice with width h, the volume rate through the orifice, $v_{max} \pi d_p h$, should be equal to the volume rate of fluid that is displaced as the piston advances, $\omega U_o \pi d_p^2 / 4$. By equating the two volume rates, $v_{max} \approx \omega U_o d_p / (4h)$. Consequently, the average value of the fluid velocity in the neighborhood of the piston head is $v_f = \xi \omega U_o$, where $1 < \xi < d_p / (4h)$, and from Equation (2-2), one obtains

$$v_j \frac{\partial \theta}{\partial x_j} \sim \frac{\xi U_o \omega \theta}{d_p}. \tag{2-3}$$

The term $\omega\theta$ in Equation (2-3) is of the order of $\partial\theta/\partial t$, and Equation (2-3) becomes

$$v_j \frac{\partial\theta}{\partial x_j} \sim \frac{\xi U_o}{d_p}\frac{\partial\theta}{\partial t}. \tag{2-4}$$

Equation (2-4) indicates that when the amplitude of oscillation, U_o, is smaller than a fraction of the piston diameter ($\xi U_o/d_p \ll 1$ with $\xi > 1$), the convected derivative term in Equation (2-1) can be neglected. This means that the linearized version of Equation (2-1) can be considered only when the piston motion is extremely small (a small fraction of the piston diameter). When the piston motion is of the order of the piston diameter the convected derivative term, $v_j \frac{\partial\theta}{\partial x_j}$, has a significant contribution and cannot be neglected.

2.1 ONE-DIMENSIONAL APPROXIMATION OF THE ENERGY EQUATION

In this section, an approximate one-dimensional version of Equation (2-1) is developed in an attempt to relate the temperature of the fluid with temperature readings along the outer surface of the damper casing. In order to simplify the sign convention, the virtual damper shown in Figure 2-1 (center), in which the fluid is moving through a stationary orifice, is adopted. Viscous heating in this configuration is equivalent to viscous heating in real dampers, like the one depicted in Figure 2-1 (top), where the piston head is moving through the fluid. The configuration shown in Figure 2-1 (center) is convenient as a positive piston velocity generates a positive fluid-particle velocity, and the velocity of a fluid-particle relative to the orifice is merely the absolute fluid-particle velocity.

In this analysis, it is assumed that the temperature of the fluid is a function of the position, x, and time, t, so that all fluid particles that belong to a given cross-section of the damper have the same temperature, $\theta(x, t)$. As fluid is forced to flow through the stationary orifice located at $x = 0$,

fluid temperature increases due to viscous heating. By neglecting viscous heating generated along the damper casing, the term $\tau_{ik} \frac{\partial v_i}{\partial x_k}$ in Equation (2-1) can be considered to be a power source distribution (energy per time per unit volume) that is centered at the piston head. The width of the distribution, $p(x)$, is merely the length of the orifice. For the analysis presented here the distribution for the heat source $p(x)$ is approximated with the Dirac distribution (delta function, Lighthil 1989) and with a rectangular function distribution with a width equal to the length of the orifice.

It is first assumed that energy does not conduct through the cylindrical housing of the damper to the surrounding environment, and that, as the piston is moving back and forth, heat transfers only from the piston head (distributed heat source) to neighboring sections of the damper. The transfer of heat along the length of the damper occurs via the fluid, the piston rod and the damper casing. Since metals are better conductors of heat than oil, the transfer of heat along the length of the damper is due mainly to the metallic components of the damper (for instance the coefficient of thermal conductivity of steel is approximately 30 J/(m sec° C) whereas that of oil is only 4.4 J/(m sec° C) (Shackelford et al. 1994). This heat transfer mechanism along the longitudinal direction of the damper is expressed with an overall coefficient of thermal conductivity, k_l, its value being close to the value of the thermal conductivity of steel. With these assumptions, the heat transfer equation given by Equation (2-1) can be contracted to an approximate one-dimensional energy equation expressed at a cross-section of the damper having area A_p

$$\rho C_p \frac{D\theta(x,t)}{Dt} = k_l \frac{\partial^2 \theta(x,t)}{\partial x^2} + \frac{P(t)\dot{u}(t)}{A_p} p(x) \tag{2-5}$$

in which $P(t)$ and $\dot{u}(t)$ are the force and velocity on the piston rod, and $(P(t)\dot{u}(t)/A_p)p(x)$ is a power source distribution. $D\theta/Dt$ is the total time derivative of the temperature

$$\frac{D\theta(x,t)}{Dt} = \frac{\partial}{\partial t}\theta(x,t) + \dot{u}(t)\frac{\partial}{\partial x}\theta(x,t) \tag{2-6}$$

in which $\dot{u}(t)$ is an average section velocity at location x and time t. Volume-rate conversion yields that the average section velocity should be independent of x and therefore is equal to the piston velocity.

Since the piston motions have finite duration, the conduction of heat through the damper casing into the surrounding environment must be considered. For thin tubes, the rate of heat conduction per unit length of the damper is proportional to the circumference of the damper, πd_p, and to the temperature gradient between the fluid temperature, $\theta(x,t)$, and the outside temperature, $\theta_o(x,t)$. Denoting with ε the thickness of a thin shock tube, the rate of energy loss per unit length is given by $(k_r \pi d_p / \varepsilon)[\theta(x,t) - \theta_o(x,t)]$, where k_r is the coefficient of thermal conductivity along the radial direction of the damper. In this case, the energy equation at a cross-section of the damper takes the form

$$\rho C_p \frac{D\theta(x,t)}{Dt} + k_r \frac{\pi d_p}{\varepsilon A_p}[\theta(x,t) - \theta_o(x,t)] = k_l \frac{\partial^2 \theta(x,t)}{\partial x^2} + \frac{P(t)\dot{u}(t)}{A_p} p(x). \tag{2-7}$$

In reality, for cylindrical dampers (thick tubes) the rate of heat conduction per unit length given by the second term of the left hand side of Equation (2-7) is the solution of the radial flow of heat between two coaxial cylinders

$$\dot{q}(t) = \frac{k_r 2\pi}{A_p ln\left[1 + \frac{2\varepsilon}{d_p}\right]}[\theta(x,t) - \theta_o(x,t)] \tag{2-8}$$

and a more appropriate equation for cylindrical dampers is thus

$$\rho C_p \frac{D\theta(x,t)}{Dt} + \frac{k_r 2\pi}{A_p ln\left[1+\frac{2\varepsilon}{d_p}\right]}[\theta(x,t)-\theta_o(x,t)] = k_l \frac{\partial^2\theta(x,t)}{\partial x^2} + \frac{P(t)\dot{u}(t)}{A_p}p(x). \qquad (2\text{-}9)$$

Figure 2-2 shows the difference between the thick and thin tube formulations as function of ε/d_p, together with the corresponding values for the three dampers of interest in this study. Despite the approximations introduced, and assuming that one can decide on realistic values for the coefficients of thermal conductivity along the longitudial direction, k_l, and radial direction, k_r, the solution of the nonlinear partial differential equation given by Equation (2-9) is a formidable task.

2.2 SOLUTIONS TO THE ENERGY EQUATION UNDER SMALL AMPLITUDE MOTIONS

The problem of viscous heating under small-amplitude motions is of interest in wind induced vibrations of bridges and buildings where the amplitude of the piston motion remains small; however the duration of motion may be large. At this limit nonlinear fluid dampers tend to behave like linear viscous dampers.

Using the linear viscous assumption, Makris (1998) has presented various solutions of equations (2-5) and (2-7) under harmonic and triangular wave excitations after adopting for the heat source distribution, $p(x)$, a Dirac distribution (delta function); and a rectangular function distribution with a width equal to the length of the orifice at the piston head. Here we only present the solution of (2-5) (adiabatic damper housing) with a rectangular distribution, $p(x,l)$, defined as

$$p(x,l) = \frac{1}{l}\left[h\left(x+\frac{l}{2}\right) - h\left(x-\frac{l}{2}\right)\right] \qquad (2\text{-}10)$$

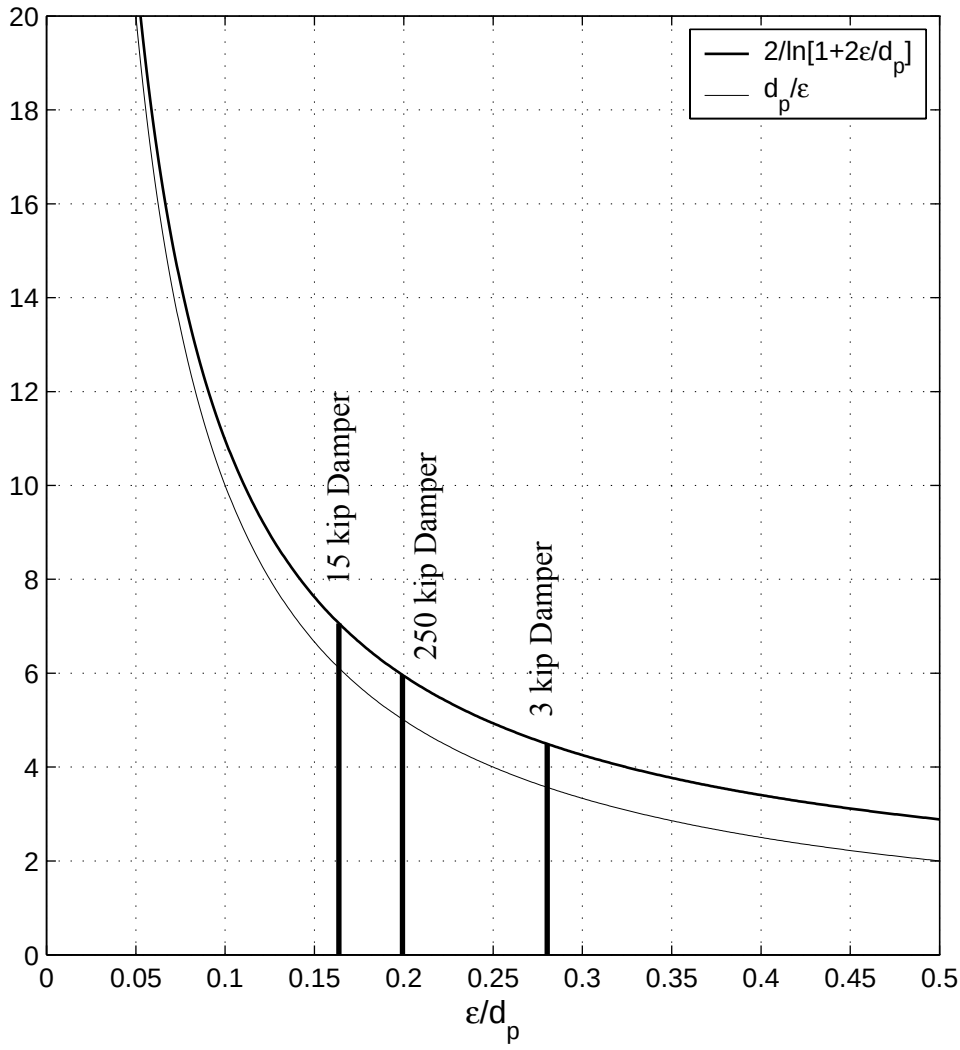

Figure 2-2. The thick and thin tube formulations as a function of ε / d_p, together with the corresponding values for the three dampers of interest in this study.

where l = width of the piston head; and $h(z)$ = Heaviside function. The distribution given by (2-10) is illustrated in Figure (2-1). With this distribution, the solution of (2-5) is (Makris 1998)

$$\theta(x,t) = \frac{1}{4\alpha l k_s}\Delta p V_o \int_0^t [\cos 2\omega_o(t-\xi)+1]\cdot\left\{erfc\left[\frac{1}{2}\left(\frac{x}{l}-\frac{1}{2}\right)\frac{l\sqrt{\alpha}}{\sqrt{\xi}}\right]-erfc\left[\frac{1}{2}\left(\frac{x}{l}+\frac{1}{2}\right)\frac{l\sqrt{\alpha}}{\sqrt{\xi}}\right]\right\}d\xi \tag{2-11}$$

(in which $k_s = k_l = k_r$ = the value of the thermal conductivity of steel, 15 Joule / sec m °C $\leq k_s \leq$ 10 Joule / sec m °C).

The experimental program that follows in Chapter 3 shows that Equation (2-11) predicts the temperature rise at various locations of a 250 kip damper with fidelity. Eight such dampers (four at each end) have been installed in the 91/5 overpass in Orange County, California (Makris and Zhang 2004). A photograph showing the installed damper is presented in Figure 1-1. One of the reasons that Equation (2-11), which is the solution for an adiabatic damper housing, offers such an accurate representation is that the coefficient, $(k_s \pi d_p)/(\varepsilon A_p)$, in the second term on the left-hand side of Equation (2-7) is two orders of magnitude smaller than the coefficient of the first term, ρC_p.

2.3 SOLUTION TO THE ENERGY EQUATION UNDER LONG-STROKE MOTION

2.3.1 Temperature Rise During Monotonic Loading

When the piston stroke is of the order of the piston diameter, the total time derivative in the heat transfer equation given by Equations (2-7) or (2-9) has to be considered. The presence of the convected time derivative term complicates substantially the solution of the heat equation. Nevertheless, for the special case of a linear motion (step velocity history) a closed form expression for the

temperature rise on the piston head during this monotonic loading can be obtained. This monotonic loading can also be understood as a half-cycle motion during a triangular wave input. The solution although restricted to a half cycle, offers significant insight into the viscous heating problem since it shows that when the amplitude of motion is finite the temperature rise depends only on the pressure drop and not on the amplitude of the stroke.

Concentrating on the case of a positive constant piston-velocity, $\dot{u}(t) = V_0 h(t-0)$, and assuming the case where the heat-source distribution, $p(x)$, is approximated with the Dirac delta function, $\delta(x-0)$, the Laplace transform of Equation (2-7) gives

$$\frac{d^2\theta(x,s)}{dx^2} - \alpha V_0 \frac{d\theta(x,s)}{dx} - (\alpha s + \beta)\theta(x,s) = -C\frac{V_0^2}{k_l A_p}\frac{1}{s}\delta(x-0) \tag{2-12}$$

where s is the Laplace variable, $\alpha = \rho C_p / k_l$ and $\beta = (k_r/k_l)\cdot \pi d_p/(\varepsilon A_p) \approx \pi d_p/(\varepsilon A_p)$ if one assumes that $k_r \approx k_l \approx k_s$, where k_s is the coefficient of thermal conductivity of steel. The reference temperature is equal to zero, $\theta(x,0) = 0$. Equation (2-12) is a linear ordinary differential equation with respect to x and can be solved using the Fourier integral theorem.

Defining the parameter, $\gamma = \beta + \alpha^2 V_0^2/4$, the solution of (2-12) in the Laplace space is

$$\theta(x,s) = \frac{1}{2}\frac{CV_0^2}{k_s A_p}\frac{1}{s}\frac{e^{-\left(\sqrt{\alpha s+\gamma}-\frac{\alpha V_0}{2}\right)x}}{\sqrt{\alpha s+\gamma}}. \tag{2-13}$$

The temperature rise on the piston head is given by setting $x = 0$; and the Laplace inversion of Equation (2-13) for $x = 0$ gives

$$\theta(0,t) = \frac{1}{2}\frac{CV_0^2}{k_s A_p}\frac{1}{\sqrt{\gamma}} Erf\left[\sqrt{\frac{\gamma}{\alpha}}t\right], \quad \dot{u}(t) \geq 0 \tag{2-14}$$

where Erf{.} is the error function (Abramowitz and Stegun 1970). For finite velocities the term $\alpha^2 V_0^2/4$ in γ dominates over β. Furthermore, CV_0/A_p is the pressure drop, Δp, while $\alpha = \rho C_p/k_s$. Accordingly, Equation (2-14) further simplifies to

$$\theta(0,t) = \frac{\Delta p}{\rho C_p} Erf\left[\frac{V_0}{2}\sqrt{\alpha t}\right], \quad \dot{u}(t) \geq 0\,. \tag{2-15}$$

Equation (2-15) shows that when the piston motion is finite the temperature rise on the piston head depends only on the pressure drop. This result is recovered in the next section, where the temperature rise within the damper is computed by considering a macroscopic energy balance over the entire body of fluid within the damper.

The long-term temperature rise in the damper during this monotonic loading can be computed by recalling that

$$s\theta(x,s)\big|_{s=0} = \theta(x,t)\big|_{t=\infty}; \tag{2-16}$$

and accordingly

$$\theta(x,\infty) = \frac{1}{2}\frac{CV_0^2}{k_s A_p}\frac{e^{-\left(\sqrt{\gamma}-\frac{\alpha V_0}{2}\right)x}}{\sqrt{\gamma}}\,. \tag{2-17}$$

Using the binomial expansion of the square root, $\sqrt{1+\zeta} = 1 + \frac{\zeta}{2} + \ldots$, Equation (2-17) simplifies to

$$\theta(x, \infty) = \frac{\Delta p}{\rho C_p} e^{-\frac{\beta}{\alpha V_0} x} . \tag{2-18}$$

The ratio $\beta/\alpha = k_s \pi d_p/(\rho C_p \varepsilon A_p)$ where k_s is the coefficient of thermal conductivity of steel which approximates the coefficient of thermal conductivity along the radial direction, d_p is the piston head diameter, ρ is the density of the fluid, C_p is the heat capacity coefficient at constant pressure, ε is the thickness of the shock tube and A_p is the area of the piston head. Table 2-1 indicates the values of β/α that correspond to the three dampers studied in this report. These values are $\beta/\alpha = 0.263$, 0.047 and 0.013 for the 3 kip, 15 kip and 250 kip dampers, respectively.

Figure 2-3 plots the computed distribution of the temperature along the casing of the three dampers of interest ($\beta U_0/(\alpha V_0) = 0.057$, 0.015 and 0.005 for the 3 kip, 15 kip and 250 kip dampers, respectively). It shows that the temperature at every section of the damper is nearly the same. This analytical result is used in the forthcoming analysis to derive a macroscopic energy balance equation over the entire body of fluid within the damper.

2.4 MACROSCOPIC ENERGY BALANCE

Consider now that the amplitude of the piston motion, U_0, is sufficiently large so that most of the fluid enclosed within the damper housing travels through the piston head. In this case the heat transfer equation can be averaged over the entire damper, since the temperature at every section of the damper is nearly the same at a given time (see Figure 2-3)[1]. The macroscopic energy balance equation can be obtained from Equation (2-7) after.integrating over the piston stroke. Now the temperature at every section of the damper is nearly the same at a given time, $\frac{\partial}{\partial x}\theta(x, t) \approx 0$. Conse-

1. Experimental results presented later in this report show that for the large, 250 kip damper, the assumption that the temperature at every section of the damper is nearly the same is true only during the first two or three cycles. As loading evolves, experimental data show that the temperature rise at the center is steeper and not axisymmetric.

Table 2-1. Geometrical characteristics of the dampers considered in this study along with the physical properties of the steel and silicone oil

Quantity	3 kip Damper	15 kip Damper	250 kip Damper
Damping Coefficient C	17.69 kNsec/m (0.101 kipsec/in)	121.8 kNsec/m (0.696 kipsec/in)	965.2 kN(sec/m)$^{0.35}$ (60 kip(sec/in)$^{0.35}$)
Thickness of Damper Housing ε (m)	$7.75\text{x}10^{-3}$ (0.305 in)	$1.37\text{x}10^{-2}$ (0.539 in)	$2.97\text{x}10^{-2}$ (1.17 in)
Piston Diameter d_p (m)	$2.763\text{x}10^{-2}$ (1.088 in)	$8.37\text{x}10^{-2}$ (3.259 in)	$1.49\text{x}10^{-1}$ (5.87 in)
Rod Diameter d_r (m)	$1.100\text{x}10^{-2}$ (0.433 in)	$2.83\text{x}10^{-2}$ (1.114 in)	$5.66\text{x}10^{-2}$ (2.230 in)
Area of Piston Head A_p (m^2)	$5.05\text{x}10^{-4}$ (0.783 in^2)	$4.87\text{x}10^{-3}$ (7.549 in^2)	$1.50\text{x}10^{-2}$ (23.19 in^2)
Maximum Stroke Uo (m)	0.0381 (1.5 in)	0.152 (6 in.)	0.203 (8 in.)
Thermal Conductivity of Steel, k_s (Joule/(sec m °C))	≈ 15-30	≈ 15-30	≈ 15-30
Mass Density of Silicone Oil, ρ (kg/m^3)	≈ 950	≈ 950	≈ 950
Heat Capacity of Silicone Oil, C_p (Joule/kg°C)	≈ 2000	≈ 2000	≈ 2000
$\alpha = \rho C_p / k_s$ (sec/m^2)	$8.44\text{x}10^4$	$8.44\text{x}10^4$	$8.44\text{x}10^4$
$\beta = \pi d_p / (\varepsilon A_p)$ ($1/m^2$)	$2.22\text{x}10^4$	$3.94\text{x}10^3$	$1.06\text{x}10^3$
β / a (Hz)	0.263	0.047	0.013

quently, the term $k_l \frac{\partial^2 \theta}{\partial x^2}(x,t)$ in that equation also vanishes. Multiplying the remaining terms in Equation (2-7) by $A_p dx$ and integrating over the length of the piston stroke yields

$$\rho C_p A_p \frac{d\theta(t)}{dt} \int_{-U_0}^{U_0} dx + k_r \frac{\pi d_p}{\varepsilon} [\theta(t) - \theta_0(t)] \int_{-U_0}^{U_0} dx = P(t)\dot{u}(t) \int_{-U_0}^{U_0} p(x)dx \tag{2-19}$$

Given that $\int_{-U_0}^{U_0} p(x)dx = 1$, Equation (2-19) reduces to

$$mC_p \frac{d\theta(t)}{dt} + \frac{2\pi k_r d_p U_0}{\varepsilon}(\theta(t) - \theta_0) = P(t)\frac{du(t)}{dt}, \tag{2-20}$$

in which $m = 2\rho A_p U_0$, is the mass of the fluid that travels through the piston head as the piston moves and k_r has been taken equal to k_s = coefficient of thermal conductivity of steel.

The boundary conditions between the outer surface of the damper housing and the surrounding environment are very complex since they combine the effects of heat conduction, convection and radiation. In many occasions radiation can be superimposed on the conductive and convective heat flow through most gases (Jakob and Hawkins 1942, Kakac and Yener 1993). For the case of forced conduction one can assume that the air in the immediate vicinity of the damper maintains a nearly constant temperature, T_{air}, and in this case the convection boundary condition (Newton's law of cooling) given by

$$k_s \frac{\partial \theta}{\partial n} = h(T_{air} - \theta_o(t)), \tag{2-21}$$

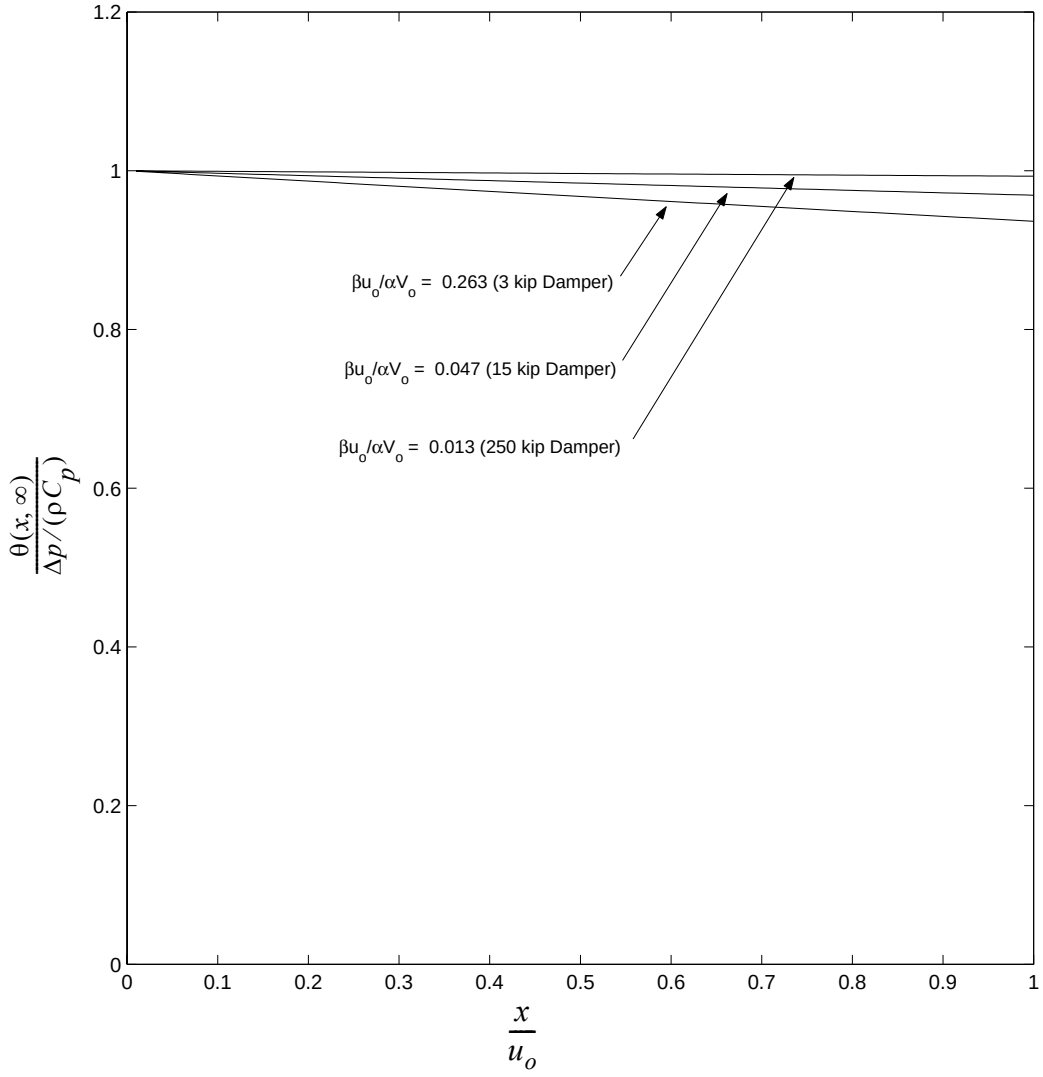

Figure 2-3. Theoretical temperature distribution along fluid dampers after a monotonic long-stroke motion.

can be applied, in which h is a combined heat transfer coefficient (Jakob and Hawkins 1942, Kakac and Yener 1993), or occasionally termed as the boundary film conductance (Boley and Weiner 1960), that combines the effects of convection, conduction and radiation. The left hand side of (2-21), $k_s\frac{\partial\theta}{\partial n}$, is the radial heat flux, which can be approximated with

$$-k_s\frac{\partial\theta}{\partial n} = \frac{2k_s(\theta(t)-\theta_o(t))}{d_p ln\left(1+\frac{2\varepsilon}{d_p}\right)} \approx \frac{k_s(\theta(t)-\theta_o(t))}{\varepsilon}. \tag{2-22}$$

The second relation in Equation (2-22) is appropriate for thin tubes only, otherwise the first relation is more appropriate for the general case. Regardless of the equation used to express the radial heat flux the form of the governing equation that describes this one-dimensional model is the same.

Substitution of the thin tube approximation of Equation (2-22) into (2-21) gives

$$\frac{k_s(\theta(t)-\theta_o(t))}{\varepsilon} = h(\theta_o(t)-T_{air}), \tag{2-23}$$

from which

$$\theta_o(t) = \frac{k_s}{\varepsilon h + k_s}\theta(t) + \frac{\varepsilon h}{\varepsilon h + k_s}T_{air}. \tag{2-24}$$

Equation (2-24) relates the temperature history of the outer surface of the damper, $\theta_o(t)$, to the temperature history of the fluid, $\theta(t)$, and the surrounding constant air temperature, T_{air}. Substitution of Equation (2-24) into (2-20) gives

$$\frac{d}{dt}\theta(t) + \frac{2\pi k_s d_p U_o}{mC_p\varepsilon} \cdot \frac{1}{1+\gamma}\theta(t) = \frac{1}{mC_p}P(t)\dot{u}(t) + \frac{2\pi k_s d_p U_o}{mC_p\varepsilon} \cdot \frac{1}{1+\gamma}T_{air}, \tag{2-25}$$

where $\gamma = k_s / \varepsilon h$.

With the introduction of the parameter, γ, Newton's law of cooling can be rearranged in the form

$$\gamma = \frac{k_s}{\varepsilon h} = \frac{\theta_o(t) - T_{air}}{\theta(t) - \theta_o(t)}. \tag{2-26}$$

In the event that Newton's law of cooling is a sound approximation, the combined heat transfer coefficient, h, is independent of temperature and the parameter $\gamma = k_s / \varepsilon h$ is a constant. Accordingly, the adoption of Newton's law of cooling implies that the right hand side of Equation (2-26) remains a constant throughout the history of loading.

2.5 LINEAR SOLUTION

Assuming that Newton's law of cooling indeed applies to this problem and that the parameter γ given by (2-26) is indeed constant, Equation (2-25) is a linear differential equation with constant coefficients

$$\frac{d\theta(t)}{dt} + \lambda\theta(t) = \frac{1}{mC_p}P(t)\dot{u}(t) + \lambda T_{air} \tag{2-27}$$

where $\lambda = \frac{2\pi k_s d_p U_o}{mC_p\varepsilon}\frac{1}{1+\gamma}$.

The solution of Equation (2-27) under harmonic and triangular wave motion have been presented by Makris (1998). Under harmonic motion, $u(t) = U_o sin(\omega t)$, the resulting force in a viscous damper is $P(t) = C\omega U_o cos(\omega t)$ and the solution of Equation (2-27) is

$$\theta(t) = T_{air} + \frac{1}{2}\frac{\Delta p_{max}}{\rho C_p}\frac{1}{4+\left(\frac{\lambda}{\omega}\right)^2}\left[cos(\omega t)\left(\frac{\lambda}{\omega}(cos(\omega t)+2sin(\omega t))\right)+2\frac{\omega}{\lambda}-(\frac{\lambda}{\omega}+2\frac{\omega}{\lambda})e^{-\lambda t}\right] \quad (2\text{-}28)$$

where $\Delta p_{max} = C\omega U_o / A_p$ is the maximum pressure drop between the two sides of the piston head. Equation (2-28) is a closed form expression that gives the temperature of the internal fluid of viscous dampers as a function of the force output and the frequency of loading.

In the event that the external temperature on the damper housing, $\theta_o(t)$, is known through measurements, Newton's Law of cooling can be rearranged to give an expression for the internal oil temperature, $\theta(t)$, as a function of the external temperature, $\theta_o(t)$, the γ parameter, and the ambient temperature, T_{air} (Black and Makris, 2000)

$$\theta(t) = \frac{(\gamma+1)}{\gamma}\theta_o(t) - \frac{1}{\gamma}T_{air}. \quad (2\text{-}29)$$

2.6 NONLINEAR SOLUTION

Figure 2-4 plots the evolution of parameter $\gamma = (\theta_o(t) - T_{air})/(\theta(t) - \theta_o(t))$ with the rise in external damper temperature as the three dampers considered here are subjected to continuous cycling at various frequencies (presented in Chapter 4). The plots clearly show that the γ parameter does not retain a constant value as the cycling of the damper continues, and therefore, Newton's law of cooling is a gross approximation.

Prior to loading, all the temperatures appearing in the ratio given by Equation (2-26) are equal indicating an indeterminate value for γ. This intermediate value of γ at the initiation of loading is a constant which can be identified from the recorded data shown in Figure 2-4. For the 3 kip damper

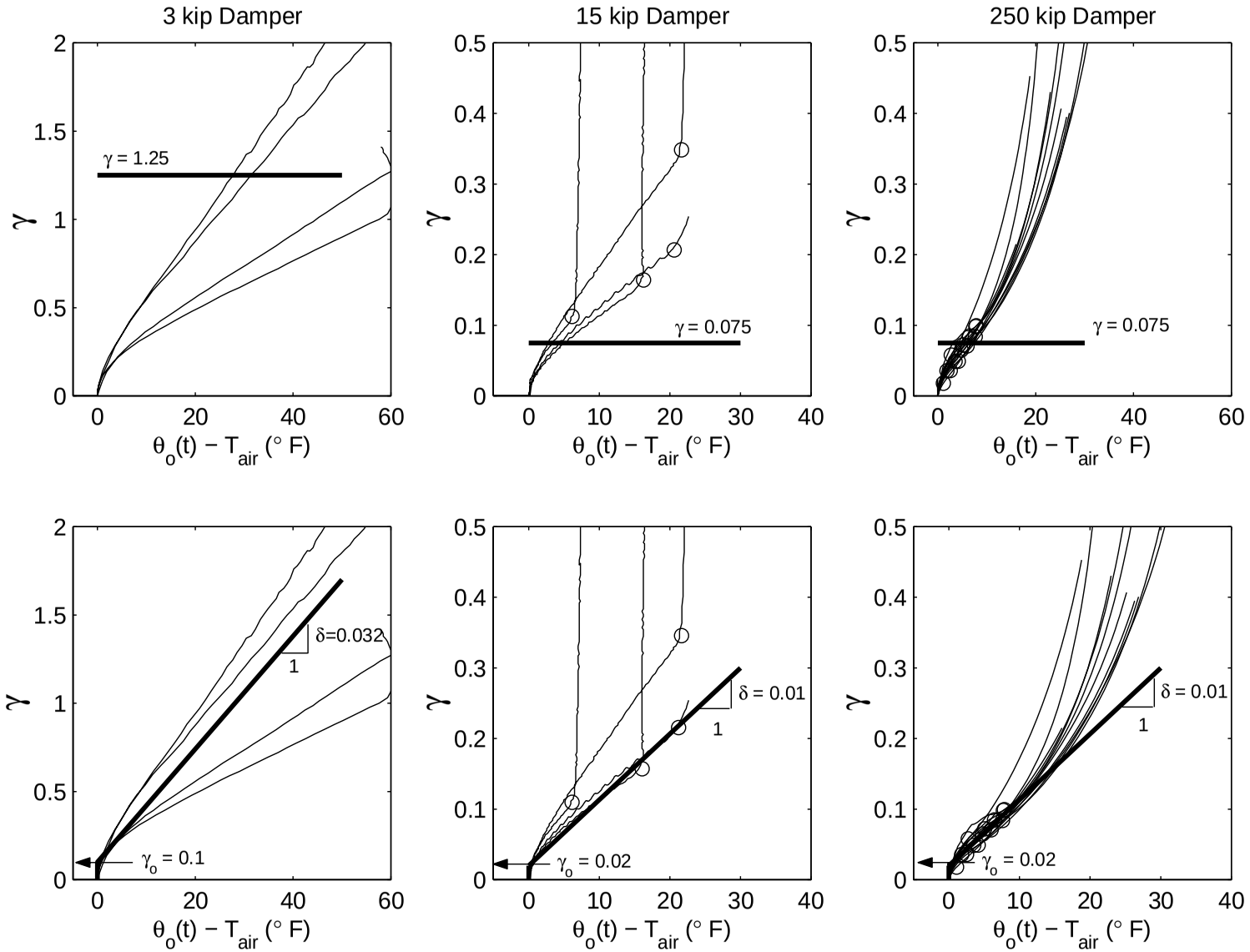

Figure 2-4. Thin lines: Evolution of parameter γ with external damper temperature as the three dampers of interest are subjected to continuous cycling. Heavy lines indicate a constant γ (top); and a linear γ with a nonzero initial value (bottom). The circles indicate the end of loading.

$\gamma_o \approx 0.1$, whereas, for the 15 kip and the 250 kip damper $\gamma_o \approx 0.02$. Subsequently as loading proceeds, parameter γ increases at a nearly linear rate so that

$$\gamma(t) = \gamma_o + \delta[\theta_o(t) - T_{air}]. \tag{2-30}$$

For the 15 and 250 kip dampers, experimental data suggests a value of $\delta \approx 0.01\ [F]^{-1}$. With the two parameter model given by Equation (2-30), a more realistic law of cooling is

$$\frac{\theta_o(t) - T_{air}}{\theta(t) - \theta_o(t)} = \gamma_o + \delta[\theta_o(t) - T_{air}] \tag{2-31}$$

which after rearranging gives

$$\theta(t) = \frac{\delta\theta_o^2(t) + (1 + \gamma_o - \delta T_{air})\theta_o(t) - T_{air}}{\delta\theta_o(t) - \delta T_{air} + \gamma_o}. \tag{2-32}$$

Equation (2-32) is a two parameter model for the law of cooling of fluid dampers and expresses the temperature of the internal fluid as a function of the external temperature of the damper casing, $\theta_o(t)$, and the temperature of the surrounding air, T_{air}.

For both the 15 kip and the 250 kip dampers, the experimental data shown in Figure 2-4 suggests[1] that the values of the two parameters appearing in Equation (2-32) are $\gamma_o = 0.02$ and $\delta = 0.01[F]^{-1}$. The performance of Equation (2-32) in predicting the internal temperature is examined in Chapters 4 and 5.

1. It should be noted that the line in the center column of Figure 2-4, which deviates substantially from the other three lines, was calculated from data recorded from the lowest amplitude test. For this amplitude, the recorded internal temperature is less representative of the actual internal temperature at mid-stroke as will be discussed in the following chapter.

When the two parameter law of cooling is adopted, Equation (2-28) is not valid. In this case, the time dependence of the external temperature, $\theta_o(t)$, is expressed as a function of the internal temperature of the silicone fluid, $\theta(t)$, via Equation (2-31) which gives

$$\theta_o(t) = \frac{1}{2\delta}\{A + \delta\theta(t) + [\delta^2\theta^2(t) + B\theta(t) + C]^{1/2}\} \tag{2-33}$$

where the constant parameters A, B and C are given by $A = \delta T_{air} - 1 - \gamma_o$, $B = 2\delta\gamma_o - 2\delta - 2\delta^2 T_{air}$ and $C = 1 + 2\gamma_o + 2\delta T_{air} + \gamma_o^2 - 2\gamma_o\delta T_{air} + \delta^2 T_{air}$.

Substitution of (2-33) into (2-20) yields the nonlinear governing differential equation

$$\frac{d\theta(t)}{dt} + \lambda\left[\theta(t) - \frac{1}{2\delta}\{A + \delta\theta(t) + [\delta^2\theta^2(t) + B\theta(t) + C]^{1/2}\}\right] = \frac{1}{mC_p}P(t)\dot{u}(t) + \lambda T_{air} \tag{2-34}$$

which can be solved numerically for the internal temperature, $\theta(t)$, using a standard state-space formulation (Matlab 1992). The performance of Equation (2-34) in predicting the internal temperature knowing only the damper properties and the loading history is evaluated in Chapter 4.

3 EXPERIMENTAL STUDIES UNDER SMALL AMPLITUDE MOTION — WIND LOADING

When fluid dampers are used to suppress wind-induced vibrations the piston displacement and velocities are relatively small. The problem of heating under small amplitude and prolonged duration motions was studied experimentally at the Earthquake Engineering Research Center laboratory at the University of California, Berkeley. Figure 3-1 (top) shows a photograph of the experimental setup with six internal thermocouple probes and six external thermocouples mounted on the damper shell. The setup includes a self-equilibrating reaction frame and a 300 kip actuator along with a 1000 gpm proportional valve. Figure 3-1 (bottom) shows a schematic of the locations of the thermocouples. The thermocouples labelled (1) through (6) are internal thermocouples which are in contact with the silicone oil of the damper. Thermocouples (1) and (4) are at the mid-stroke position, installed 90° apart along the circumference of the damper shell; while thermocouples (2) and (5) are at + 4in. and thermocouples (3) and (6) are at the end-of-stroke location (+8 in.). The thermocouples labelled (7) through (12) are external thermocouples.

Figure 3-2 (left) plots the recorded temperature histories at the mid-stroke position under harmonic loading with amplitude $u_o = 0.5$ in. and frequency $f = 0.66$ Hz for a duration of loading equal to 23 minutes (920 cycles). The recorded temperature histories with thermocouples No. 1 and No. 4 shows that the temperature rise is not axisymmetric. The temperature at thermocouple No. 4 increases much more rapidly at the beginning of loading and subsequently the temperature at both

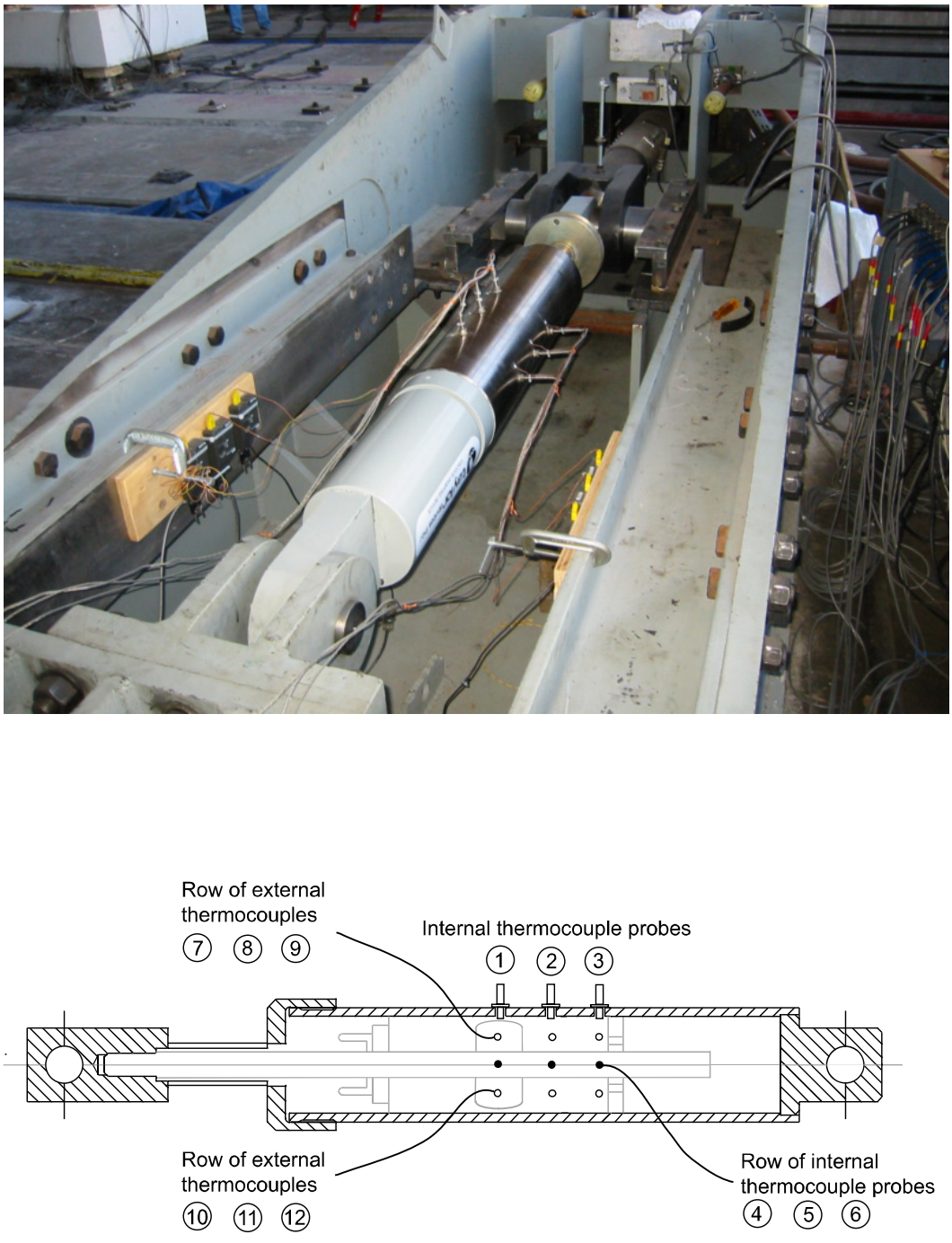

Figure 3-1. Experimental setup for testing the 250 kip damper from the 91/I5 overpass (top). Schematic of the fluid damper indicating the locations of the six internal thermocouple probes ((1) through (6)) and the six external thermocouples ((7) through (12)) (bottom).

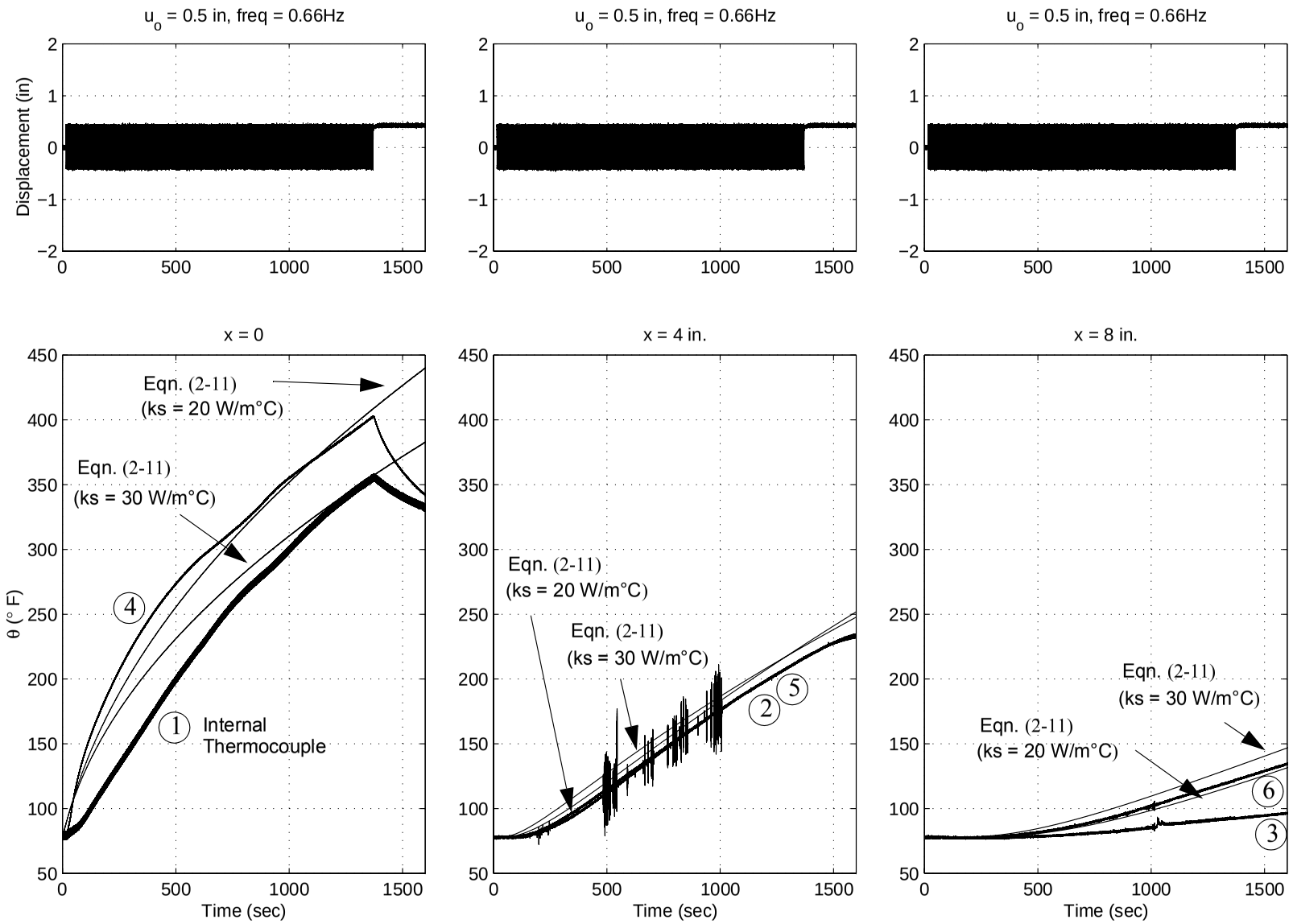

Figure 3-2. Recorded loading histories (top) and temperature histories (bottom) at x = 0 (left column), 4 in. (center column), and 8 in. (right column) under harmonic loading with piston amplitude u_o = 0.5 in. and frequency f = 0.66 Hz.

thermocouples rise at approximately the same rate. Upon termination of loading, the two thermocouples indicate that same temperature within five minutes (300 sec). Together with experimental data, Figure 3-2 plots the prediction of the analytical expression given by Equation (2-11) when the coefficient of thermal conductivity is taken as either $k_s = 20$ Joules/sec m °C or 30 Joules/sec m °C. Figure 3-2 shows that the prediction of Equation (2-11) is very good.

Figure 3-2 (center) plots the recorded temperature histories at $x = 4.0$ in. under the same loading. Now the recorded temperature histories from the two thermocouples placed 90° apart are almost identical while the temperature rise for a given time at $x = 4.0$ in. is less than the temperature rise at $x = 0$ in.; since the location, $x = 4.0$ in. is further away from the heat source. The analytical expression given be Equation (2-11) offers an outstanding prediction (for $x = 4.0$ in.) not only for peak values but also for the entire shape of the temperature curve through the history of loading.

An equally accurate prediction is achieved with Equation (2-11) when $x = 8.0$ in. for the temperature rise at the end-of-stroke location. In this location, the temperature rise is not axisymmetric, however, the prediction of Equation (2-11) is in close agreement with the higher of the two temperature histories. The temperature rise prediction of the end-of-stroke location is of prime interest since we are concerned with the temperature that the end-seals will experience.

The outstanding performance of the analytical expression (2-11) is also demonstrated in Figure (3-3) which plots the recorded temperature histories at mid-stroke ($x = 0$ in.), at $x = 4.0$ in. and at end-of-stroke ($x = 8.0$ in.) under harmonic loading with amplitude $u_o = 2.0$ in. and frequency $f = 0.2$ Hz for a duration of loading equal to 13 minutes (156 cycles).

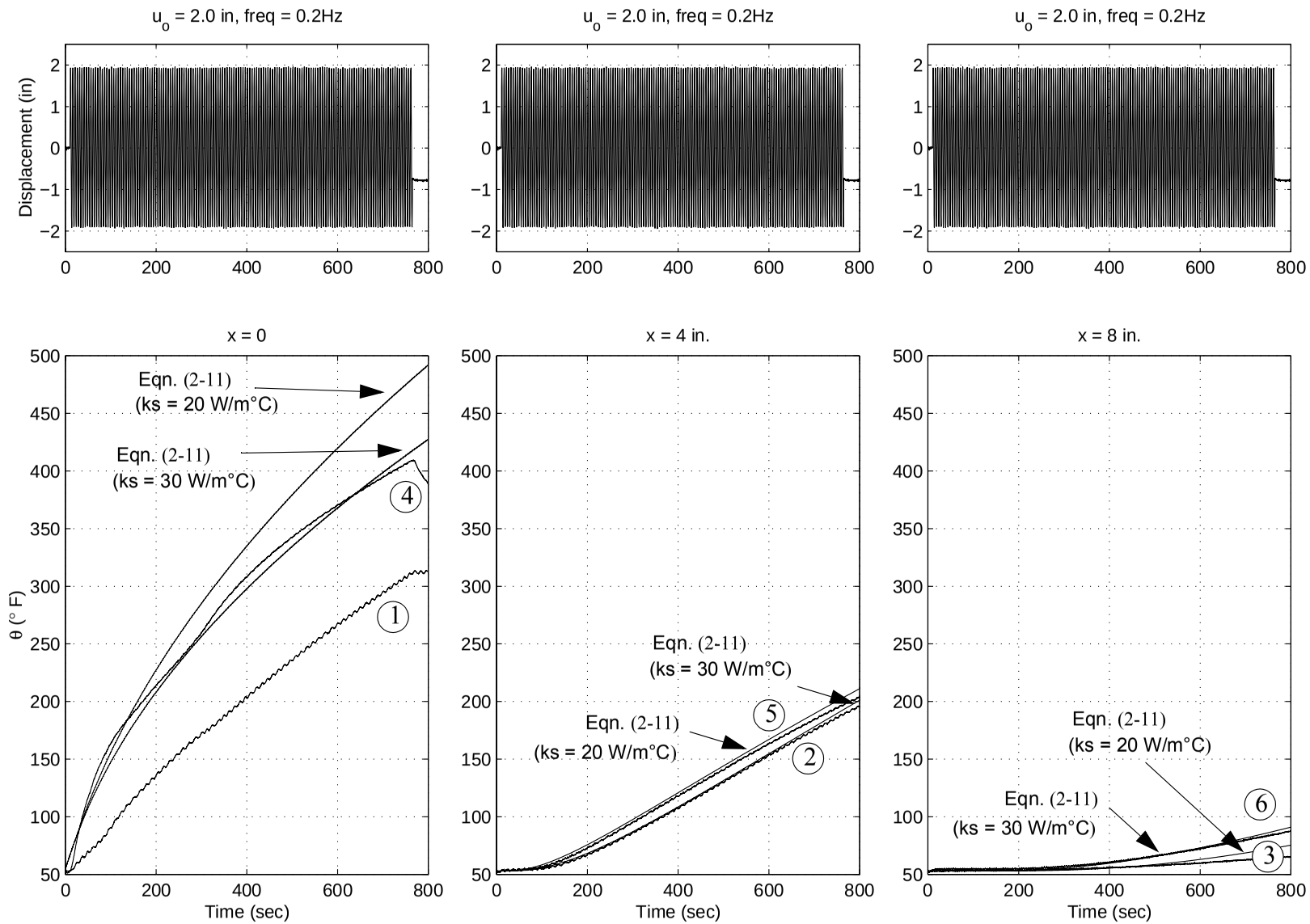

Figure 3-3. Recorded loading (top) and temperature histories (bottom) at x = 0 (left column), 4 in. (center column), and 8 in. (right column) (right column) under harmonic loading with piston amplitude u_o = 2.0 in. and frequency f = 0.2 Hz.

The analytical expression give by (2-11) not only predicts with fidelity the peak values but also matches the history of the temperature rise throughout loading which demonstrates a negative curvature when $x = 0$ in.; and a positive curvature when $x = 8.0$ in.

Figure 3-4 plots the recorded temperature histories within the fluid of the damper under harmonic loading with amplitude $u_o = 0.5$ in. and frequency $f = 0.25$ Hz. During the first test the loading was accidentally interrupted for 60 seconds and subsequently restarted. The same test was repeated and is shown in Figure 3-5. The recorded histories in Figure 3-4 are of interest since they show that the interruption influences the temperature rise at $x = 0$; however, it is almost unnoticeable at $x = 8$ in. Furthermore, when the loading was resumed the temperature history reassumed the initial backbone curve. For this loading ($u_o = 0.5$ in., $f = 0.25$ Hz) the prediction of the analytical expression in Equation (2-11) is not as good as it was in Figures 3-2 and 3-3; nevertheless, at $x = 8$ in., which is the location of highest interest, Equation (2-11) predicts the temperature of the hottest thermocouple. When the test was repeated (see Figure 3-5) Equation (2-11) is in excellent agreement with the prediction of the less hot thermocouple placed at $x = 8$ in.

In conclusion, the experimental work presented in this chapter shows that in the 250 kip damper tested, the temperature rise is not axisymmetric. For instance, after 4 hours of loading the temperature along the circumference of the damper near the end-seals ($x = 8$ in.) may differ by more than 50 °F. The recorded data shows that the closed form expression given by Equation (2-11) can be used with confidence to estimate the internal temperature of fluid dampers at all locations when loaded harmonically with small amplitude motion. In most cases the agreement between the recorded data and the mathematical prediction is very good and thus Equation (2-11) should offer dependable results for a variety of dampers manufactured by different vendors. One of the reasons

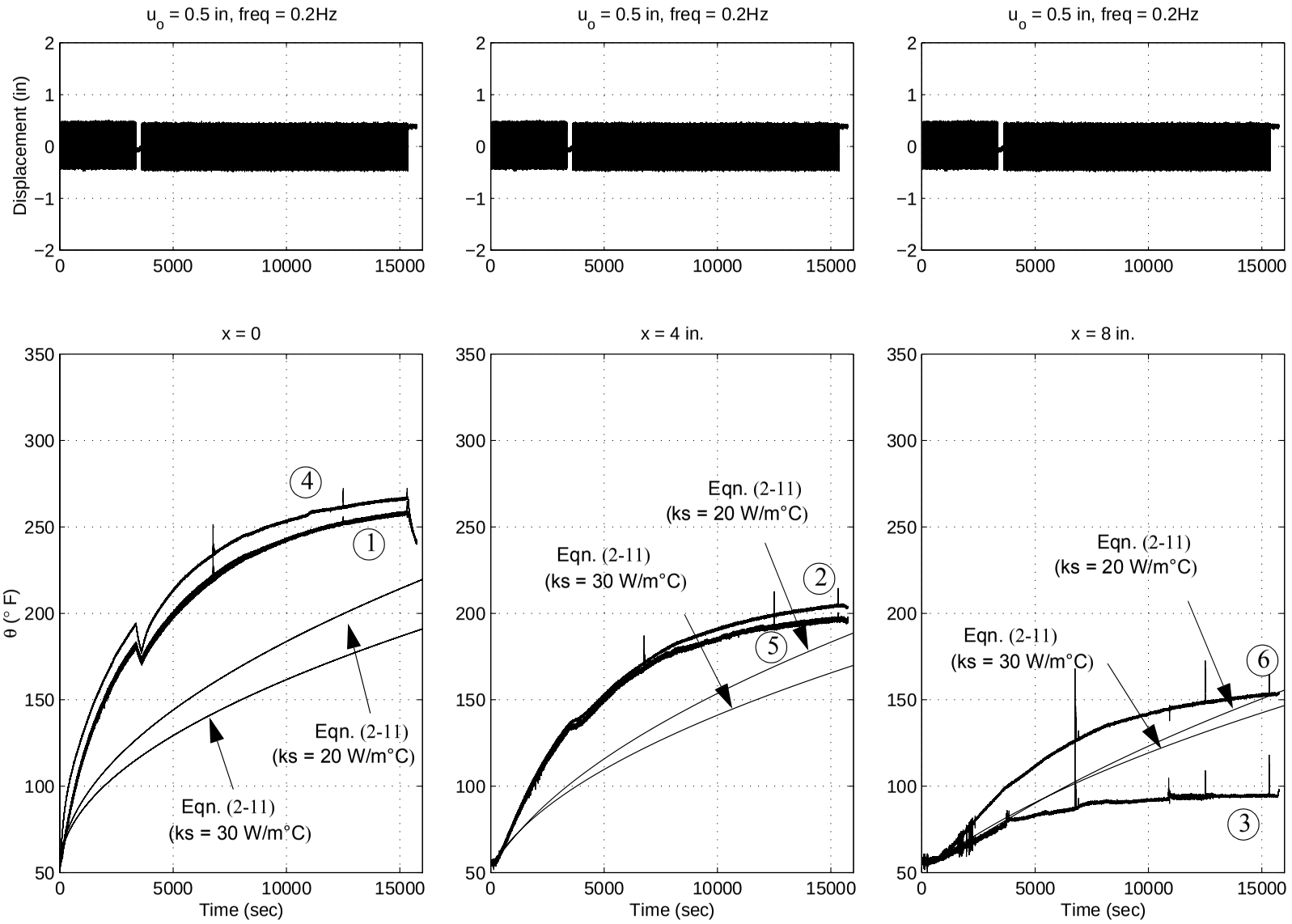

Figure 3-4. Recorded displacement histories (top) and temperature histories (center and bottom) for x = 0 (left column), 4 in. (center column), and 8 in. (right column) for an harmonic loading test with u_o = 0.5 in. and frequency = 0.2 Hz.

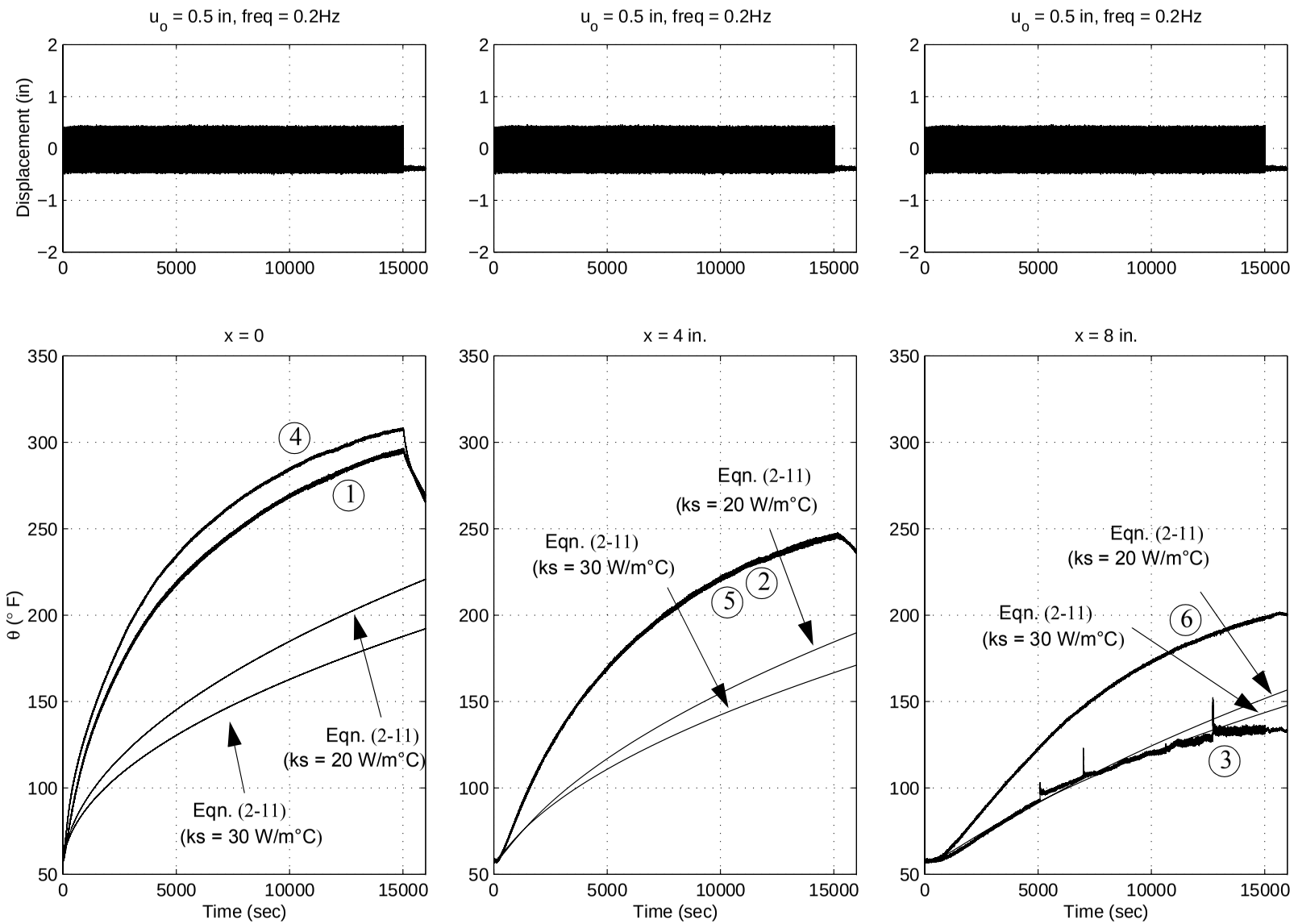

Figure 3-5. Recorded displacement histories (top) and temperature histories (center and bottom) for x = 0 (left column), 4 in. (center column), and 8 in. (right column) for an harmonic loading test with u_o = 0.5 in. and frequency = 0.2 Hz.

that Equation (2-11), which is the solution for an adiabatic damper housing, offers such accurate results is because the ration $\beta / \alpha = (k_s \pi d_p) / (\rho C_p \varepsilon A_p)$ in Equation (2-7) for the 250 kip damper is as low as 0.013.

4 EXPERIMENTAL STUDIES UNDER LARGE AMPLITUDE MOTION — EARTHQUAKE LOADING

This chapter describes the experimental testing of three fluid dampers — a 3 kip, 15 kip and a 250 kip damper. The objective of the testing is to characterize the mechanical and thermal behavior of the dampers and verify the validity of the approximate analytical expressions for long-stroke motions presented in Chapter 2. The geometrical characteristics of the dampers, as well as, the physical properties of the steel and silicone oil are given in Table 2-1.

The three dampers shown in Figure 1-2 are fluid orifice dampers with similar external and internal characteristics. In order to collect temperature readings from the internal fluid, ports have been drilled through the damper housing and high-pressure, high-temperature thermocouple probes—which are in direct contact with the internal oil—have been installed. The external temperature was measured at various locations via fine-gauge, K-type thermocouples. Each damper was subjected to a number of harmonic tests with varying amplitudes and frequencies in order to properly characterize their thermal properties.

The subsequent sections of this chapter present a description of each damper, the experimental setup and results, along with a comparison of the measured internal temperature and the predictions given by the analytical solutions presented in Chapter 2.

4.1 COMPONENT TESTING OF THE 3 KIP DAMPER

The 3 kip damper has a mid-stroke length of 12 in. and a maximum stroke of ±1.5 in. The damper has a linear force-deformation relation, $P(t) = C[\dot{u}(t)]$, where $C = 17.69$ (kNsec)/m $= 0.101$ (kipsec)/in.

4.1.1 Experimental Setup

The 3 kip damper was tested at the structural laboratory at Davis Hall, at the University of California, Berkeley in the summer of 2000 and spring of 2001. The experimental setup for the testing of the 3 kip damper is shown in Figure 4-1. A hydraulic actuator imposes a prescribed displacement history along the axis of the damper. The force developed in the damper is measured through a stationary load cell connected between the damper and the reaction frame (left end in Figure 4-1). The imposed displacement history is measured with a linear variable differential transducer (LVDT) located within the actuator.

Temperature histories are recorded at three locations. The thermocouple labelled by the circled 1 in Figures 4-1 and 4-3, was inserted along the length of the piston rod and positioned internally near the moving surface of the piston head. This was achieved by drilling a 6.5 in. (16.5 cm) long bore along the piston rod which terminates at the piston head. A high-temperature, high-pressure thermocouple probe was inserted through the damper housing at the end of the stroke (labelled by the circled 2 in Figures 4-2 and 4-3). In addition, an external thermocouple, labelled by the circled 3, was placed on the damper housing near the end-of-stroke location. A thermally-conductive paste was used to ensure integral contact between the external thermocouple and the damper housing, as well as, at the end of the hole bored down the length of the piston rod.

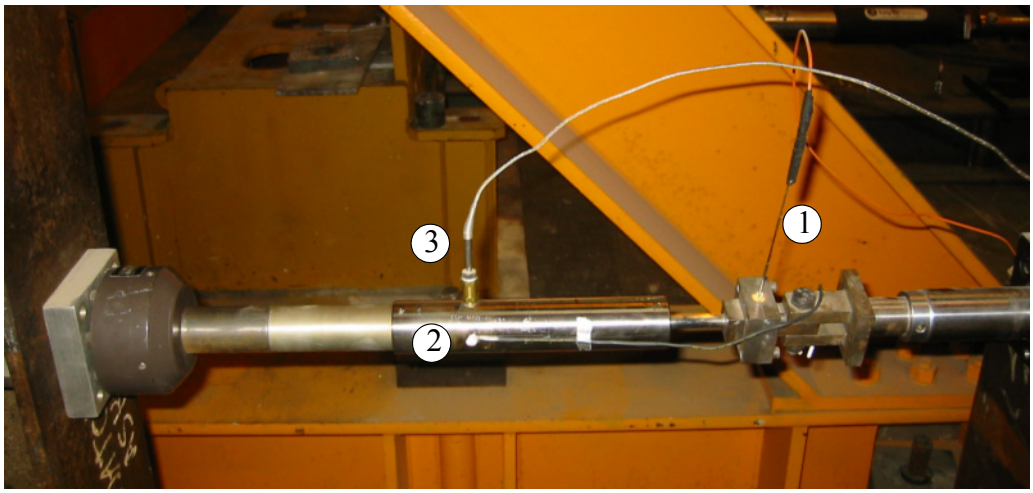

Figure 4-1. View of the experimental setup for the testing of a 3 kip damper. The damper is mounted between the piston of the actuator (right) and the load cell (left) which is fixed to a steel reaction frame.

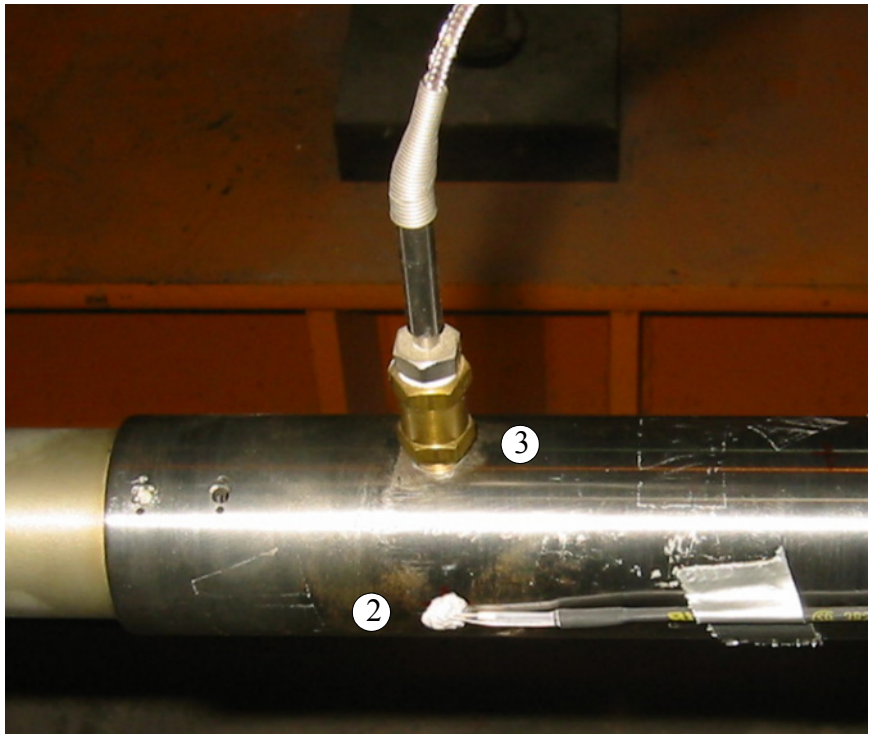

Figure 4-2. Close-up view showing the external thermocouple with its end inserted in highly thermally conductive paste (2), and the high-pressure, high-temperature thermocouple probe inserted through the damper housing (3).

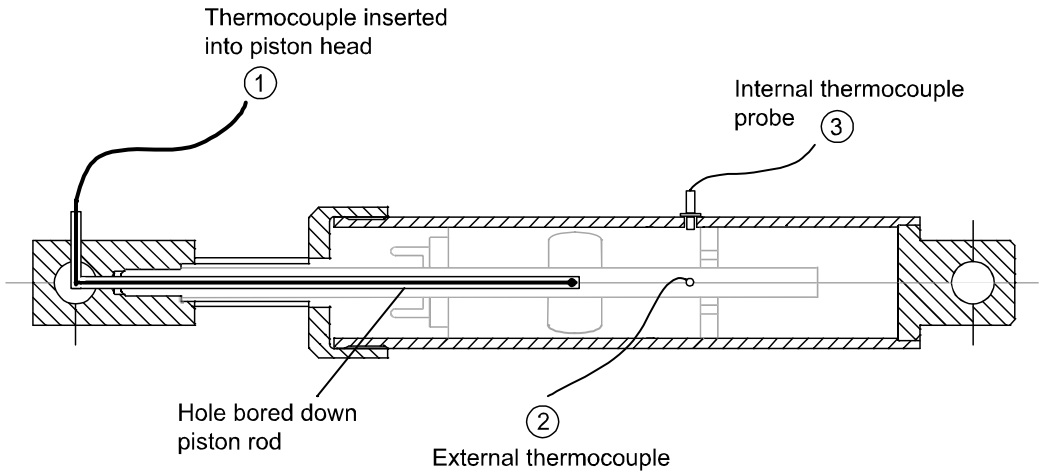

Figure 4-3. Schematic of the 3 kip damper indicating the locations of the thermocouple inserted down the piston rod (1); the external thermocouple (2); and the internal thermocouple probe (3).

4.1.2 Experimental Results

Table 4-1 summarizes the 6 tests performed on the 3 kip damper, with the corresponding results presented in Figures 4-4 through 4-9. The top plot in each figure shows the input time history, while the bottom plots shows the recorded internal and external temperature histories, together with predicted temperature histories of the internal silicone fluid that undergoes shearing action. The lines with the circled numbers are the recorded temperature histories at the positions indicated on the inset damper schematic and Figure 4-3. The dashed lines labeled "Eqn. (2-28)" and "Eqn. (2-34)" are predictions of internal fluid temperature based on the approximate macroscopic energy balance formulation. The solution of the linear differential equation considering a one parameter cooling law is given by Equation (2-28); whereas, the solution of the nonlinear differential equation (Equation (2-34)), which incorporates the two parameter cooling law, is obtained numerically. The dashed lines labeled "Eqn. (2-29)" and "Eqn. (2-32)" are predictions of the internal fluid temperatures by reading the external temperature on the damper housing in association with the one parameter cooling law (Equation (2-29)) and the two parameter cooling law (Equation (2-32)). For the 3 kip damper, when Newton's law of cooling is adopted, an average value of $\gamma = 1.25$ is used, whereas, when the two parameter cooling law is adopted $\gamma_o = 0.1$, and $\delta = 0.032$ (see Figure 2-4).

Figure 4-4 shows the results of the first test conducted on the 3 kip damper. The line labelled by the circled 1 plots the recorded temperature history at the piston head (via the thermocouple inserted down the piston rod), lines 2 and 3 plot the external and internal temperatures at the end-of-stroke location (+1.5 in.). Figure 4-4 shows that the internal temperature measured at the end of the stroke is substantially less than that recorded at the piston head. This observation suggests that the internal oil temperature measured at the end of the stroke is likely not a representative measure

Table 4-1. Experimental Tests Performed on the 3 kip Damper

Test No.	Amplitude (in)	Frequency (Hz)	Velocity (in/sec)	Duration (cycles)
1	1.4	0.25	2.20	~ 420
2	1	0.5	3.14	~ 420
3	1.4	0.5	4.40	~ 210
4	1.0	1.0	6.28	~ 160
5	1.4	1.0	8.79	~ 80
6	0.5	2.0	6.28	~ 200

of the internal oil temperature throughout the damper. The linear and nonlinear analytical solutions given by Equation (2-28) and the solution of Equation (2-34) quickly reach a steady-state value—a stable temperature with continued loading—which is substantially less than the observed temperature increase, while the predictions of the internal temperature given the external temperature (Equations (2-29) and (2-32)) overestimate the observed temperature.

Figures 4-5 and 4-6, which plot the results of tests 2 and 3, respectively, show similar trends to those seen in test number 1, with the predictions of Equations (2-28) and the solution of (2-34) reaching a steady-state at temperatures much less than the observed internal temperature. The estimates of internal temperature based on the recorded external temperatures (given by Equations (2-29) and (2-32)), however, accurately represent the recorded internal temperatures for both tests.

Figures 4-7 and 4-8 present the results of tests 4 and 5, respectively. It is seen that the internal temperature predicted by Equations (2-28) and (2-34) reach their steady-state more gradually than the first 3 tests, although, still at levels below the observed temperature. The predictions of internal temperature estimated from the external readings give relatively accurate estimates of the observed temperature.

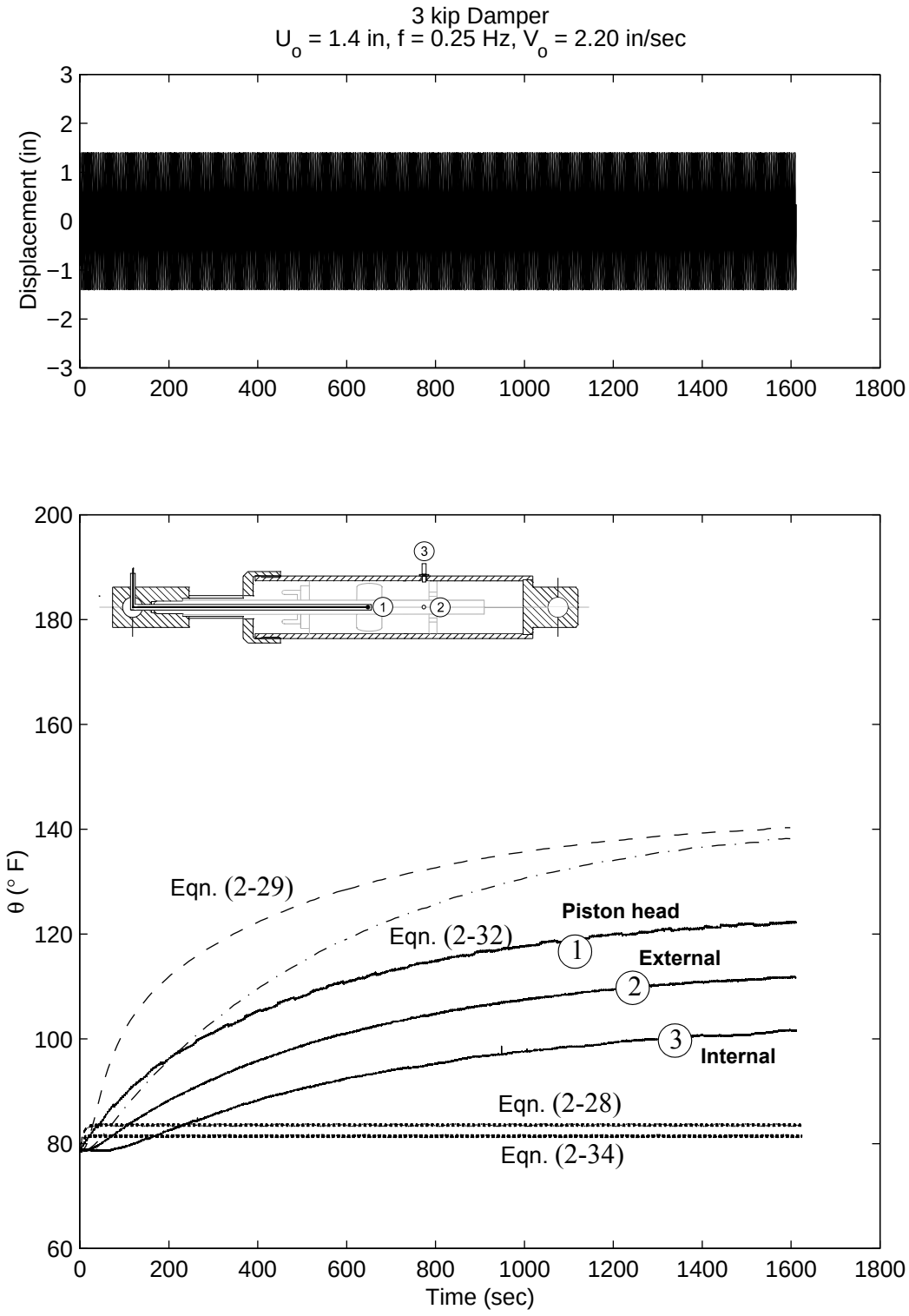

Figure 4-4. Plot showing the harmonic input with amplitude, U_o = 1.4 in. and frequency, f = 0.25 Hz imposed on the 3 kip damper (top); and a comparison of the measured temperature histories with the analytical solutions (bottom).

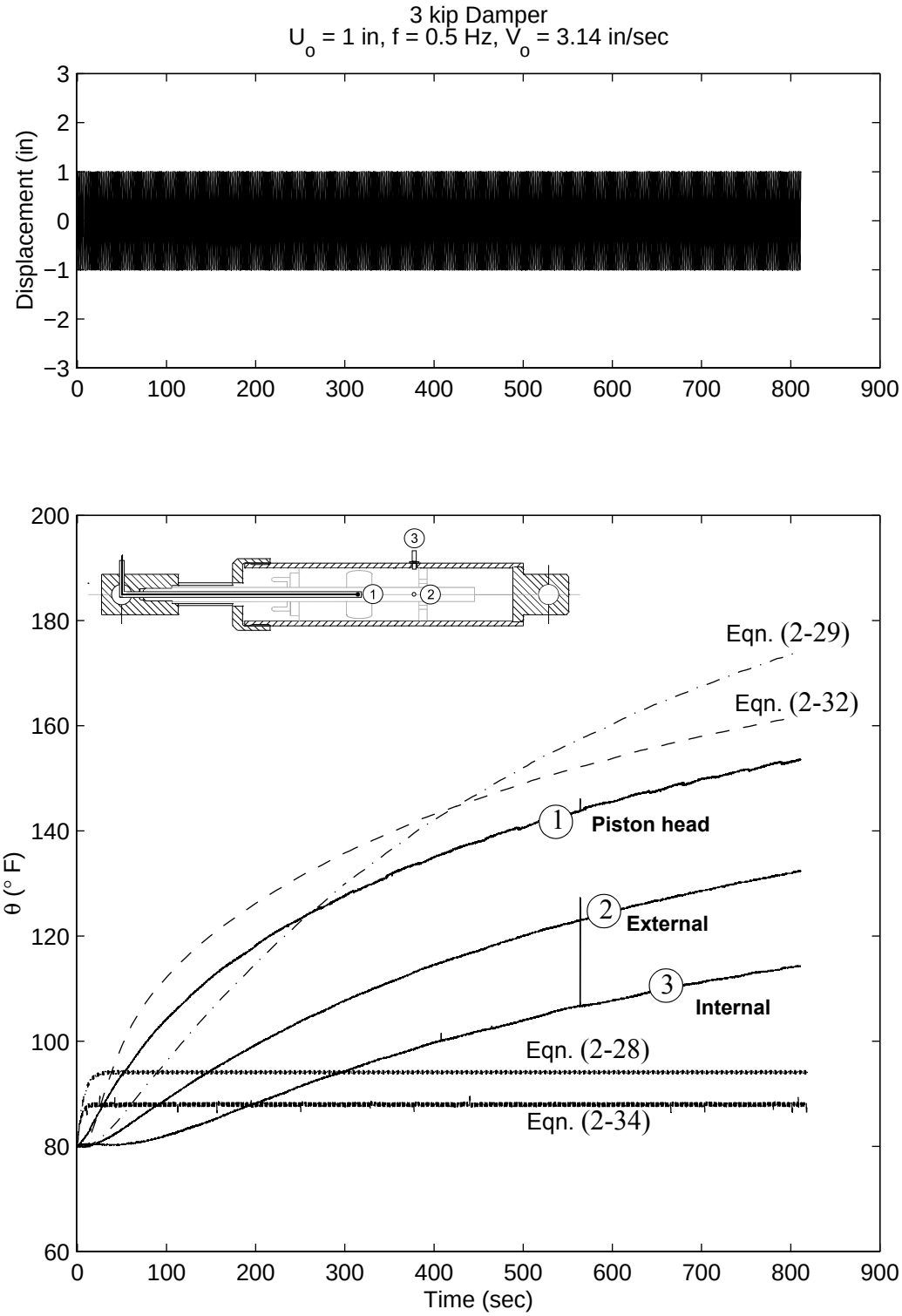

Figure 4-5. Plot showing the harmonic input with amplitude, U_o = 1.0 in. and frequency, f = 0.5 Hz imposed on the 3 kip damper (top); and a comparison of the measured temperature histories with the analytical solutions (bottom).

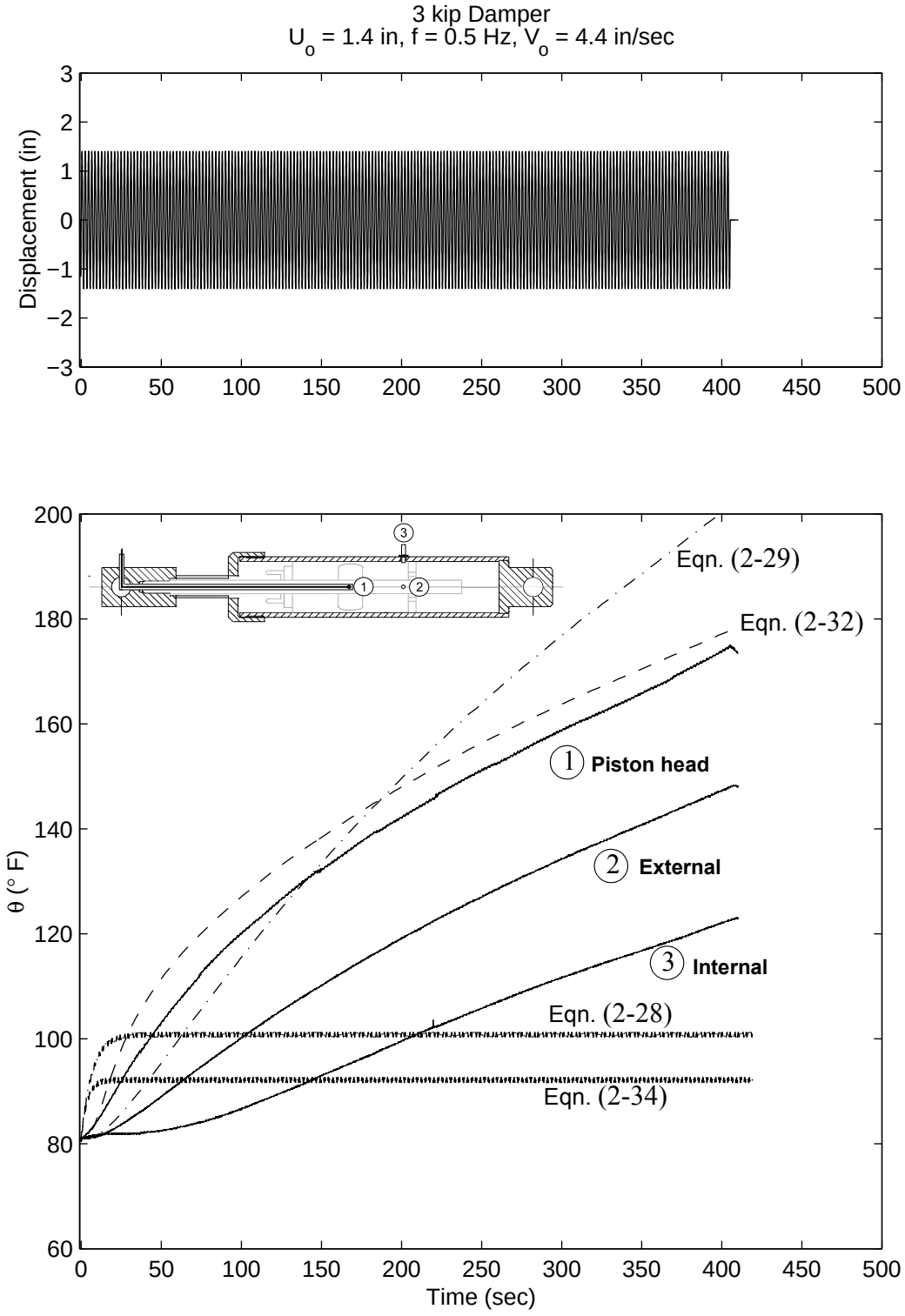

Figure 4-6. Plot showing the harmonic input with amplitude, U_o = 1.4 in. and frequency, f = 0.5 Hz, imposed on the 3 kip damper (top); and a comparison of the measured temperature histories with the analytical solutions (bottom).

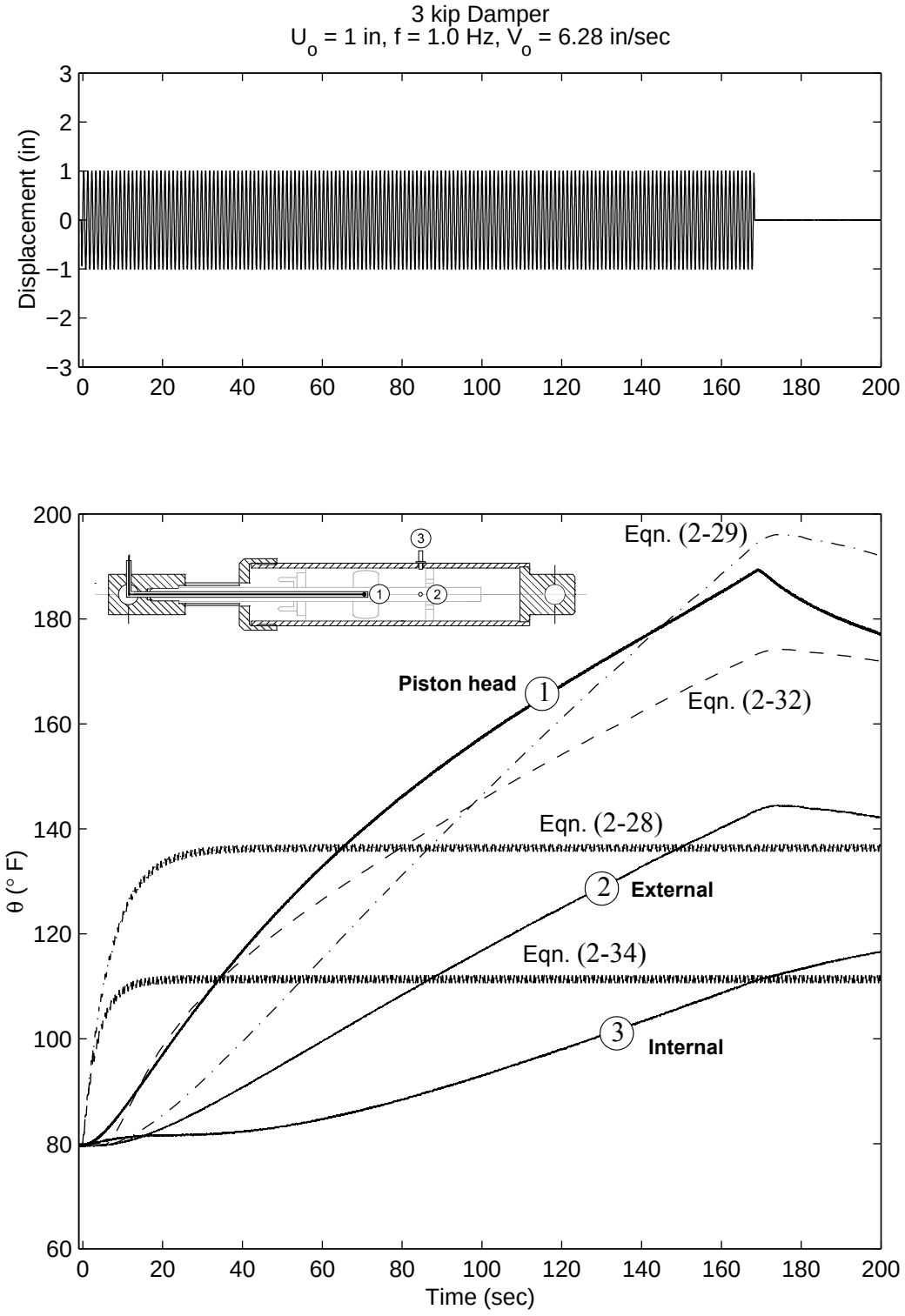

Figure 4-7. Plot showing the harmonic input with amplitude, U_o = 1.0 in. and frequency, f = 1.0 Hz imposed on the 3 kip damper (top); and a comparison of the measured temperature histories with the analytical solutions (bottom).

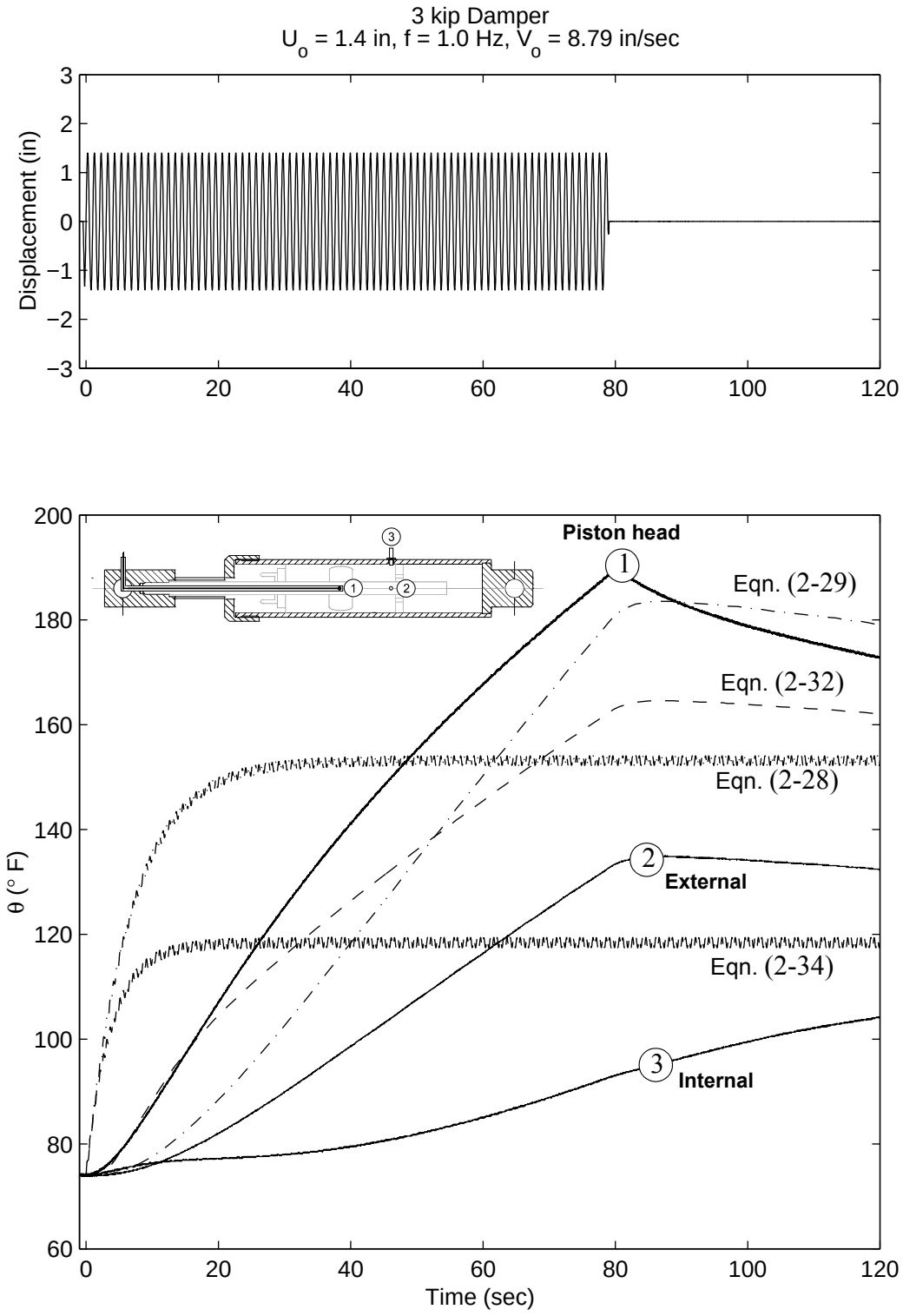

Figure 4-8. Plot showing the harmonic input with amplitude, U_o = 1.4 in. and frequency, f = 1.0 Hz imposed on the 3 kip damper (top); and a comparison of the measured temperature histories with the analytical solutions (bottom).

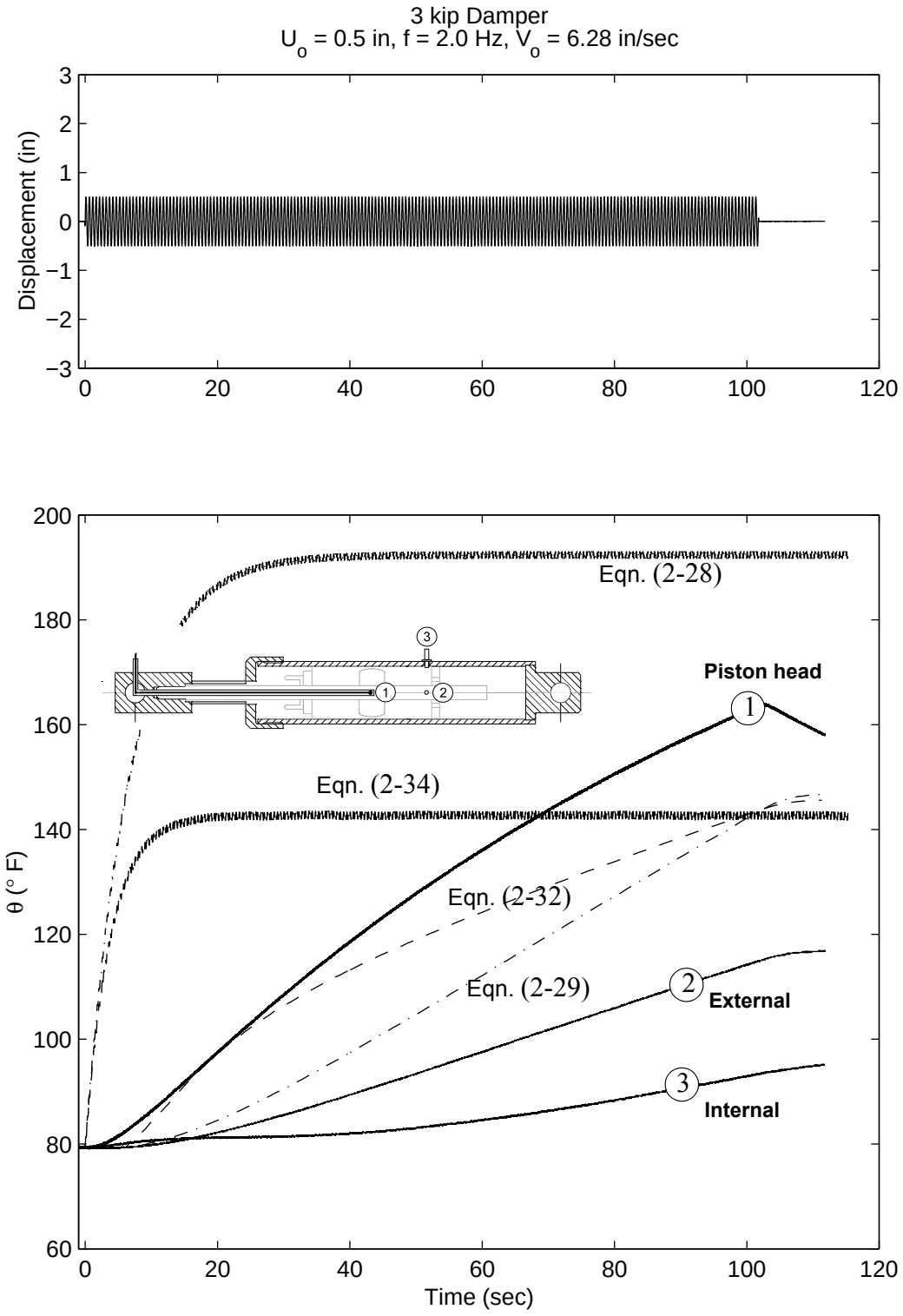

Figure 4-9. Plot showing the harmonic input with amplitude, U_o = 0.5 in. and frequency, f = 2.0 Hz imposed on the 3 kip damper (top); and a comparison of the measured temperature histories with the analytical solutions (bottom).

The results of test number 6 are shown in Figure 4-9. Although tests 4 and 6 have the same input velocity, the linear solution, given by Equation (2-28), over-estimates the internal temperature for test number 6, whereas, it predicts an internal temperature much lower than that observed for test number 4. This observation is contradicted by the experimental data which shows that the temperature increase at the piston head is similar for both tests, reaching approximately $160°$ F at roughly the same duration of loading (100 sec). Evidence of a slow rate of heat transfer along the length of the damper is clearly seen for the relatively low amplitude input in test number 6 (± 0.5 in.) as the temperature increase observed at the end of the stroke (+1.5 in.) is much less than at the piston head ($15°$ F opposed to $80°$ F).

4.1.3 Conclusions - 3 kip Damper

In general, it is seen that the linear and nonlinear analytical expressions (Equations (2-28) and the solution of Equation (2-34)) better represent the observed internal oil temperature for increasing input velocity. The internal oil temperature predicted by the analytical expressions, in all cases, rises more rapidly than the observed behavior and reaches a steady-state. This steady-state temperature was not observed in the recorded data. The predictions of internal temperature from recorded external temperatures given by Equations (2-29) and (2-32) give reasonable estimations for all tests with the exception of the lowest velocity test (test number 1).

4.2 COMPONENT TESTING OF THE 15 KIP DAMPER

The 15 kip damper has a mid-stroke length of 50 in. and a maximum stroke of ± 6 in. The damper has been studied previously by Chang et al. (2000). Similar to the 3 kip damper presented in the previous section, it has a linear force-velocity response with $P(t) = C\dot{u}(t)$, where $C = 121$ (kN sec)/m $= 0.70$ (kip sec)/in.

4.2.1 Experimental Setup

The experimental setup for the testing of the 15 kip damper is shown in Figure 4-10. The force developed in the damper is measured through a stationary load cell that is connected between the damper and the reaction frame (left end in Figure 4-10). The imposed displacement history is measured with a linear variable differential transducer (LVDT) located at the right end of the actuator.

Temperature histories are recorded at two internal and two external locations as shown in Figure 4-11 and 4-12. The temperature at the two internal locations was measured via high-pressure, high-temperature thermocouple probes (labelled by the circled 1 and 3) installed directly through the damper housing. The probes were installed near the end of the stroke, (+6 in.) and separated by $90°$ in the radial direction. The external temperature was measured using 2 Type-K thermocouples placed to coincide with the internal probes (labelled by the circled 2 and 4). The internal and external thermocouples could not be placed at the mid-stroke location as they would impede the movement of the outer sleeve of the damper housing which moves in line with the piston head.

4.2.2 Experimental Results

Table 4-2 presents a list of experimental tests performed on the 15 kip damper, with the corresponding recorded data plotted in Figures 4-13 through 4-16. The top plot in each figure shows the input time history, while the bottom plots shows the recorded internal and external temperature histories together with predicted temperature histories. The lines with the circled numbers are the recorded temperature histories at the positions indicated on the inset damper schematic and Figure 4-11. Similar to the results presented for the 3 kip damper, the dashed lines labeled “Eqn. (2-28)” and “Eqn. (2-34)” are predictions of internal fluid temperature based on the approximate macroscopic energy balance formulation. The solution of the linear differential equation considering a

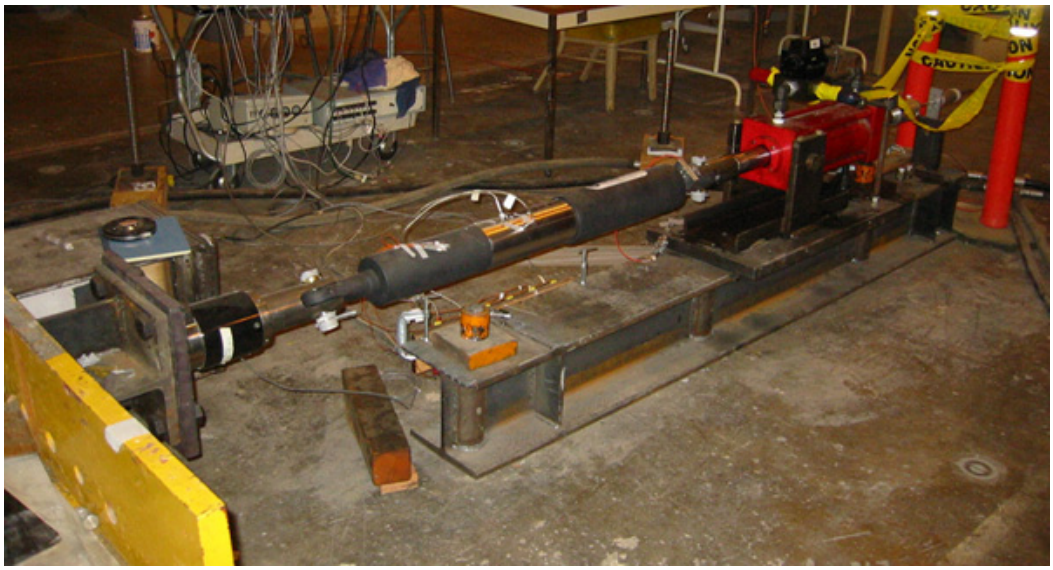

Figure 4-10. Experimental setup for testing the 15 kip damper. The damper is installed between the piston of the actuator (right) and the load cell (left) which is fixed to the reaction frame.

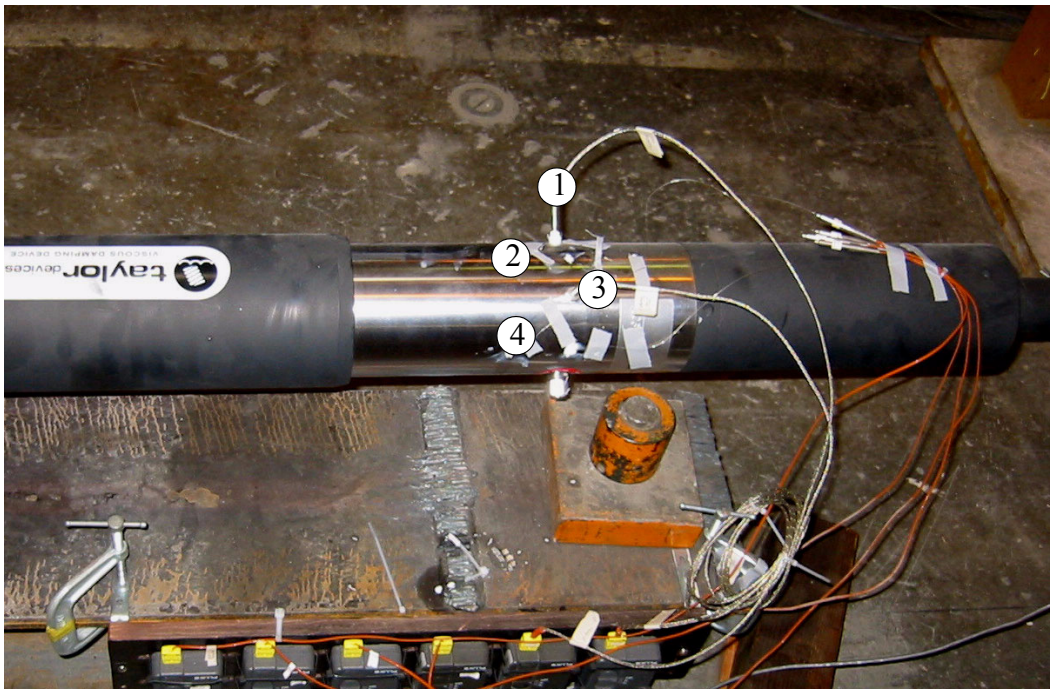

Figure 4-11. Detailed view of thermocouples. The thick wires are connected to the internal probes labelled (1) and (3), while (2) and (4) show the location of the external thermocouples.

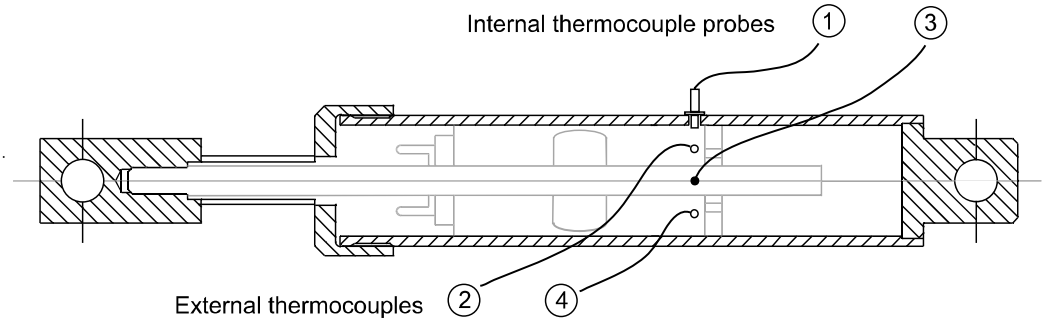

Figure 4-12. Schematic of the fluid damper indicating the locations of the internal thermocouple probes ((1) and (3)) and external thermocouples ((2) and (4)).

one parameter cooling law is given by Equation (2-28); whereas, the solution of the nonlinear differential equation (Equation (2-34)) considering a two parameter cooling law is obtained numerically. The dashed lines labeled "Eqn. (2-29)" and "Eqn. (2-32)" are predictions of the internal fluid temperatures by reading the external temperature on the damper housing in association with the one parameter cooling law (Equation (2-29)) and the two parameter cooling law (Equation (2-32)). For the 15 and 250 kip dampers, when Newton's law of cooling is adopted, an average value of $\gamma = 0.075$ is used, whereas, when the two parameter cooling law is adopted $\gamma_o = 0.02$, and $\delta = 0.01$ (see Figure 2-4).

Table 4-2. Experimental Tests Performed on the 15 kip Damper

Test No.	Amplitude (in)	Frequency (Hz)	Velocity (in/sec)	Duration (cycles)
1	1.0	1.0	6.28	~ 210
2	3.0	0.5	9.42	~ 20
3	4.0	0.5	12.57	~ 42
4	5.0	0.4	12.57	~ 19

Figure 4-13 plots the results of the first test conducted on the 15 kip damper. The solid lines labelled by the circled 1 and 3 plot the internal temperature histories recorded at the end of the stroke (+6 in.) while the circled 2 and 4 plot the external readings at the end of the stroke. The linear analytical solution for the internal temperature (Equation (2-28)) quickly reaches a steady-state, whereas, the solution of the nonlinear equation (Equation (2-34)) continues to grow reaching a temperature far in excess of that observed. The nonlinear prediction of internal temperature given external readings (given by Equation (2-32) and shown as the dashed line in the figure) captures the trend more accurately than the linear prediction which grows rapidly.

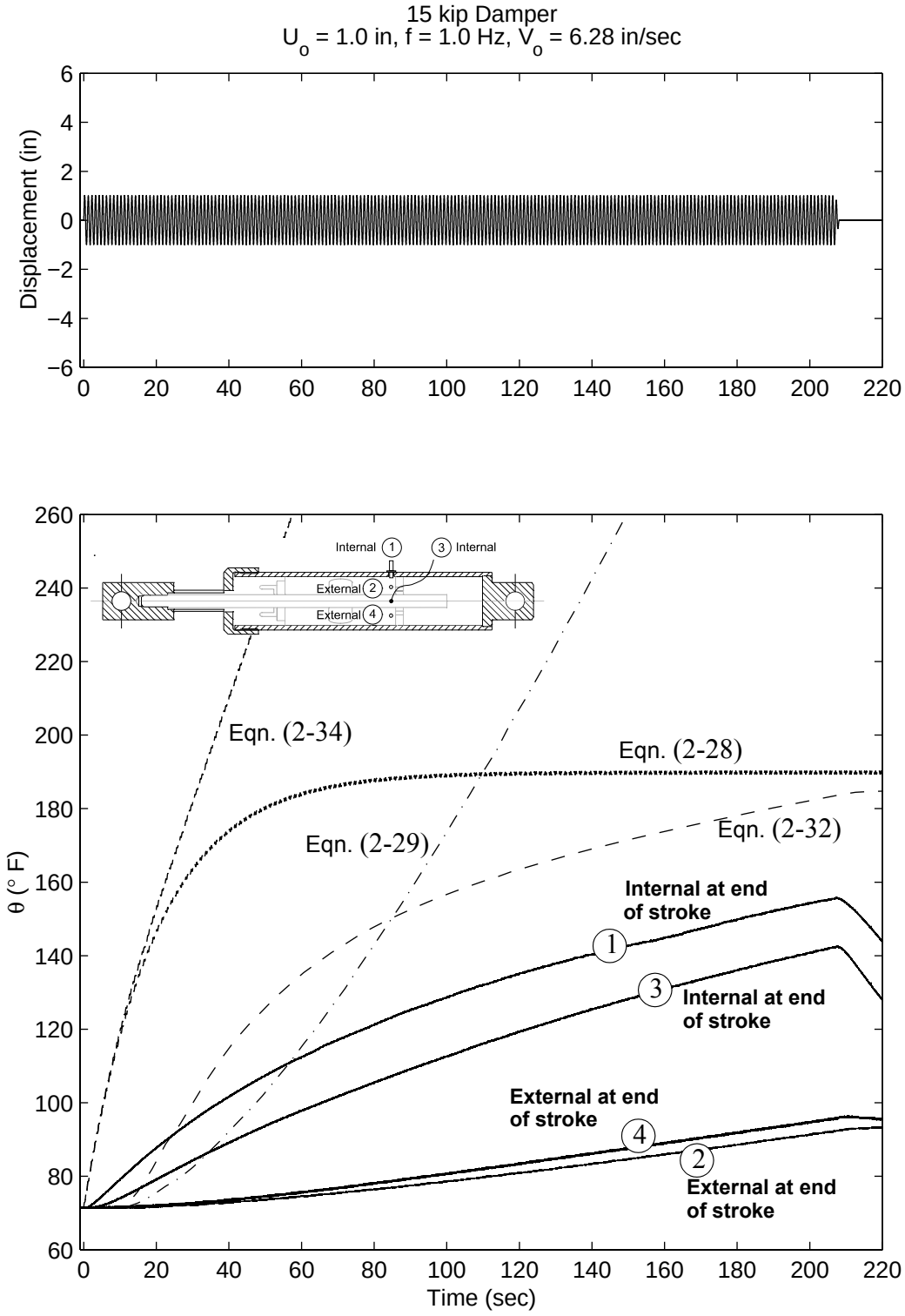

Figure 4-13. Plot showing the harmonic input with amplitude, U_o = 1.0 in. and frequency, f = 1.0 Hz imposed on the 15 kip damper (top); and a comparison of the measured temperature histories with the analytical solutions (bottom).

Figure 4-14 plots the results of the second test conducted on the 15 kip damper. The estimation of internal temperature by the analytical solutions (Equations (2-28) and the solution of (2-34)) better represent the observed temperature for this larger amplitude test. The estimation of internal temperature from external readings show reasonably accurate results.

Figures 4-15 and 4-16 present the results of the two largest amplitude tests conducted on the 15 kip damper, ±4.0 and ±5.0 in., respectively. For these tests the linear and nonlinear analytical predictions of the internal temperature given by Equation (2-28) and the solution of Equation (2-34) represent the observed internal temperature with reasonable accuracy, with the nonlinear solution predicting the internal oil temperature for the larger of the two tests with fidelity. The nonlinear prediction of the internal temperature given the external temperature (which makes use of the two parameter cooling law) accurately represents the observed internal temperature for both tests. The linear solution (given by Equation (2-29)), however, continues to grow at an increasing rate contrary to the observed trend. The difference in the two solutions is a result of the linear term in the two parameter cooling model which accounts for the fact that at larger temperatures (and thus loading durations), the rate of heat transfer is more rapid, as opposed to lower external temperatures (and durations), where there is a time lag between the external and internal temperature rise.

4.2.3 Conclusions - 15 kip Damper

In general, the linear solution given by Equation (2-28) and the solution of the nonlinear Equation (2-34) predict the observed internal temperature more accurately for the 15 kip damper than for the 3 kip damper, a fact particularly true for the larger amplitude tests (tests 2, 3 and 4). The larger amplitude motion increases the internal mixing of the oil and thus, the temperature recorded at the end of the stroke is more representative of the temperature at mid-stroke.

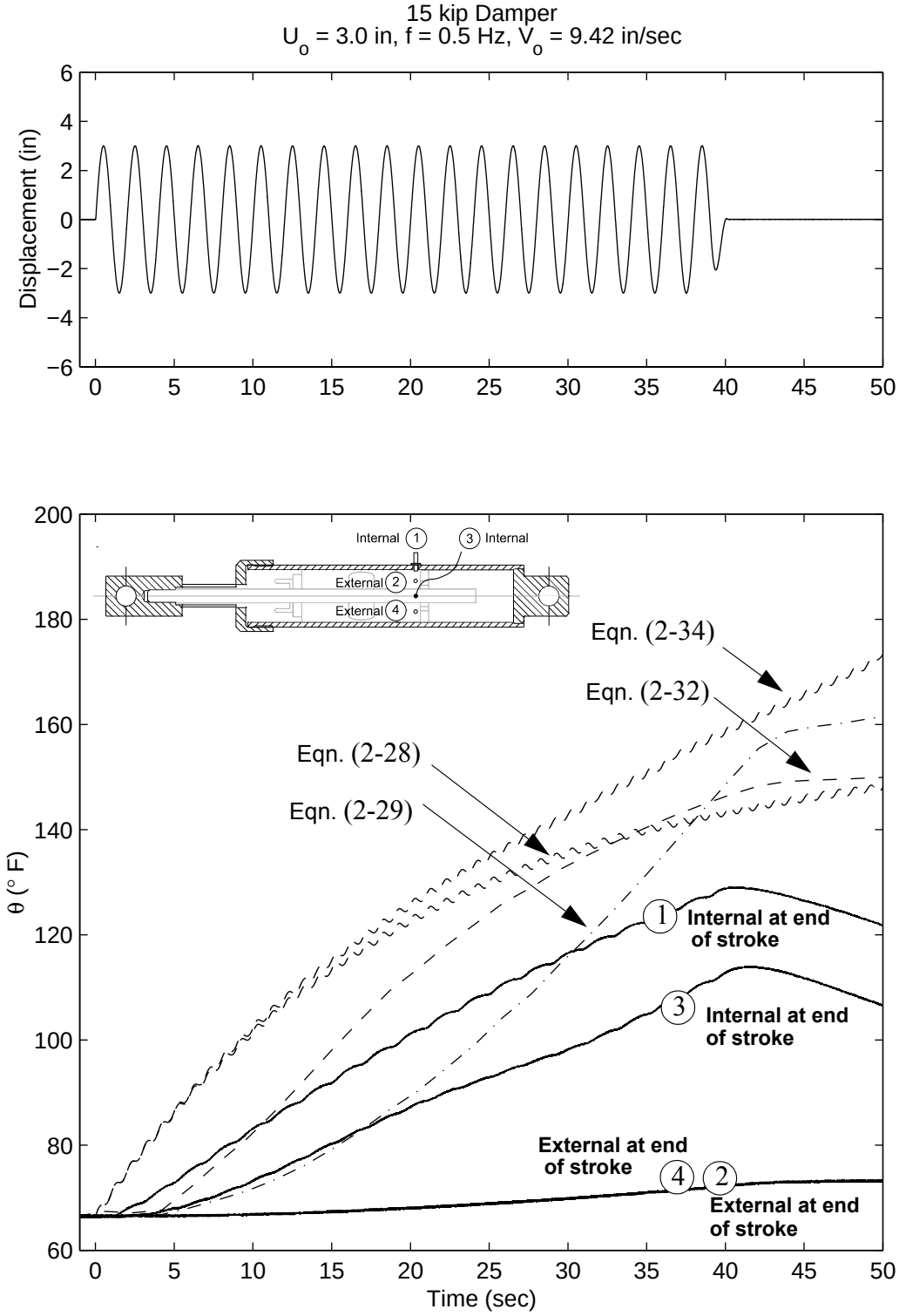

Figure 4-14. Plot showing the harmonic input with amplitude, U_o = 3.0 in. and frequency, f = 0.5 Hz imposed on the 15 kip damper (top); and a comparison of the measured temperature histories with the analytical solutions (bottom).

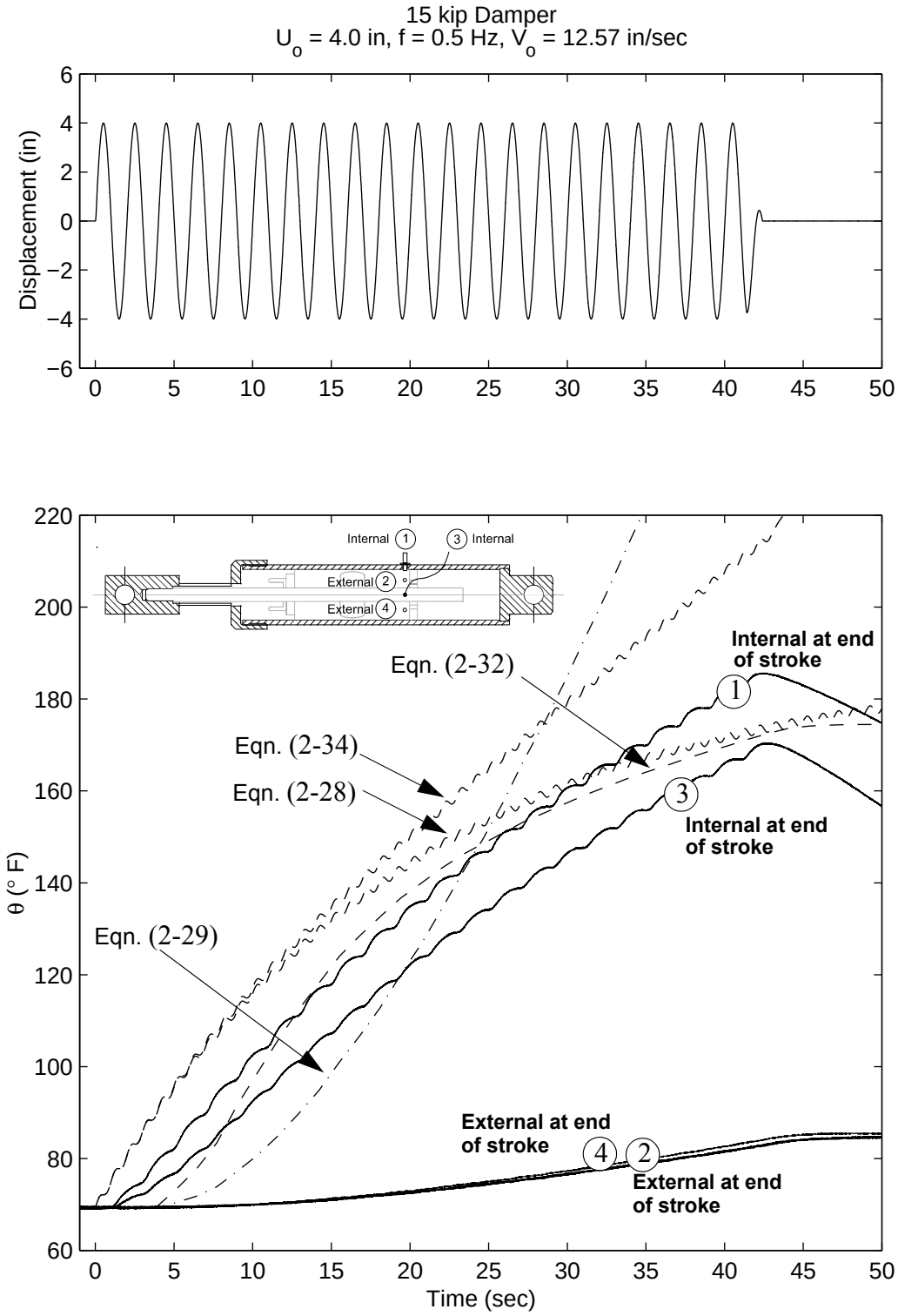

Figure 4-15. Plot showing the harmonic input with amplitude, U_o = 4.0 in. and frequency, f = 0.5 Hz imposed on the 15 kip damper (top); and a comparison of the measured temperature histories with the analytical solutions (bottom).

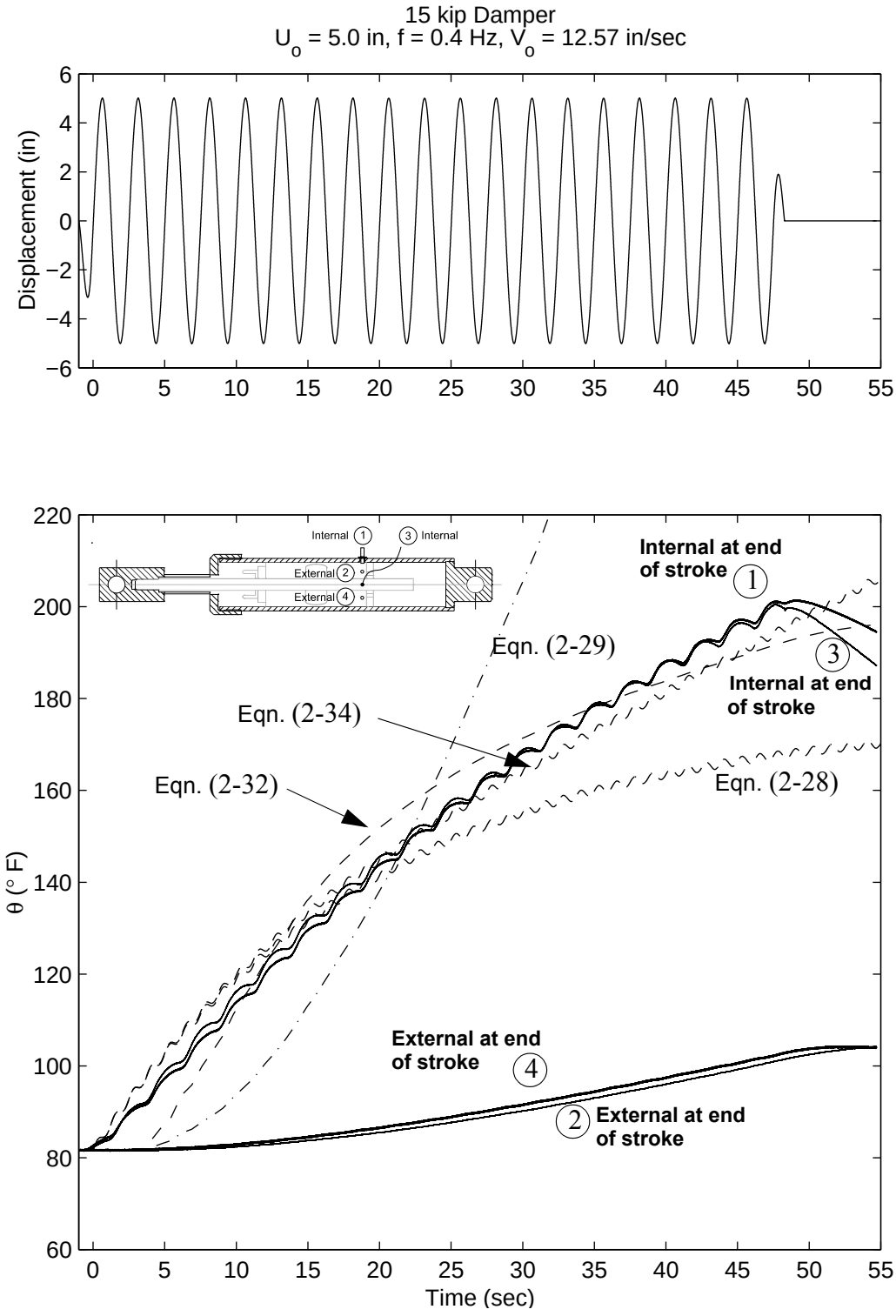

Figure 4-16. Plot showing the harmonic input with amplitude, U_o = 5.0 in. and frequency, f = 0.4Hz imposed on the 15 kip damper (top); and a comparison of the measured temperature histories with the analytical solutions (bottom).

The nonlinear prediction of the internal temperature given external readings (Equation (2-32)) is shown to predict the internal temperature for the higher amplitude tests (± 4.0 and ± 5.0 in.) with fidelity. In all tests, the nonlinear estimation is a far better approximation than the linear solution given by Equation (2-29) which does not capture the decreasing rate of temperature rise at longer durations.

4.3 COMPONENT TESTING OF THE 250 KIP DAMPER

The 250 kip damper considered in this study was originally one of two spare dampers provided for the 91/I5 overpass in the Los Angeles area (shown in Figure 4-17). The overpass uses a total of eight dampers, four at each end, to dissipate energy and control the displacement of the bridge deck during a seismic event. A photo showing the installation of four dampers at the south end of the overpass is shown in Figure 4-18. The seismic response of the 91/I5 overpass has been studied by Zhang and Makris (2002).

The 250 kip damper has a mid-stroke length of 72 in., and a maximum stroke of ± 8 in. Unlike the 3 and 15 kip dampers, the 250 kip damper has been designed to deliver the nonlinear force-velocity relation $P(t) = C|\dot{u}(t)|^{\alpha} sgn[\dot{u}(t)]$, where $C = 965.2\,\text{kN(sec/m)}^{\alpha} = 60\,\text{kip(sec/in)}^{\alpha}$ with $\alpha = 0.35$.

4.3.1 Experimental Setup

Experimental testing of the 250 kip damper was conducted at the Earthquake Engineering Research Center at the University of California, Berkeley in the spring of 2003. The setup comprises a self-equilibrating reaction frame, a 300 kip trunnion-mounted actuator with a stroke of ± 12 in. and a 1000 gpm servo-valve.

Figure 4-17. Photo showing the 91/I5 overpass located in the greater Los Angeles area. The overpass has four 250 kip dampers installed at each end. Photo taken looking south on I-5.

Figure 4-18. Photo showing four dampers installed at the south end of the 91/I5 overpass.

Similar to the 15 kip damper, the 250 kip damper was initially instrumented with thermocouple probes at the end of the stroke. Preliminary tests of the damper however, indicated that the temperature measured at this location was not representative of the temperature at mid-stroke and thus four additional internal thermocouple probes were installed — two at mid-stroke and two at +4.5 in. (approximately halfway between mid- and end-of-stroke locations). In order to position the thermocouples at these locations, the outer tube seen in Figure 4-18 had to be removed as shown in Figure 4-20. Although the outer tube plays an important role in providing increased out-of-plane rigidity, as well as, protecting the piston rod from damage, it was determined that given the laboratory setting and the level of loads likely to be imposed during testing, that the outer tube could be temporarily removed in order to make possible the temperature readings.

Figures 4-21 and 4-22 show a detailed photo of one row of thermocouples and a schematic of the thermocouple locations, respectively. The thermocouples labelled by the circled 1 through 6 are internal thermocouple probes. Thermocouples 1 and 4 are at the mid-stroke location (separated by $90°$ in the radial direction), thermocouples 2 and 5 are at +4.5 in., and thermocouples 3 and 6 are at the end of the stroke location (+8 in.). The thermocouples labelled by the circled 7 through 12 are external thermocouples located at roughly the same locations as the internal thermocouples, with 7 and 10 at mid-stroke, 8 and 11 at +4.5 in., and thermocouples 9 and 12 at the end of the stroke (+8 in.).

4.3.2 Experimental Results

A comprehensive testing program was established for the 250 kip damper in order to characterize its performance and study the force-temperature relationship of the damper. Experimental tests at four different amplitudes (4, 5, 6 and 7 inches) were performed at four different velocities (10,

Figure 4-19. Damper testing machine at the Earthquake Engineering Research Center at the University of California, Berkeley. The damper shown has a mid-stroke length of 120 inches and a force output of 450 kips at a design piston velocity of 85 in/sec.

Figure 4-20. Experimental setup for testing the 250 kip damper from the 91/I5 overpass.

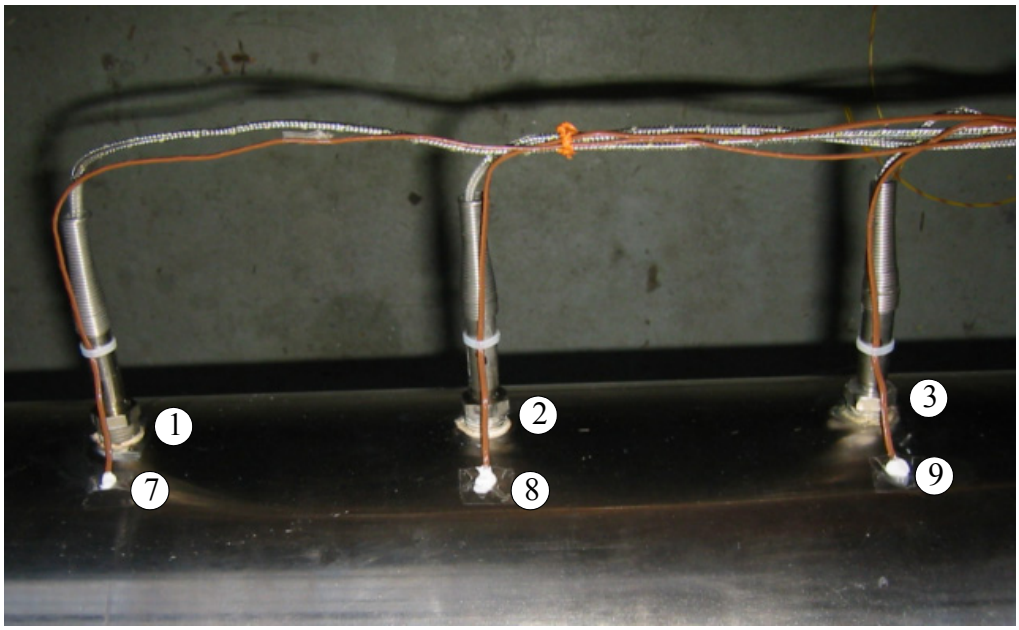

Figure 4-21. Close-up showing one row of internal thermocouple probes and one row of external thermocouples.

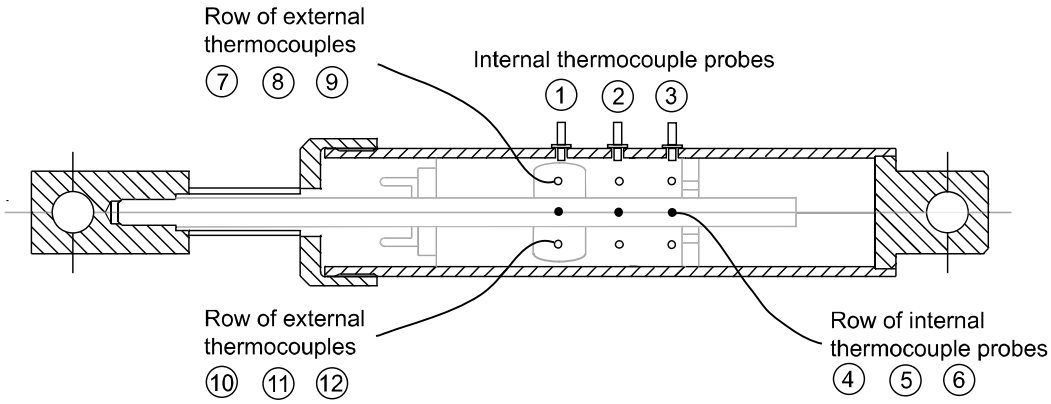

Figure 4-22. Schematic of the fluid damper indicating the locations of the six internal thermocouple probes ((1) through (6)) and the six external thermocouples ((7) through (12)).

12.5, 15 and 17.5 in/sec). Table 4-3 presents a list of the tests performed, while the corresponding data is plotted in Figures 4-23 through 4-37. The top plot in each figure shows the input time history, while the bottom plot shows the recorded internal and external temperature histories, together with predicted temperature histories of the internal silicone fluid that undergoes shearing action. The lines with the circled numbers are the recorded temperature histories at the positions indicated on the inset damper schematic and Figure 4-22. The dashed lines labeled "Eqn. (2-28)" and "Eqn. (2-34)" are predictions of internal fluid temperature based on the approximate macroscopic energy balance formulation. The solution of the linear differential equation considering a one parameter cooling law is given by Equation (2-28); while, the solution of the nonlinear differential Equation (2-34), which incorporates the two parameter cooling law, is obtained numerically. The dashed lines labeled "Eqn. (2-29)" and "Eqn. (2-32)" are predictions of the internal fluid temperatures by reading the external temperature on the damper housing in association with the one parameter cooling law (Equation (2-29)) and the two parameter cooling law (Equation (2-32)). For the 15 and 250 kip dampers, when Newton's law of cooling is adopted, an average value of $\gamma = 0.075$ is used, whereas, when the two parameter cooling law is adopted $\gamma_o = 0.02$, and $\delta = 0.01$ (see Figure 2-4).

Figures 4-23 through 4-25 plot the results of the tests performed at a velocity amplitude of 10 in/sec. Each figure plots temperature histories from all 12 thermocouples, with a selected number of histories labelled by their corresponding thermocouple number.

Table 4-3. Experimental Tests Performed on the 250 kip Damper

Test No.	Amplitude (in)	Frequency (Hz)	Velocity (in/sec)	Duration (cycles)
1	4.0	0.398	10.0	6
2	5.0	0.318	10.0	6
3	6.0	0.265	10.0	6
4[a]	7.0	0.227	10.0	6
5	4.0	0.5	12.6	6
6	5.0	0.4	12.57	6
7	6.0	0.332	12.50	6
8	7.0	0.284	12.50	6
9	4.0	0.6	15.1	6
10	5.0	0.477	15.0	6
11	6.0	0.4	15.1	6
12	7.0	0.341	15.0	6
13	4.0	0.70	17.5	6
14	5.0	0.557	17.5	6
15	6.0	0.464	17.5	6
16	7.0	0.4	17.5	6

a. Data acquisition error resulted in no usable data file

In addition to the recorded temperature histories, the linear and nonlinear analytical prediction of the internal oil temperature, given by Equation (2-28) and the solution of Equation (2-34), as well as, the linear and nonlinear prediction of internal temperature given external readings (Equations (2-29) and (2-32), respectively), are shown for comparison. It is seen in Figures 4-23 through 4-25, that Equation (2-28) and the solution of (2-34) give roughly the same value for the internal temperature with the nonlinear solution increasing at a slightly greater rate than the linear solution. Both expressions over-estimate the internal temperature—a result that is observed for all tests performed on the 250 kip damper. The predictions of internal temperature given external temperature

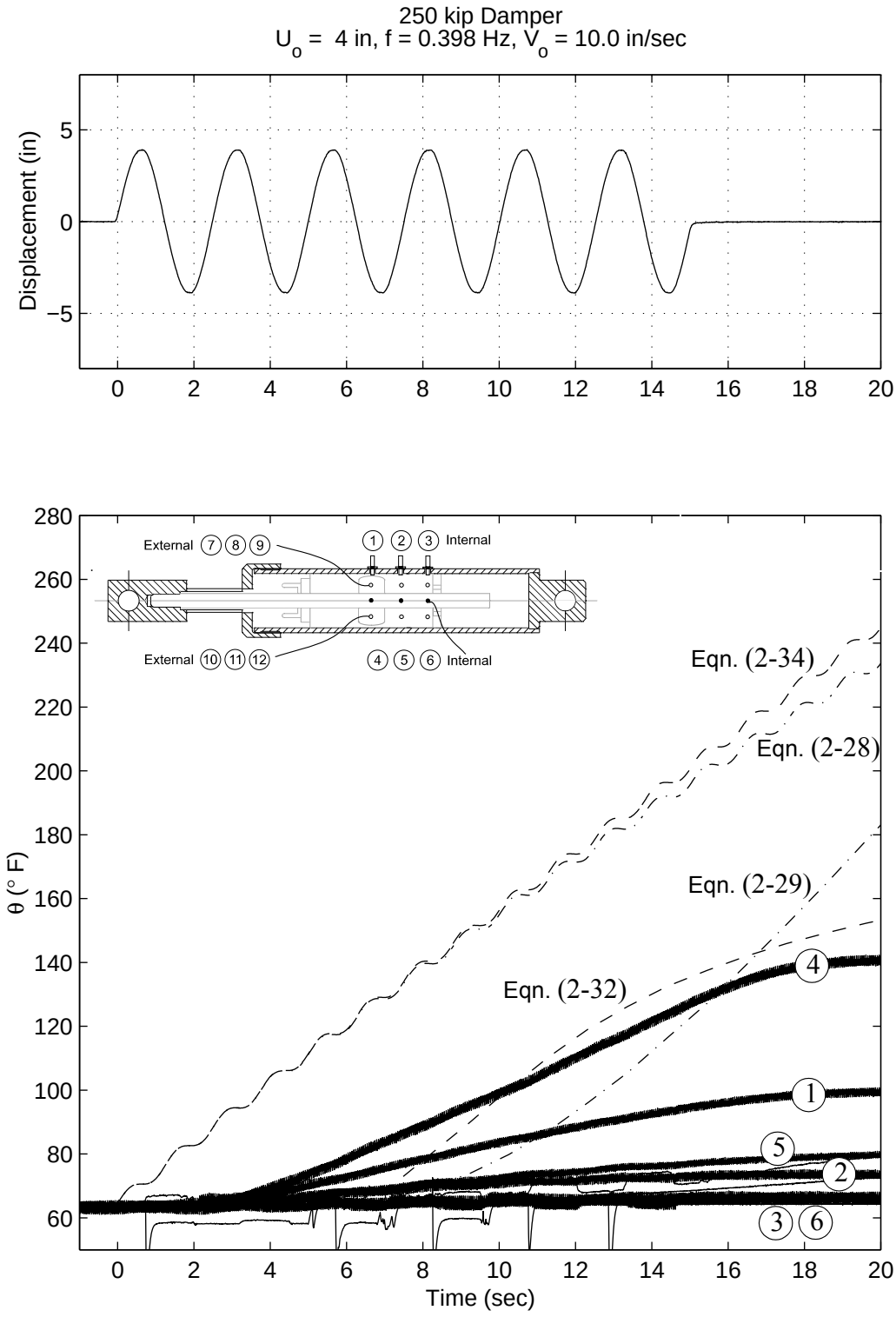

Figure 4-23. Plot showing the harmonic input with amplitude, U_o = 4.0 in. and frequency, f = 0.398 Hz imposed on the 250 kip damper (top); and a comparison of the recorded temperature histories with the analytical solutions (bottom).

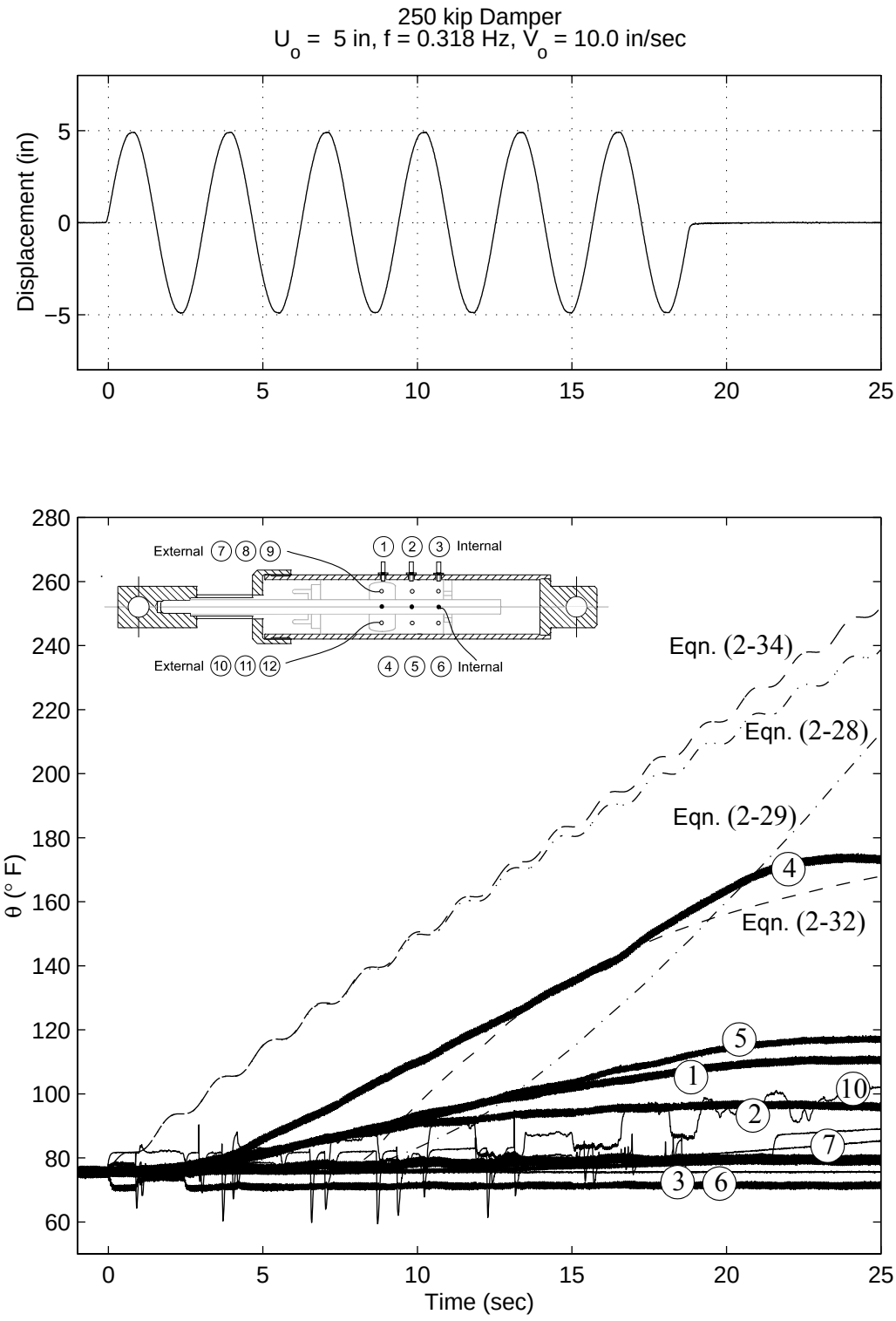

Figure 4-24. Plot showing the harmonic input with amplitude, U_o = 5.0 in. and frequency, f = 0.318 Hz imposed on the 250 kip damper (top); and a comparison of the recorded temperature histories with the analytical solutions (bottom).

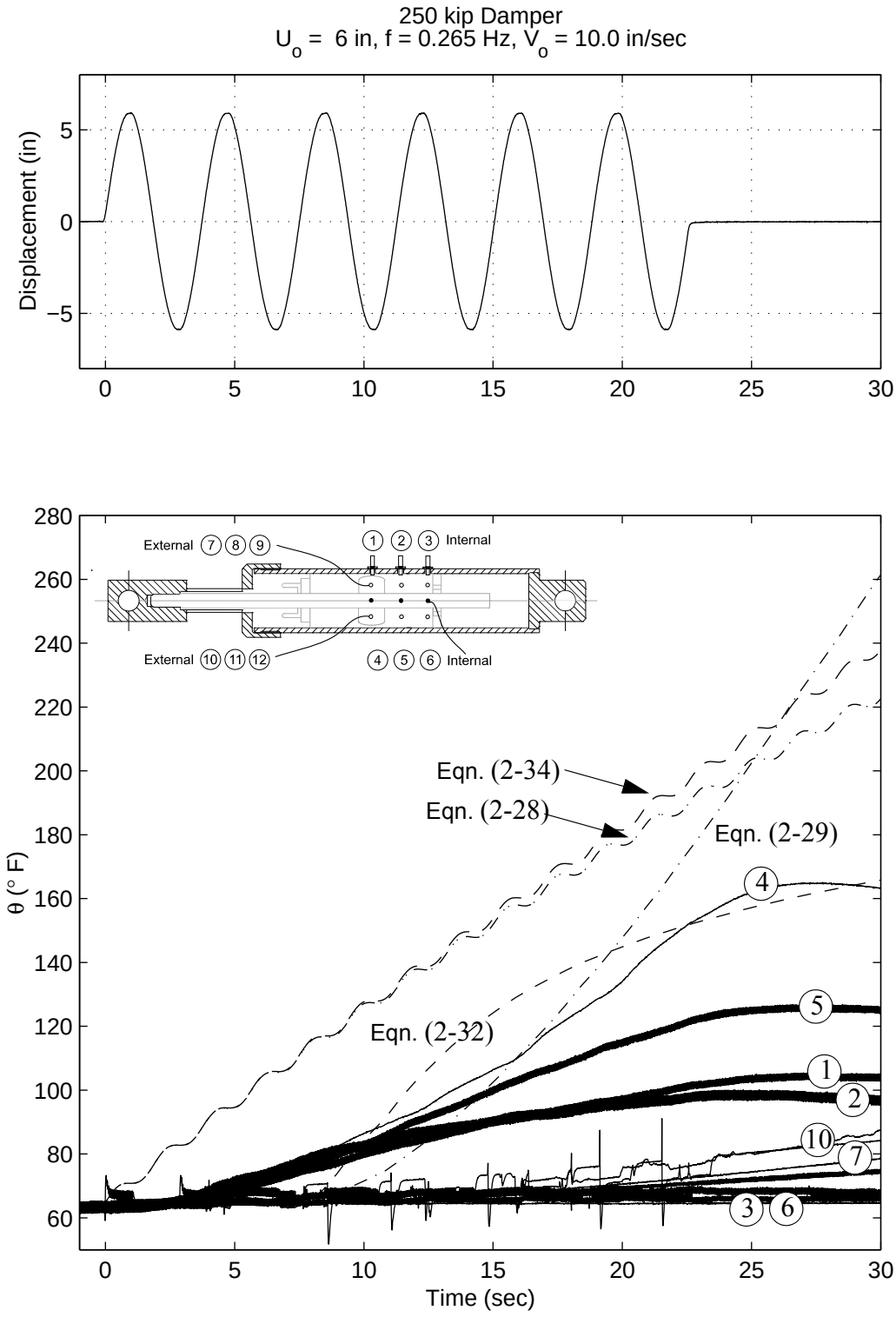

Figure 4-25. Plot showing the harmonic input with amplitude, U_o = 6.0 in. and frequency, f = 0.265 Hz imposed on the 250 kip damper (top); and a comparison of the recorded temperature histories with the analytical solutions (bottom).

result in reasonably accurate estimations of the internal oil temperature for all test performed at 10 in/sec, with the nonlinear expression matching the observed results more accurately than the linear approximation.

The non-homogeneous temperature distribution in the radial direction is clearly seen when comparing thermocouples 1 and 4 which both measure the internal temperature at the mid-stroke location. For test number 1, the difference in the two thermocouple readings is 40° F, whereas, in tests 2 and 3, the difference is in excess of 60° F. This large difference is due to internal details of the damper design (not known to the author), such as the location of the orifices in the piston head. A large variation along the length of the damper is seen by comparing one row of thermocouples. In Figure 4-25, for example, it is seen that there is roughly a 40° F temperature differential between thermocouples 4 and 5, and again between thermocouples 5 and 6, for a total temperature differential of 80° F between the mid-stroke and end-of-stroke locations. This result has important significance as it indicates that although the internal oil temperature increases substantially over a few cycles, the temperature rise at the end-of-stroke location—the location of the internal seals—is relatively small.

Figures 4-26 through 4-29 present the results of the four tests performed at a velocity amplitude of 12.5 in/sec. Similar to the tests at 10 in/sec, the recorded temperatures show a large variability both in the radial and longitudial directions. The predictions of the analytical expressions for internal temperature over-estimate the observed temperature substantially, and in general, are less accurate than the predictions for the tests conducted at 10 in/sec. The nonlinear prediction of the internal temperature given external readings (Equation (2-32)) gives very accurate results for all tests, whereas, the linear prediction (Equation (2-29)) does not. Similar to the results seen for the 15 kip

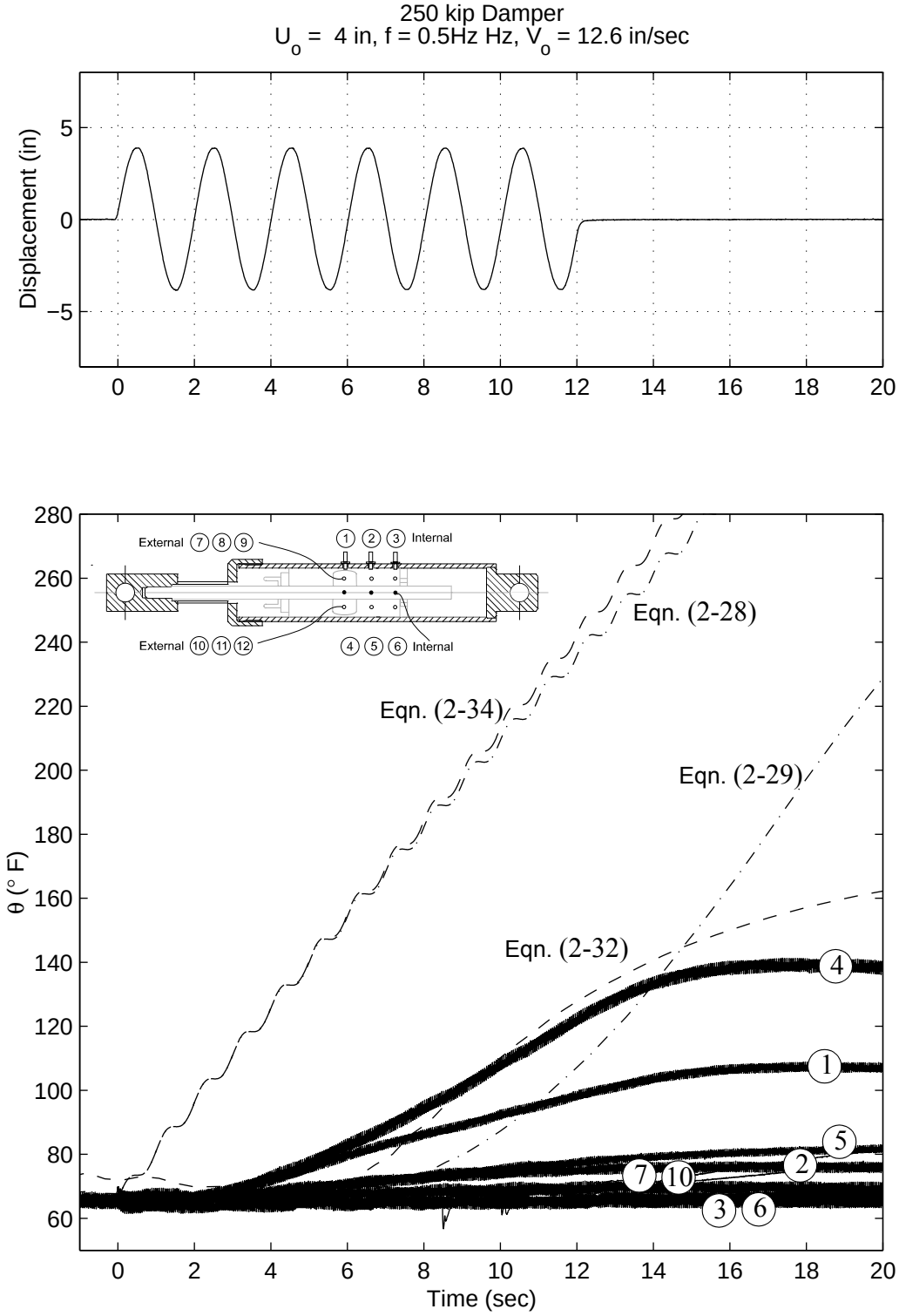

Figure 4-26. Plot showing the harmonic input with amplitude, U_o = 4.0 in. and frequency, f = 0.5 Hz imposed on the 250 kip damper (top); and a comparison of the recorded temperature histories with the analytical solutions (bottom).

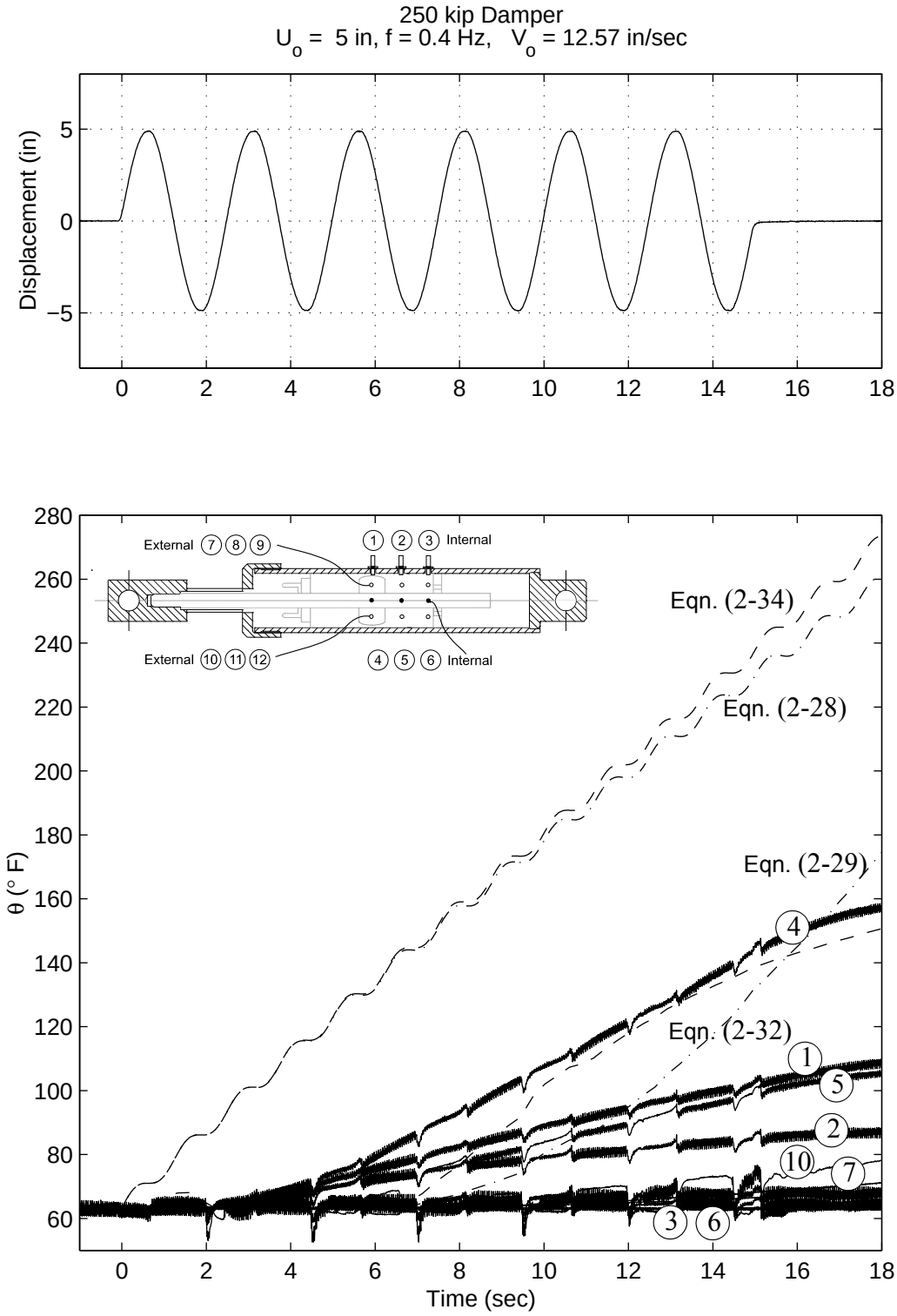

Figure 4-27. Plot showing the harmonic input with amplitude, U_o = 5.0 in. and frequency, f = 0.4 Hz imposed on the 250 kip damper (top); and a comparison of the recorded temperature histories with the analytical solutions (bottom).

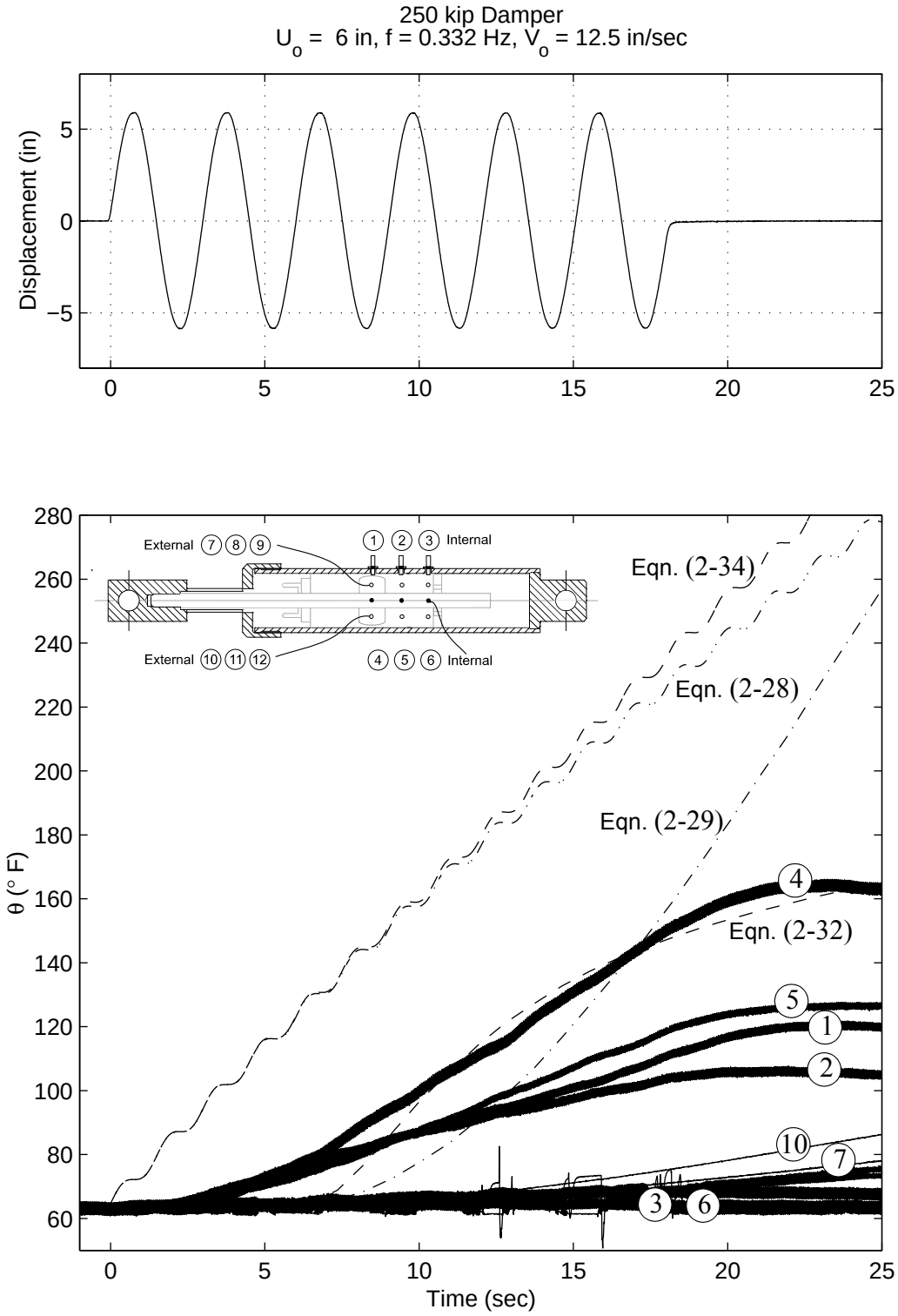

Figure 4-28. Plot showing the harmonic input with amplitude, U_o = 6.0 in. and frequency, f = 0.332 Hz imposed on the 250 kip damper (top); and a comparison of the recorded temperature histories with the analytical solutions (bottom).

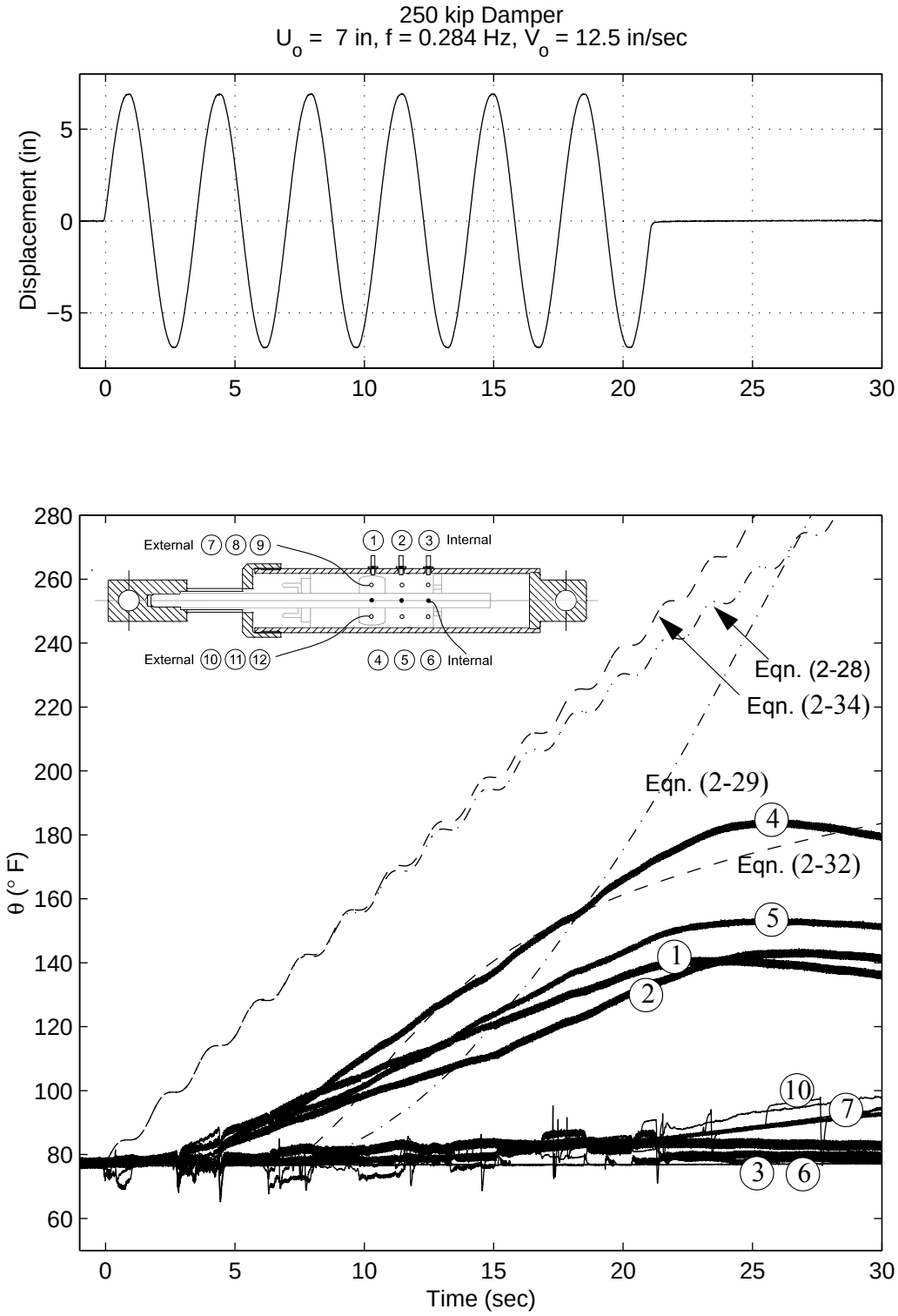

Figure 4-29. Plot showing the harmonic input with amplitude, U_o = 7.0 in. and frequency, f = 0.284 Hz imposed on the 250 kip damper (top); and a comparison of the recorded temperature histories with the analytical solutions (bottom).

damper, the linear expression does not accurately represent the observed decrease in the rate of temperature rise for higher temperatures (longer durations).

Figures 4-30 through 4-33 plot the results of the 15 in/sec tests (tests 9 through 12). Similar to the previous results for the 250 kip damper, the analytical solutions for the internal temperature over-estimates the observed internal temperatures, with maximum values in this case being in excess of $150°$ F greater than the observed internal temperature. In contrast, the predictions of the internal temperature given external readings remain reasonably accurate, with the nonlinear expression (Equation (2-32)) providing better estimates of internal temperature than the linear expression.

Finally, Figures 4-34 through 4-37 present results from the tests conducted at a velocity amplitude of 17.5 in/sec. The analytical expression over-estimate the temperature while the nonlinear prediction of the internal temperature from external readings gives reasonably accurate results — within roughly $20°$ F of the observed internal temperature.

4.3.3 Conclusions - 250 kip Damper

In general, the tests conducted on the 250 kip damper, show that the internal temperature is not radially symmetric and that although the internal oil temperature at the mid-stroke location increases substantially over a few cycles (upwards of $100°$ F), the temperature rise at the end-of-stroke location—the location of the internal seals—is relatively small. More specifically, the temperature increase at the mid-stroke location is an order of magnitude (if not two) greater than that at the end of the stroke. This observation is presented graphically in Figure 4-38 which shows the temperature increase along the length of the damper for a typical test.

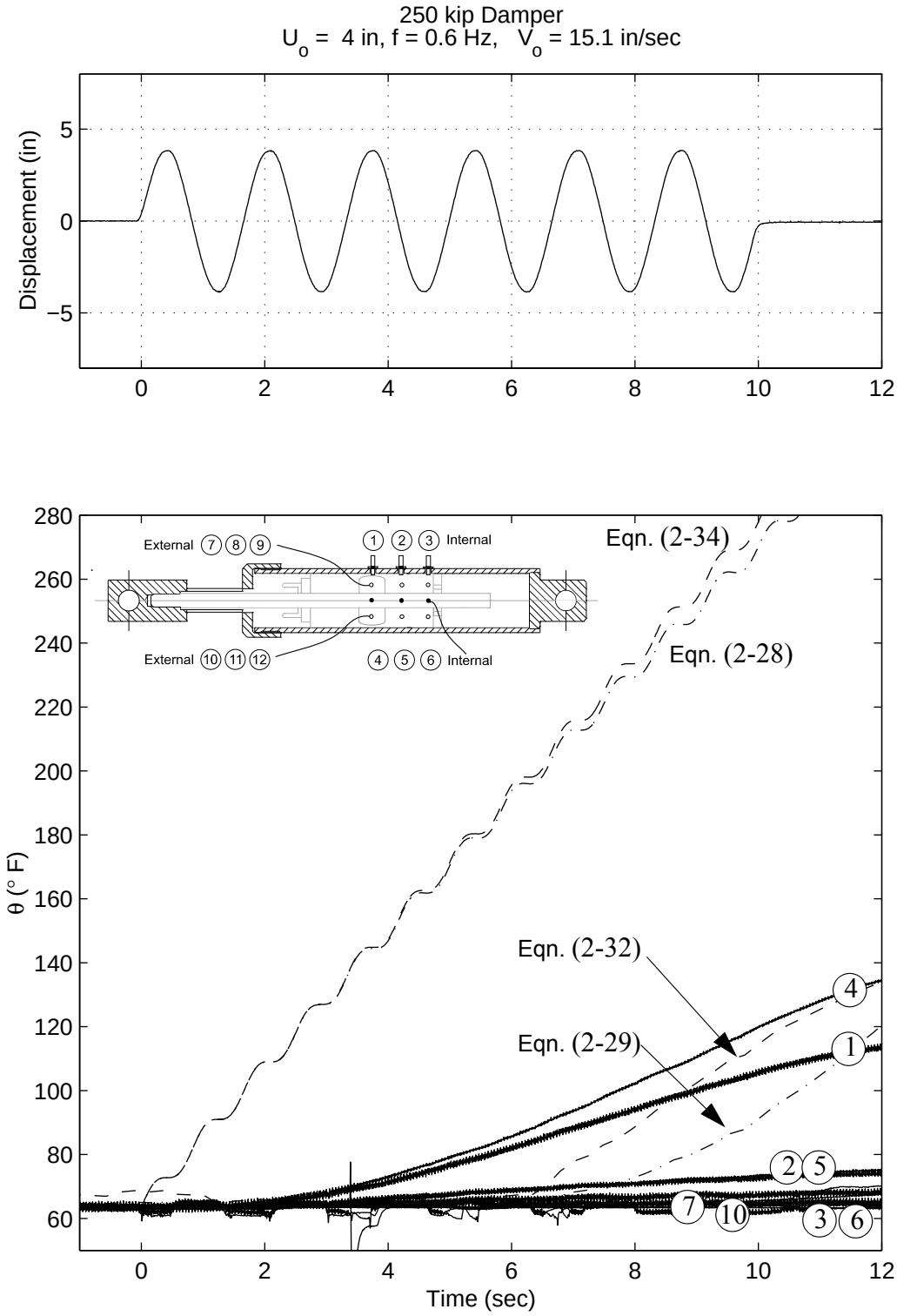

Figure 4-30. Plot showing the harmonic input with amplitude, U_o = 4.0 in. and frequency, f = 0.6 Hz imposed on the 250 kip damper (top); and a comparison of the recorded temperature histories with the analytical solutions (bottom).

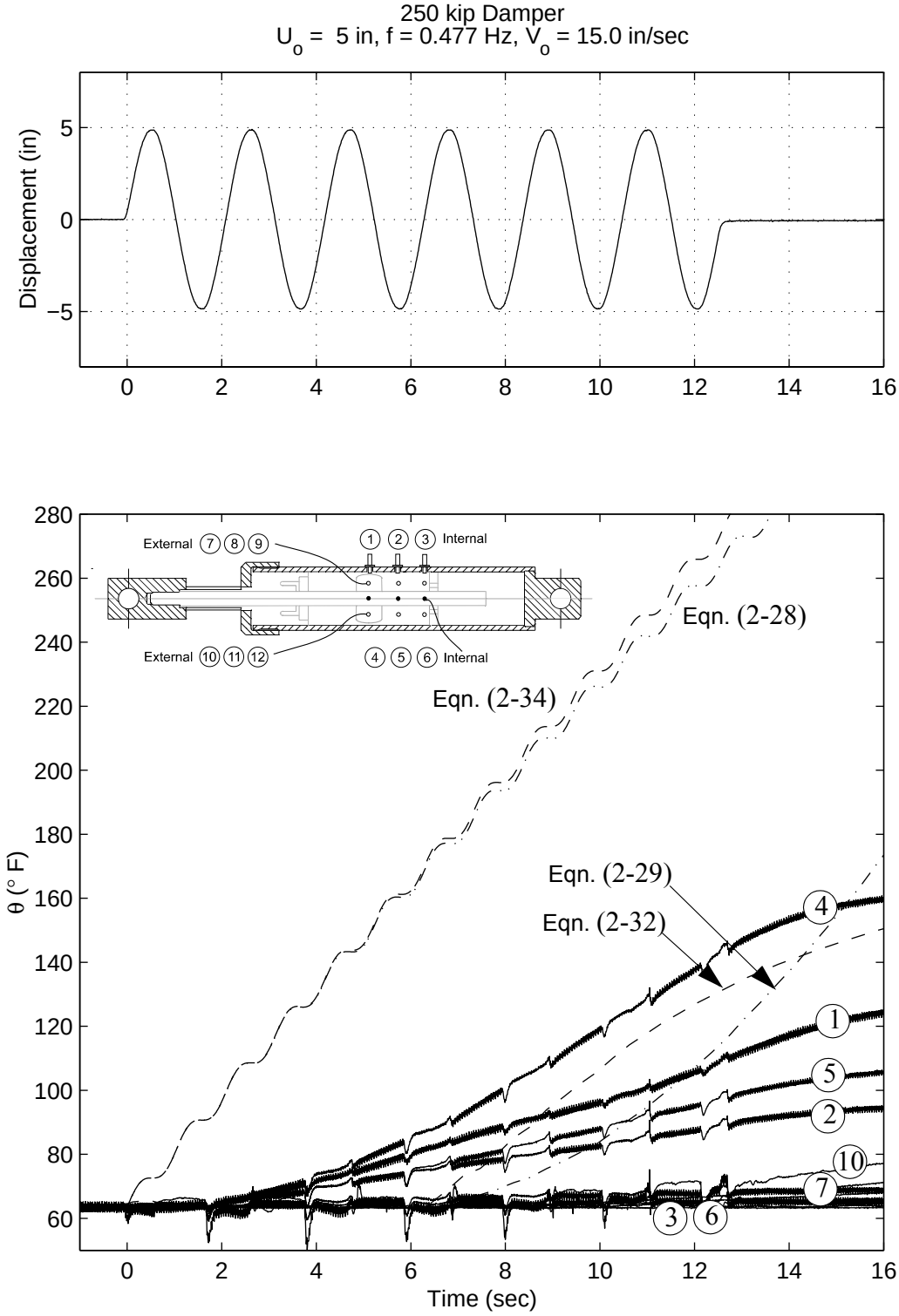

Figure 4-31. Plot showing the harmonic input with amplitude, U_o = 5.0 in. and frequency, f = 0.477 Hz imposed on the 250 kip damper (top); and a comparison of the recorded temperature histories with the analytical solutions (bottom).

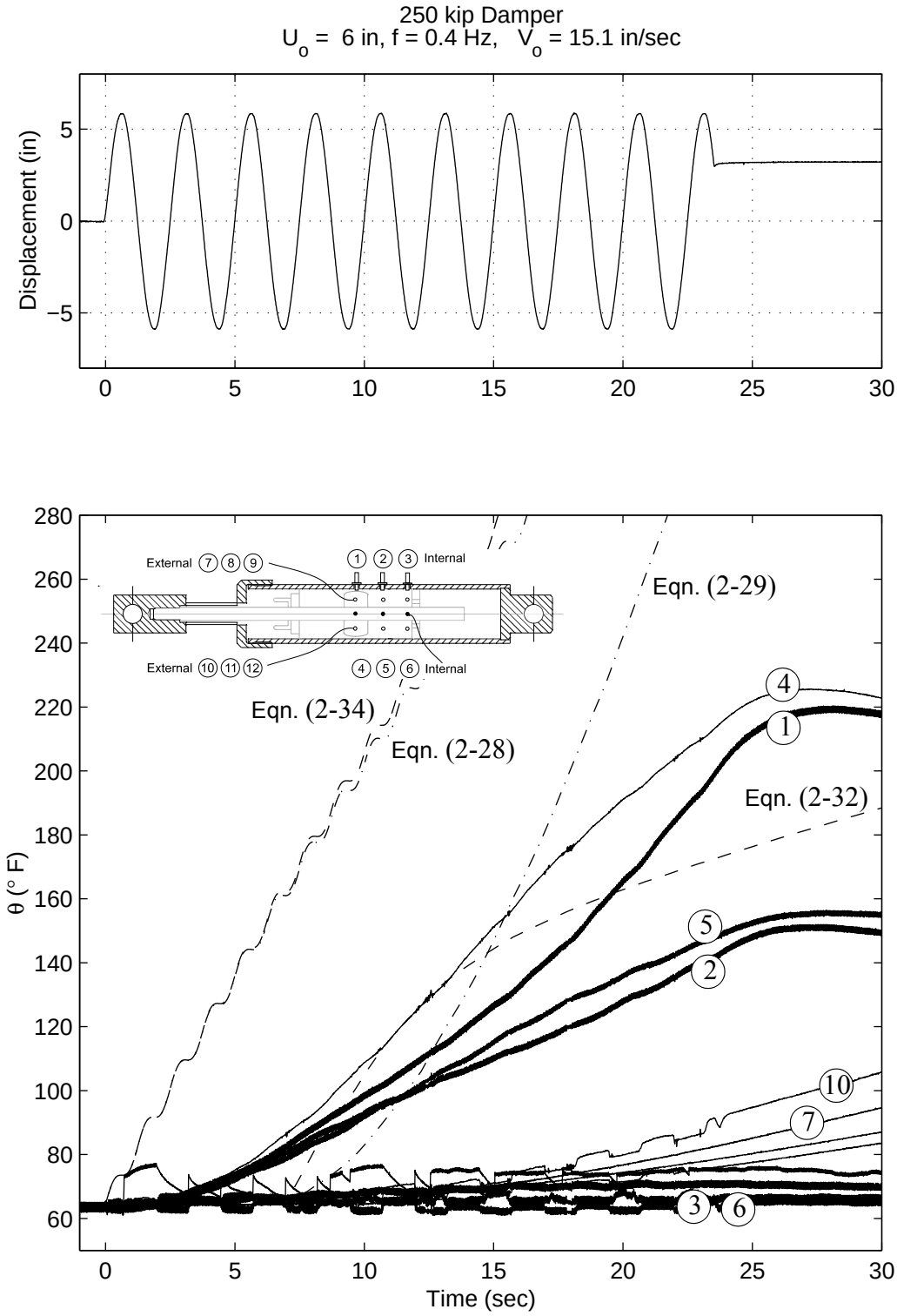

Figure 4-32. Plot showing the harmonic input with amplitude, U_o = 6.0 in. and frequency, f = 0.4 Hz imposed on the 250 kip damper (top); and a comparison of the recorded temperature histories with the analytical solutions (bottom).

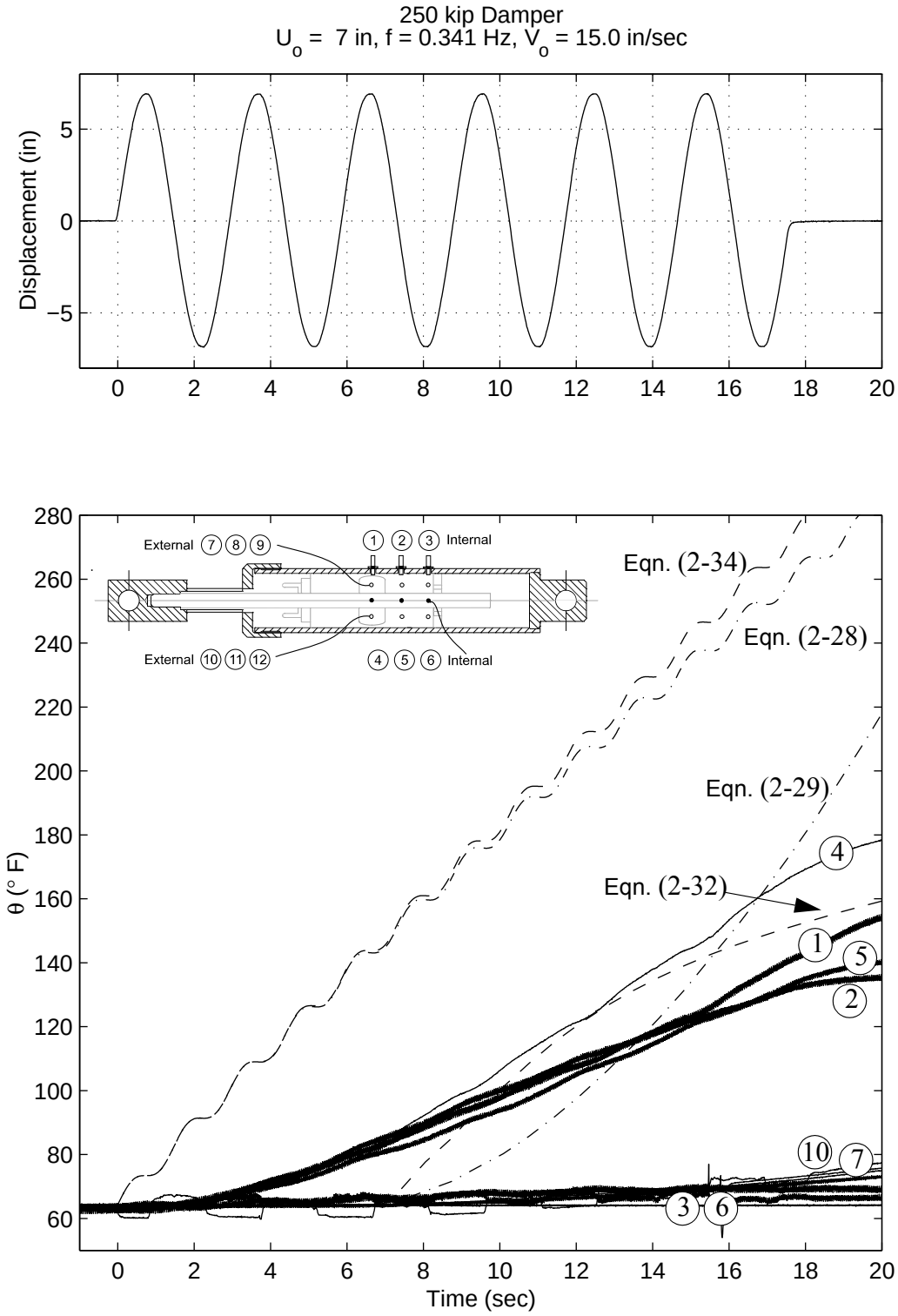

Figure 4-33. Plot showing the harmonic input with amplitude, U_o = 7.0 in. and frequency, f = 0.341 Hz imposed on the 250 kip damper (top); and a comparison of the recorded temperature histories with the analytical solutions (bottom).

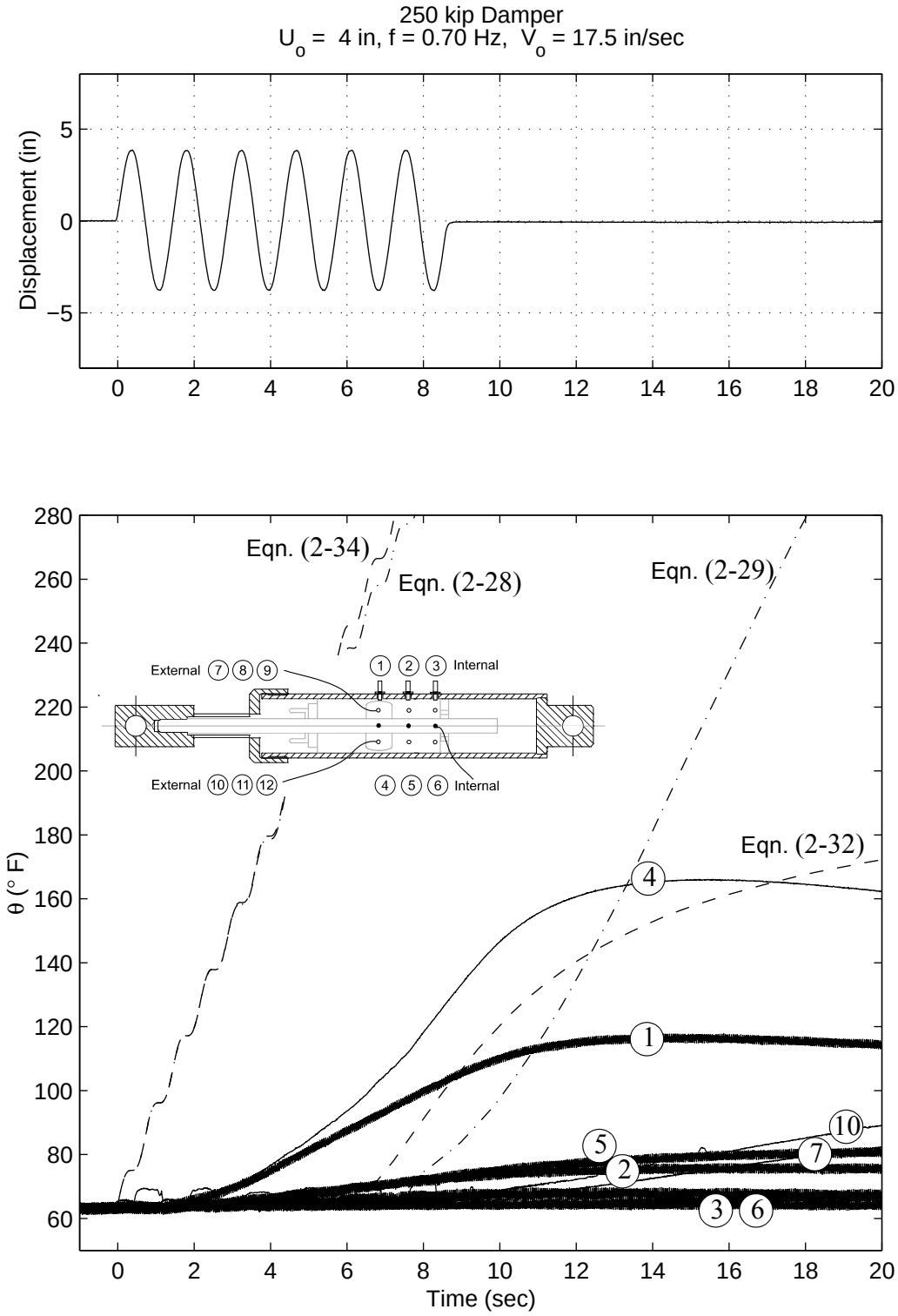

Figure 4-34. Plot showing the harmonic input with amplitude, U_o = 4.0 in. and frequency, f = 0.7 Hz imposed on the 250 kip damper (top); and a comparison of the recorded temperature histories with the analytical solutions (bottom).

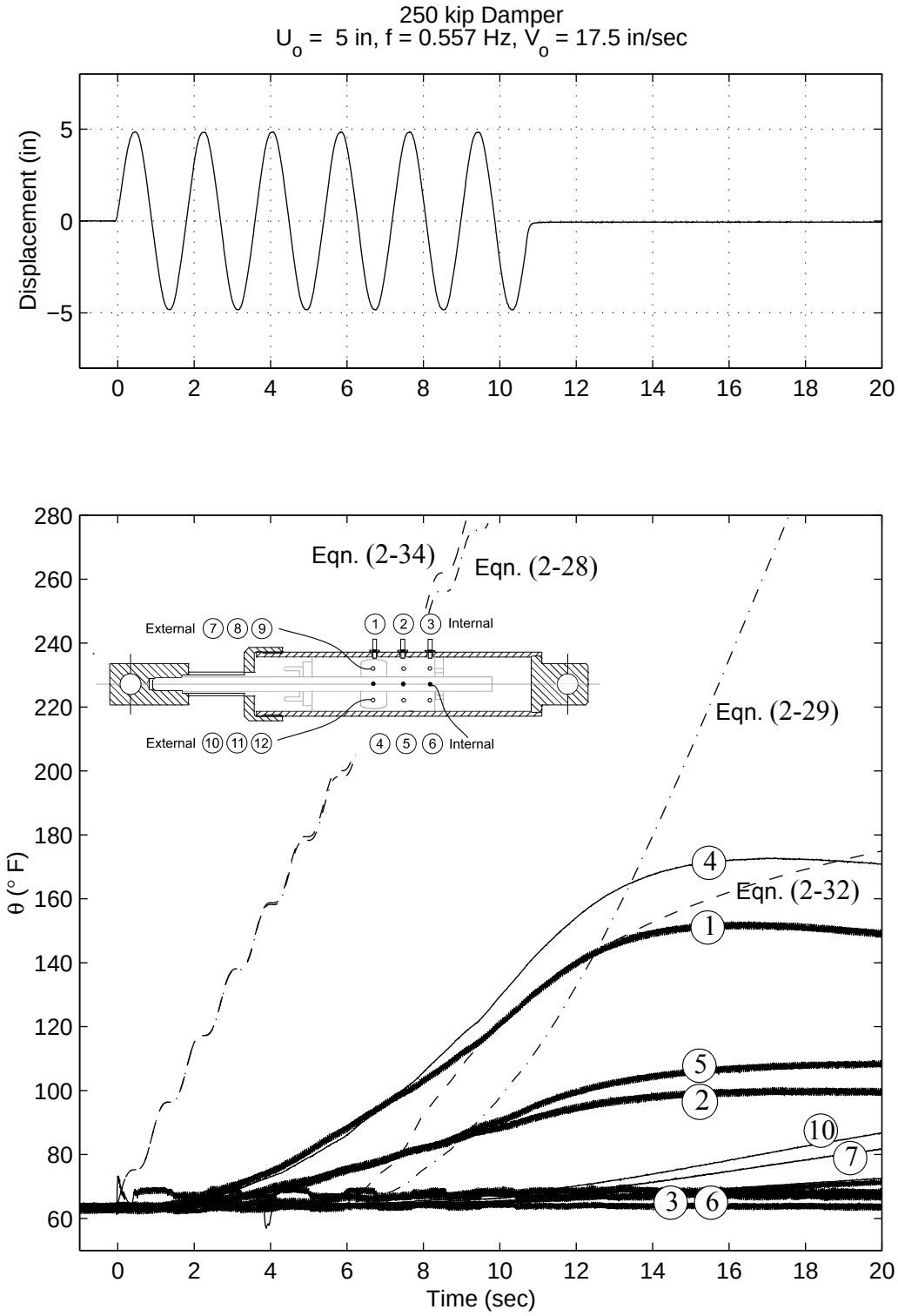

Figure 4-35. Plot showing the harmonic input with amplitude, U_o = 5.0 in. and frequency, f = 0.557 Hz imposed on the 250 kip damper (top); and a comparison of the recorded temperature histories with the analytical solutions (bottom).

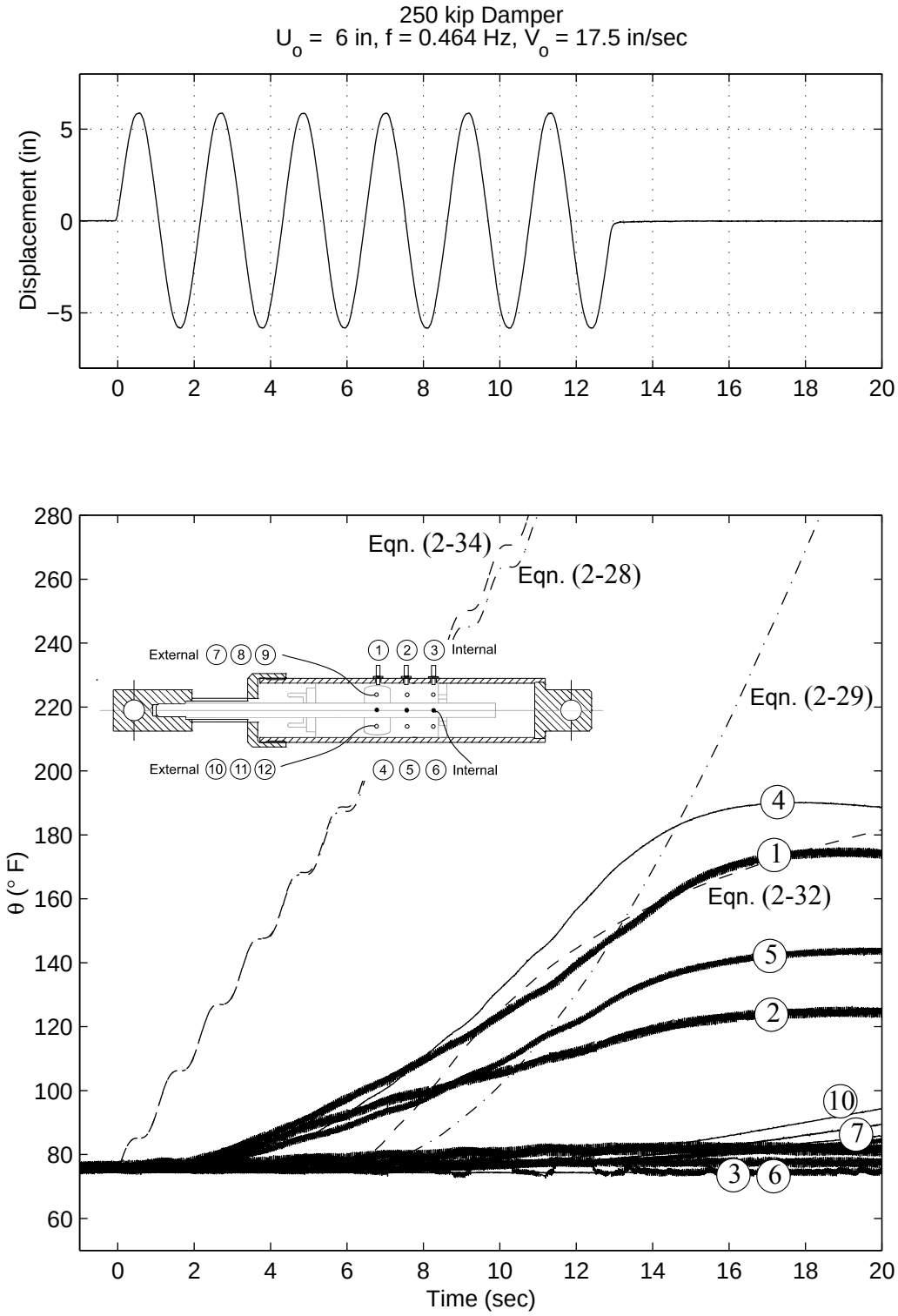

Figure 4-36. Plot showing the harmonic input with amplitude, U_o = 6.0 in. and frequency, f = 0.464 Hz imposed on the 250 kip damper (top); and a comparison of the recorded temperature histories with the analytical solutions (bottom).

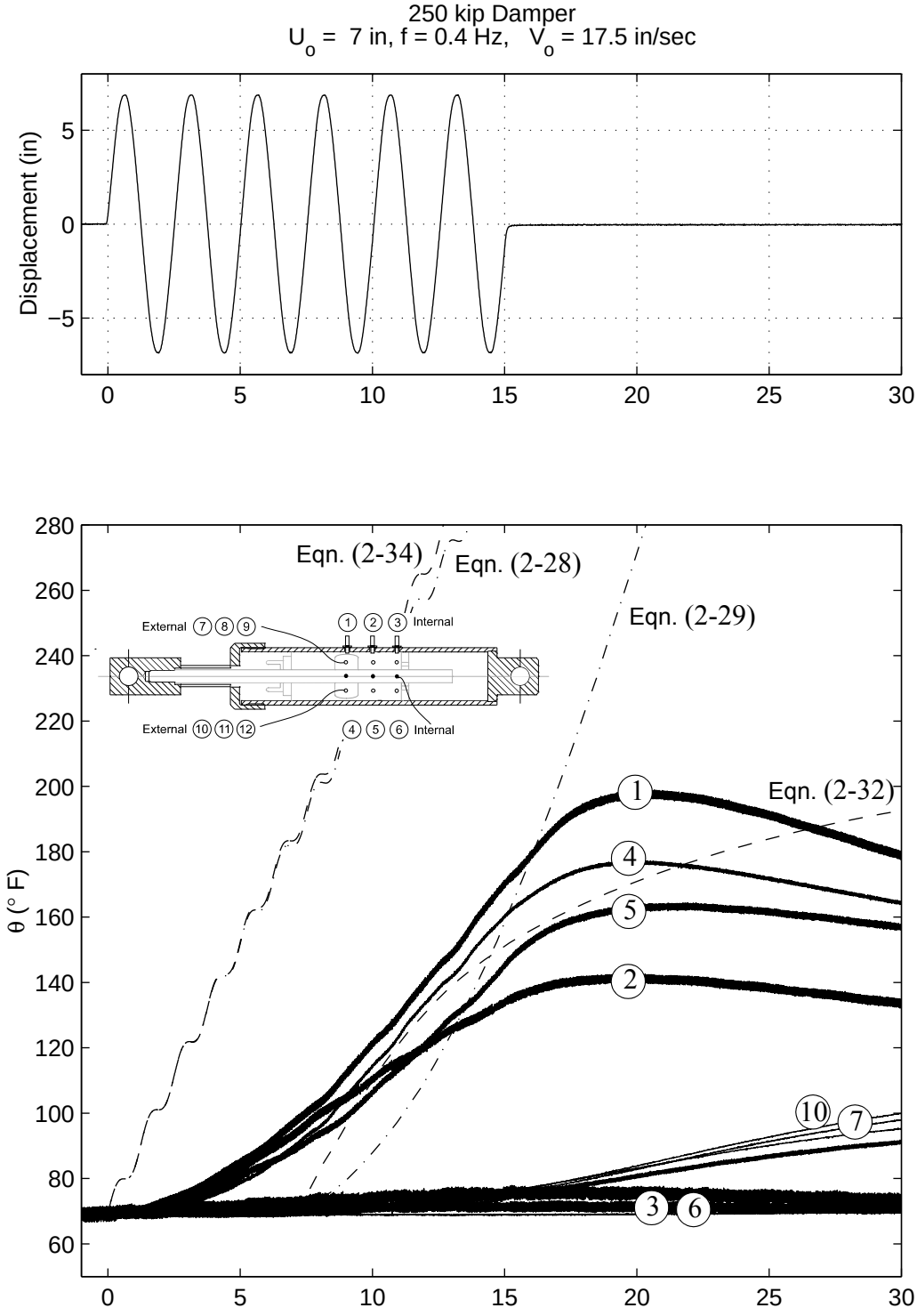

Figure 4-37. Plot showing the harmonic input with amplitude, U_o = 7.0 in. and frequency, f = 0.4 Hz imposed on the 250 kip damper (top); and a comparison of the recorded temperature histories with the analytical solutions (bottom).

The linear and nonlinear analytical expressions for internal temperature given by Equation (2-28) and the solution of Equation (2-34), respectively, over-estimate the observed temperature by a large margin for the 250 kip damper. The expressions most accurately represent the internal temperature for the low-velocity, large-amplitude (low-frequency) tests and move farther from the observed values as the testing velocity increases.

The poor prediction of the analytical expressions for the temperature rise of the internal fluid originates from the assumption that the energy input in the macroscopic energy balance equation involves a constant localized source of heat which approximates the energy input by the piston head. Large fluid dampers have massive piston heads that absorb appreciable energy before the surrounding fluid heats uniformly. This heat capacity is not accounted for in the macroscopic energy balance equation and thus it gives better results for the smaller dampers which have less massive piston heads. The time required to heat the piston head is evidenced by the lag time between the experimental and analytical results. Eventually, under repeated cycling this macroscopic energy balance equation would reasonably predict the temperature rise, however, this involves a large number of cycles that is not characteristic for damper motions under strong earthquakes which usually involve two to five strong cycles.

The linear and nonlinear expressions for the internal fluid temperature when external temperature readings on the damper housing are available, give a much better approximation than the analytical expressions. The linear expression (Equation (2-29)) gives reasonably accurate predictions but typically fails to capture the trend of the decreasing rate of temperature rise at higher temperatures (longer durations). The nonlinear expression (Equation (2-32)), which makes use of the two parameter cooling law gives an accurate prediction of the internal temperature in all tests. For most tests,

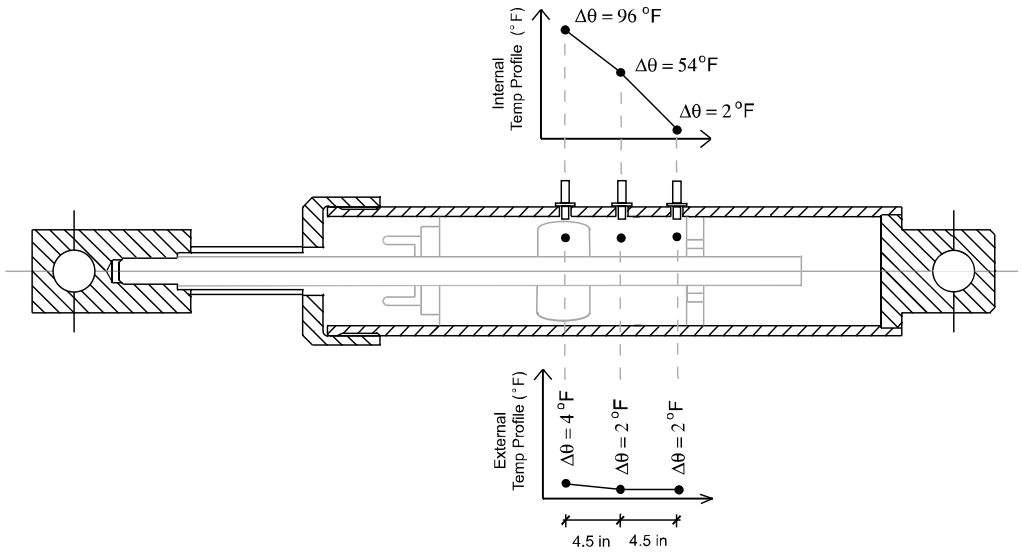

Figure 4-38. Temperature rise at end of 6 cycles along the length of the damper for test number 15, (U_o = 6 in., v_o = 17.5 in/sec), showing the large internal temperature differential between the mid-stroke and end-of-stroke locations (top) and small external temperature differential (bottom).

the estimation of Equation (2-32) is within a few degrees of the observed internal temperature and at most underestimates the internal temperature by roughly 20° F.

5 CHARACTERIZATION OF DAMPER BEHAVIOR

5.1 MACROSCOPIC MODELLING OF FORCE-VELOCITY RELATION

A power-law force-velocity behavior for viscous damping, $P(t) \propto |\dot{u}(t)|^{\alpha}$, was originally proposed in the 1920's. Jacobsen (1930) states that experimental records of free vibrations of damped structures can be accurately modelled empirically using combinations of constant friction ($\alpha = 0$), viscous friction (friction proportional to first power of velocity ($\alpha = 1$) and friction proportional to the nth power of velocity ($\alpha = n$).

Orificed fluid dampers designed for structural application utilize a series of specially designed passages to alter flow characteristics. The orifice configuration is usually designed to achieve a specified α value in the power-law force-velocity relationship $P(t) \propto |\dot{u}(t)|^{\alpha}$. It is well established that viscous fluid dampers that find applications in civil structures can therefore be suitably modeled by the nonlinear force-velocity relation

$$P(t) = C|\dot{u}(t)|^{\alpha} sgn[\dot{u}(t)] , \tag{5-1}$$

where $P(t)$ = piston force, $\dot{u}(t)$ = piston velocity, α = a predetermined fractional exponent ($0 < \alpha \leq 1$), C = a damping constant with dimension $(force) \cdot (time/length)^{\alpha}$ and $sgn[\ ]$ is the signum function. When $\alpha = 1$ Equation (5-1) reduces to the linear, purely viscous case

$$P(t) = C\dot{u}(t) , \tag{5-2}$$

which is often desirable for seismic applications as the force is near zero in the region of maximum deformation (zero velocity).

Figure 5-1 (top) presents a comparison between a typical hysteresis loop recorded during testing of the 3 kip damper and the force-velocity relationship given by Equation (5-2). For this figure, the velocity in Equation (5-2) is obtained by differentiating the recorded displacement, and the damping coefficient, C, was determined by fitting a straight line on the plot of peak force output versus peak stroke velocity for all tests. From Figure 5-1 (bottom), which plots the average peak force from the first three cycles against the peak velocity, it is seen that the damping coefficient for the 3 kip damper is 0.101 kip sec/in (17.69 kN sec/m).

Figure 5-2 presents a comparison between a recorded hysteresis loop for one of the tests conducted on the 15 kip damper and the prediction of Equation (5-2) with $C = 0.696$ kip sec/in (121.8 kN sec/m). This value for the damping coefficient was determined from the results of all tests as shown in Figure 5-2 (bottom).

Unlike the 3 and 15 kip dampers, the 250 kip damper was designed to give the nonlinear force-deformation behavior

$$P(t) = C|\dot{u}(t)|^{\alpha} sgn[\dot{u}(t)] \tag{5-3}$$

where $C = 60$ kip $(\text{sec/in})^{\alpha}$ ($C = 965.2$ kN $(\text{sec/m})^{\alpha}$), and $\alpha = 0.35$. Figure 5-3 (top) presents a comparison between a hysteresis loop for one of the 250 kip damper tests and the force-velocity relationship given by Equation (5-3). The value for the damping coefficient was determined by fitting the line $P(t) = C[v(t)]^{\alpha}$ to the experimental data as shown in Figure 5-3 (bottom).

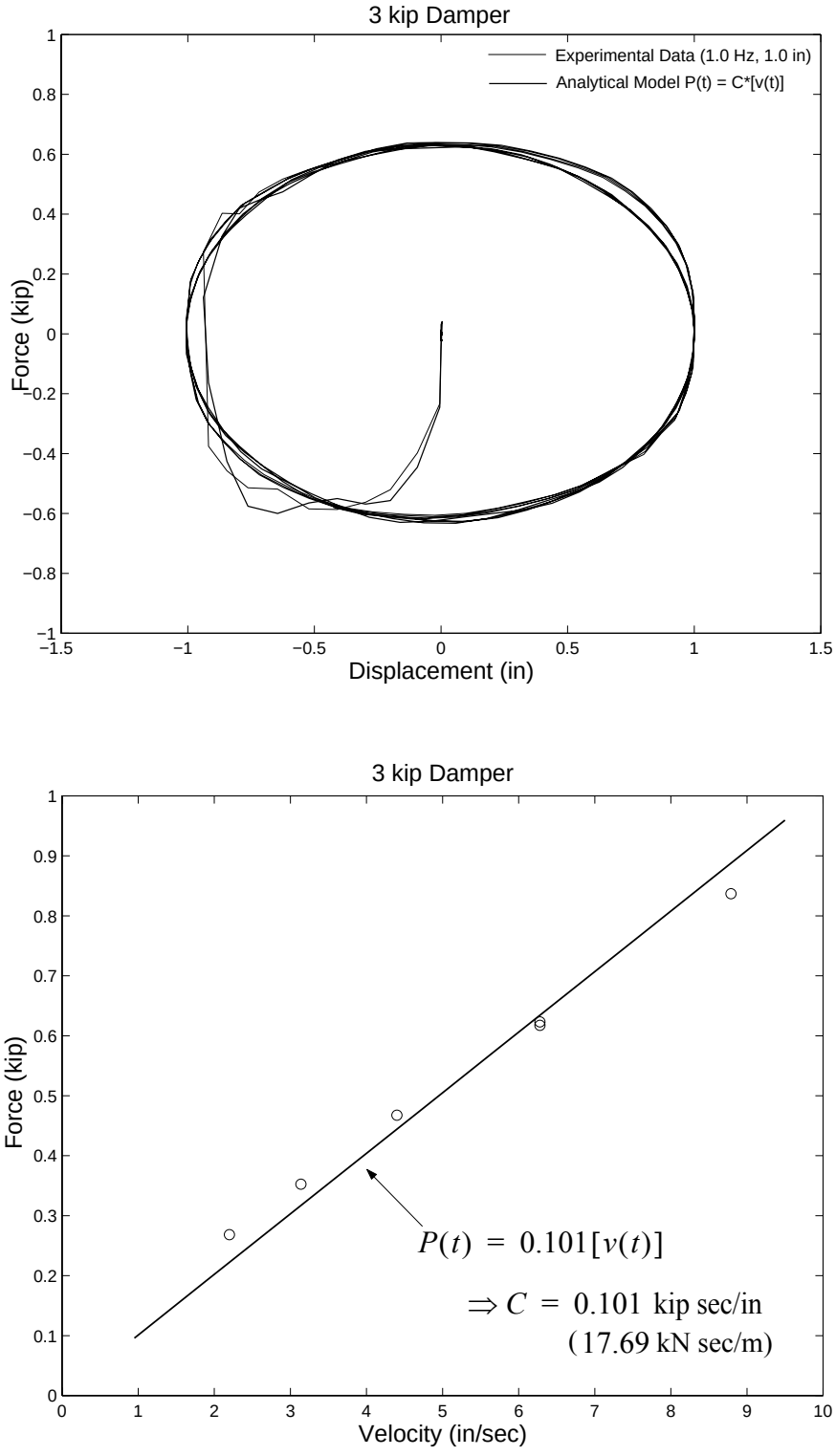

Figure 5-1. Comparison of recorded and predicted hysteresis loop for the 3 kip damper (top), and the determination of the damping coefficient from experimental data for the 3 kip damper (bottom).

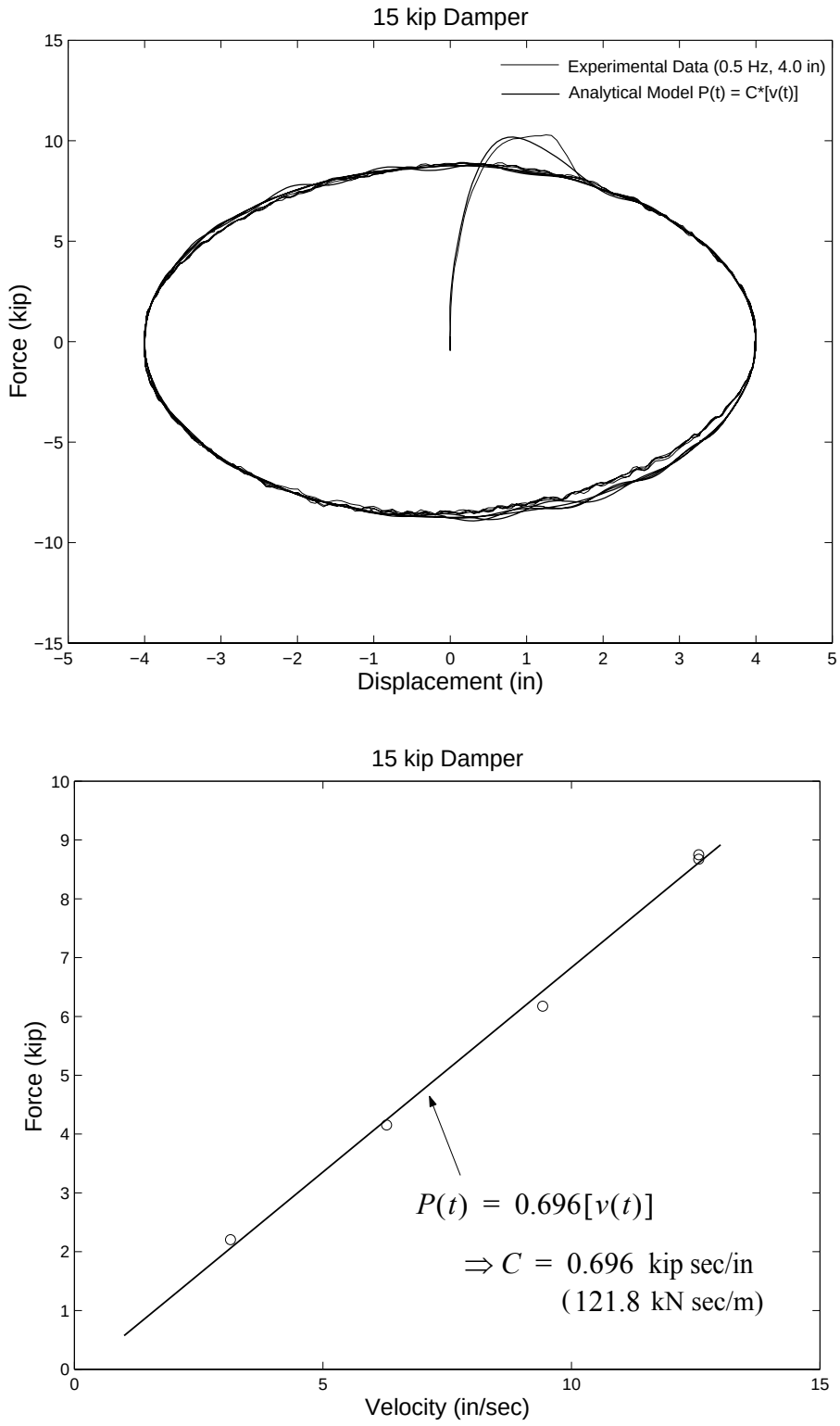

Figure 5-2. Comparison of recorded and predicted hysteresis loop for the 15 kip damper (top), and the determination of the damping coefficient from experimental data for the 15 kip damper (bottom).

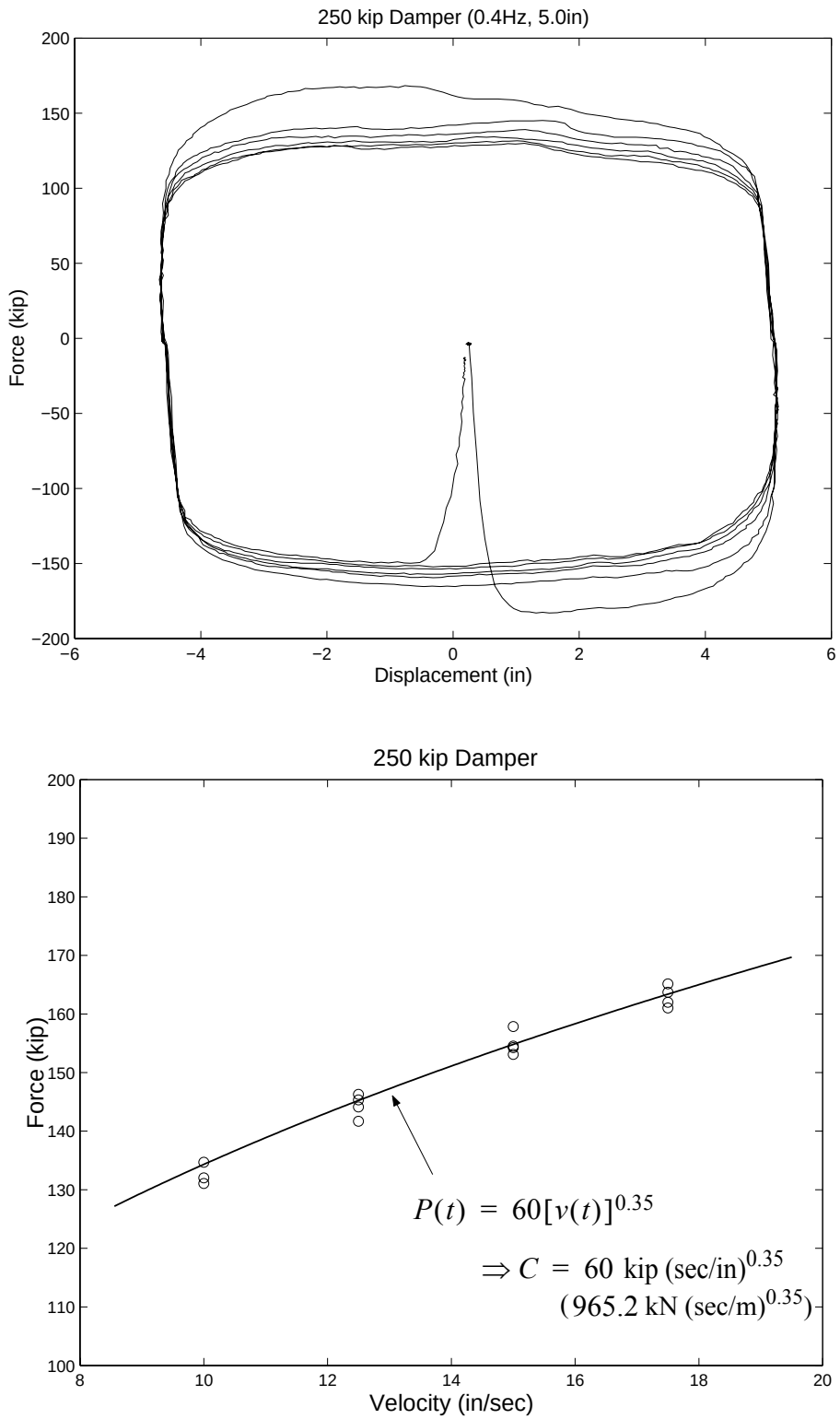

Figure 5-3. Comparison of recorded and predicted hysteresis loop for the 250 kip damper (top), and the determination of the damping coefficient from experimental data for the 250 kip damper (bottom).

For all three dampers, it is seen that the predicted force-deformation behavior given by Equation (5-2) for the linear 3 and 15 kip dampers, and Equation (5-1) for the nonlinear 250 kip damper, matches the recorded behavior with fidelity.

5.2 ESTIMATION OF INTERNAL TEMPERATURE FROM EXTERNAL TEMPERATURE READINGS

It was shown in Chapter 2 that the observed heat exchange between the internal fluid and the external damper casing/ambient air is accurately characterized by a two-parameter cooling law. This cooling law (Equation (2-29)) was re-arranged to give an expression (Equation (2-32)) which one can use to estimate the internal temperature given external readings. This expression, which is presented again here, is

$$\theta(t) = \frac{\delta\theta_o^2(t) + (1 + \gamma_o - \delta T_{air})\theta_o(t) - T_{air}}{\delta\theta_o(t) - \delta T_{air} + \gamma_o} \tag{2-32}$$

where $\gamma_o = 0.02$ and $\delta = 0.01[F]^{-1}$ for the larger 15 and 250 kip dampers.

Figure 5-4 plots the ratio of the change in internal temperature, $\Delta\theta(t)$, to the change in external temperature, $\Delta\theta_o(t)$, for the 4 largest amplitude tests conducted on the 15 kip damper. The solid line plots the ratio of the change in experimental internal and external data, $\Delta\theta(t)/\Delta\theta_o(t)$, whereas, the dashed line plots the ratio of the change in internal temperature estimated by Equation (2-32) to the change in measured external temperature, $\Delta\theta_{Eqn.(2-32)}(t)/\Delta\theta_o(t)$. The figure shows that for the larger two amplitude tests, the ratio making use of Equation (2-32) results in a very accurate prediction. The ratio $\Delta\theta_{Eqn.(2-32)}(t)/\Delta\theta_o(t)$ for the lower two amplitude tests over-predicts the internal temperature—a result of the external temperature being measured at the end of stroke. At the end-of-stroke location, the internal fluid has not been mixed for the lower amplitude

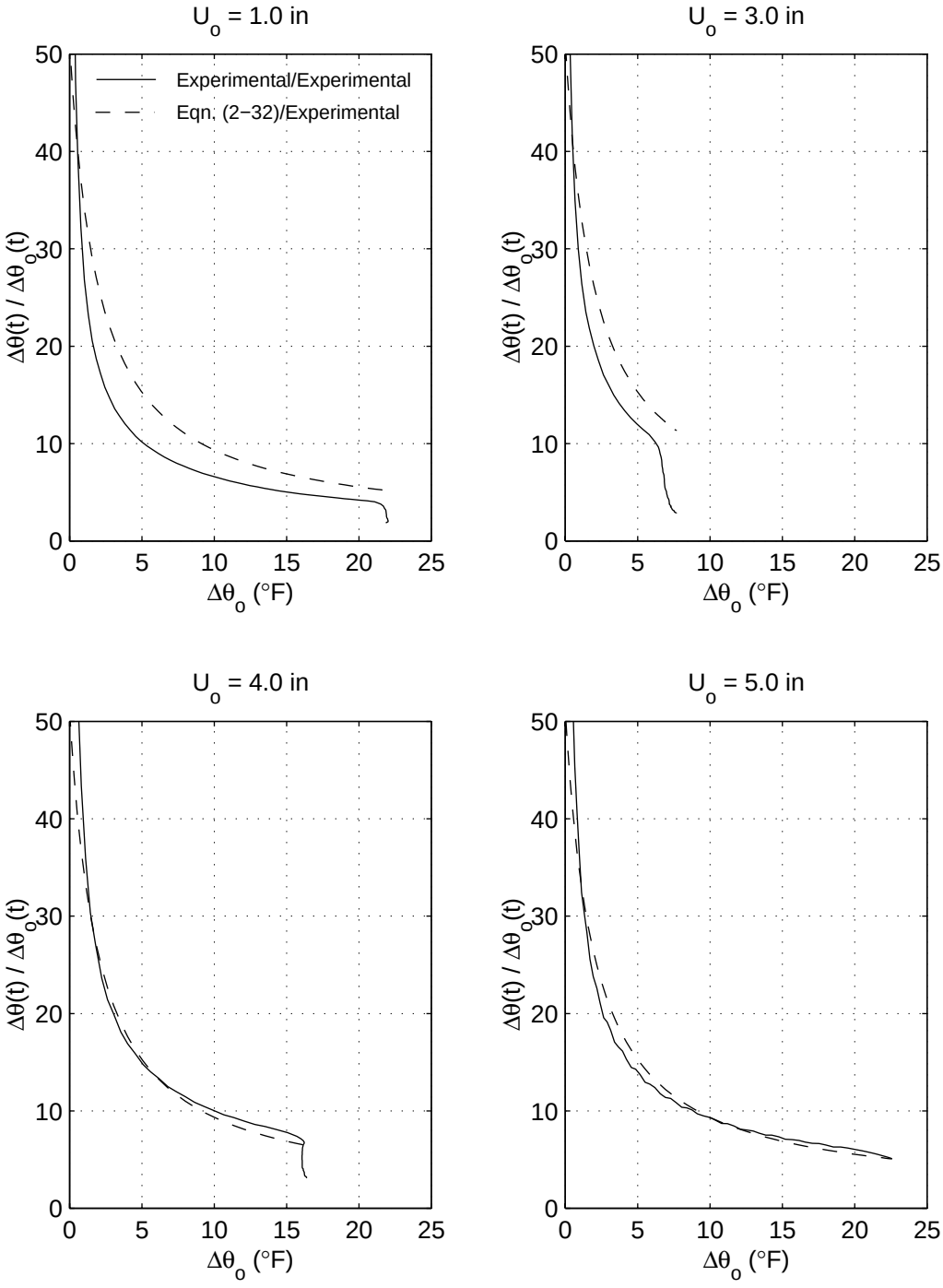

Figure 5-4. Ratio of change in internal to change in external temperature for tests conducted on the 15 kip damper. The solid lines plot ratios of experimental data, whereas, the dashed lines plot the ratio of change in Eqn. (2-32) to the recorded external temperature.

tests, and the external temperature rises more rapidly in relation to the internal temperature as heat conduction along the steel tube exceeds that through the internal oil.

Figures 5-5 through 5-8 plot the ratio of the change in internal temperature, $\Delta\theta(t)$, to the change in external temperature, $\Delta\theta_o(t)$, for all tests conducted on the 250 kip damper. It is seen that the dashed line representing $\Delta\theta_{Eqn.(2-32)}(t)/\Delta\theta_o(t)$, follows closely the ratio of the experimental data $\Delta\theta(t)/\Delta\theta_o(t)$ for all testing amplitudes and velocities. In the majority of the plots, the difference between the ratios making use of the measured and estimated internal temperature is, for practical purposes, negligible, and at no point is the difference greater than 10-15%.

Figures 5-4 through 5-8 confirm that Equation (2-32) is an accurate way to estimate the internal oil temperature resulting from large amplitude motion given the external temperature. The figures also show that the parameters $\gamma_o = 0.02$ and $\delta = 0.01[F]^{-1}$ are sufficient to estimate the internal temperature for larger dampers of varying sizes as it is equally applicable to both the 15 kip and 250 kip dampers.

5.3 FORCE-TEMPERATURE BEHAVIOR

This section examines the effect of temperature on the force output generated by the dampers in this study.

3 kip Damper

Figure 5-9 plots the time history results for test number 5 conducted on the 3 kip damper. The plot shows displacement, force, velocity and internal temperature as a function of time. The maximum values of force and velocity at every tenth cycle are indicated on the corresponding plots. It is seen that the peak force maintains a constant value even for this long-stroke, long-duration motion.

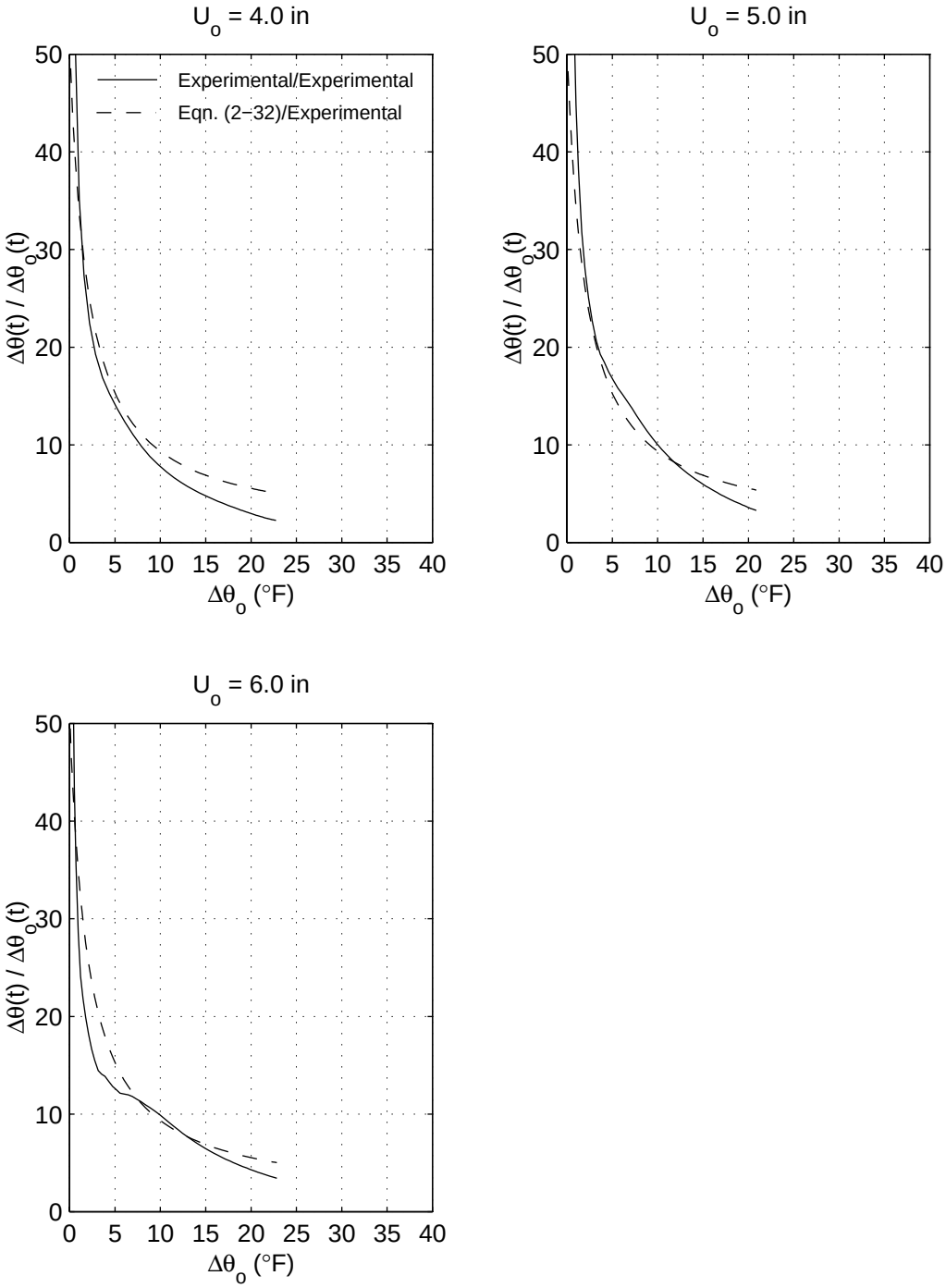

Figure 5-5. Ratio of change in internal to change in external temperature for tests conducted on the 250 kip damper with velocity amplitude Vo = 10 in/sec. The solid lines plot ratios of experimental data, whereas, the dashed lines plot the ratio of Eqn. (2-32) to the recorded external temperature.

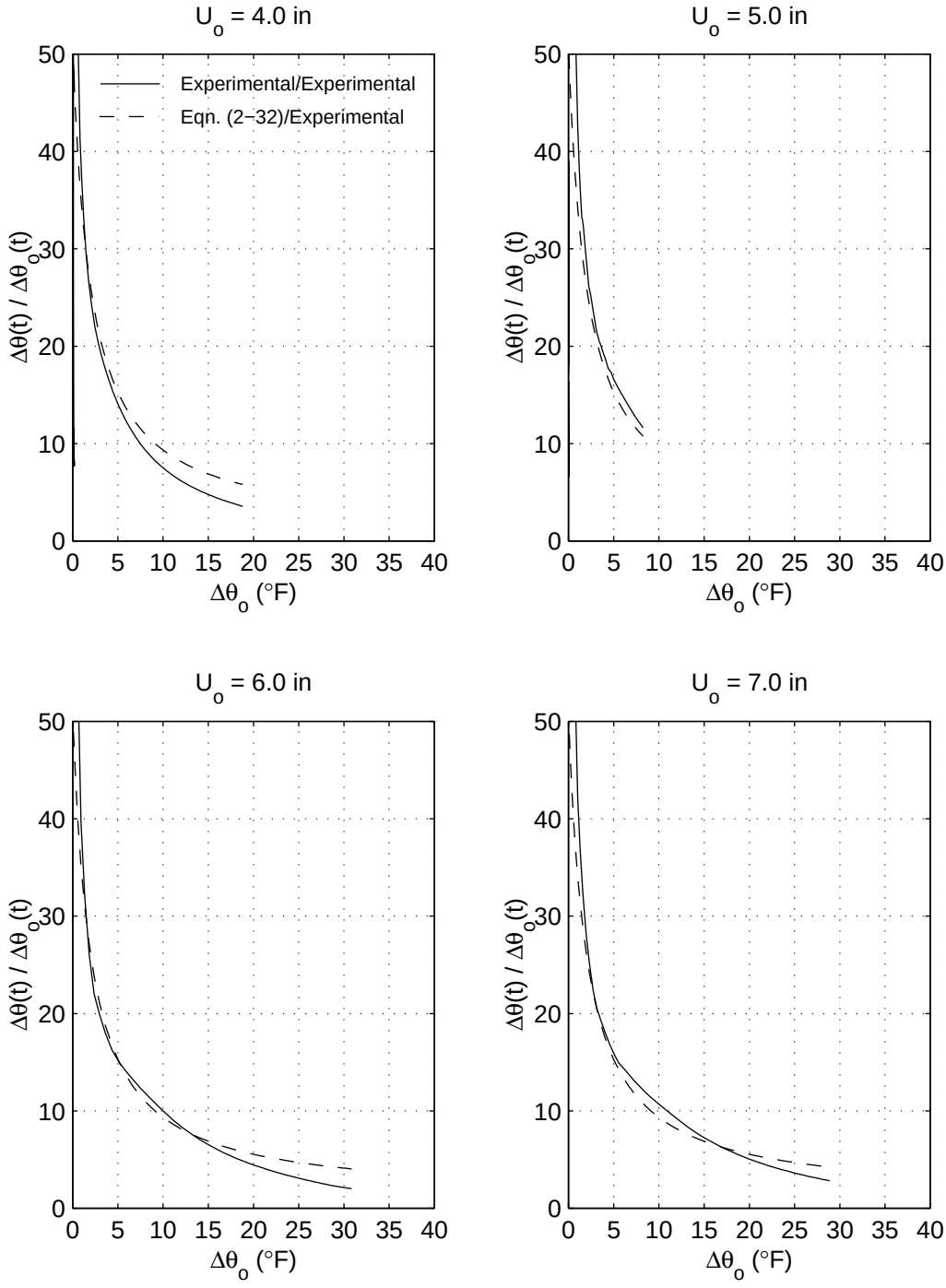

Figure 5-6. Ratio of change in internal to change in external temperature for tests conducted on the 250 kip damper with velocity amplitude Vo = 12.5 in/sec. The solid lines plot ratios of experimental data, whereas, the dashed lines plot the ratio of Eqn. (2-32) to the recorded external temperature.

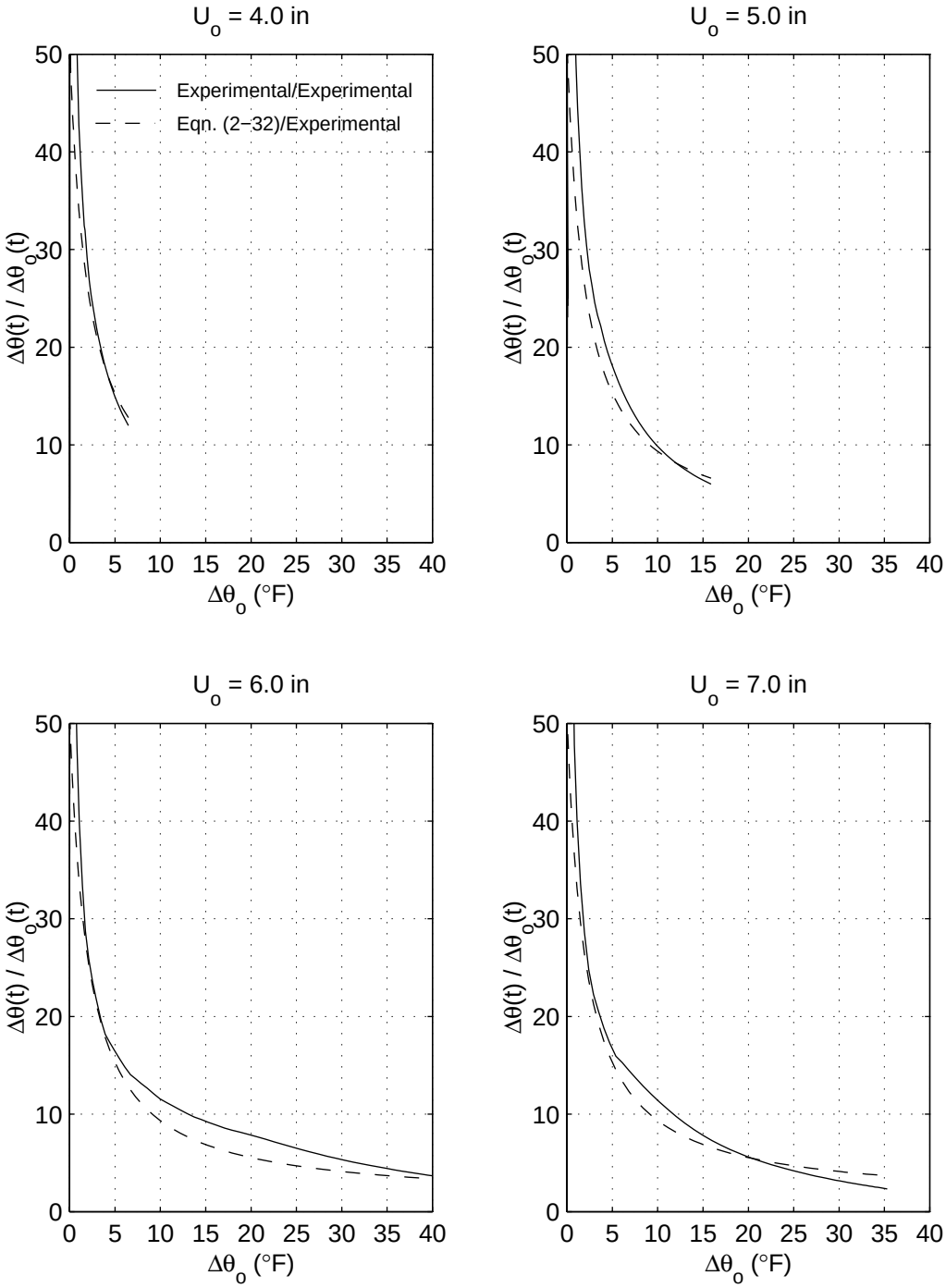

Figure 5-7. Ratio of change in internal to change in external temperature for tests conducted on the 250 kip damper with velocity amplitude Vo = 15 in/sec. The solid lines plot ratios of experimental data, whereas, the dashed lines plot the ratio of Eqn. (2-32) to the recorded external temperature.

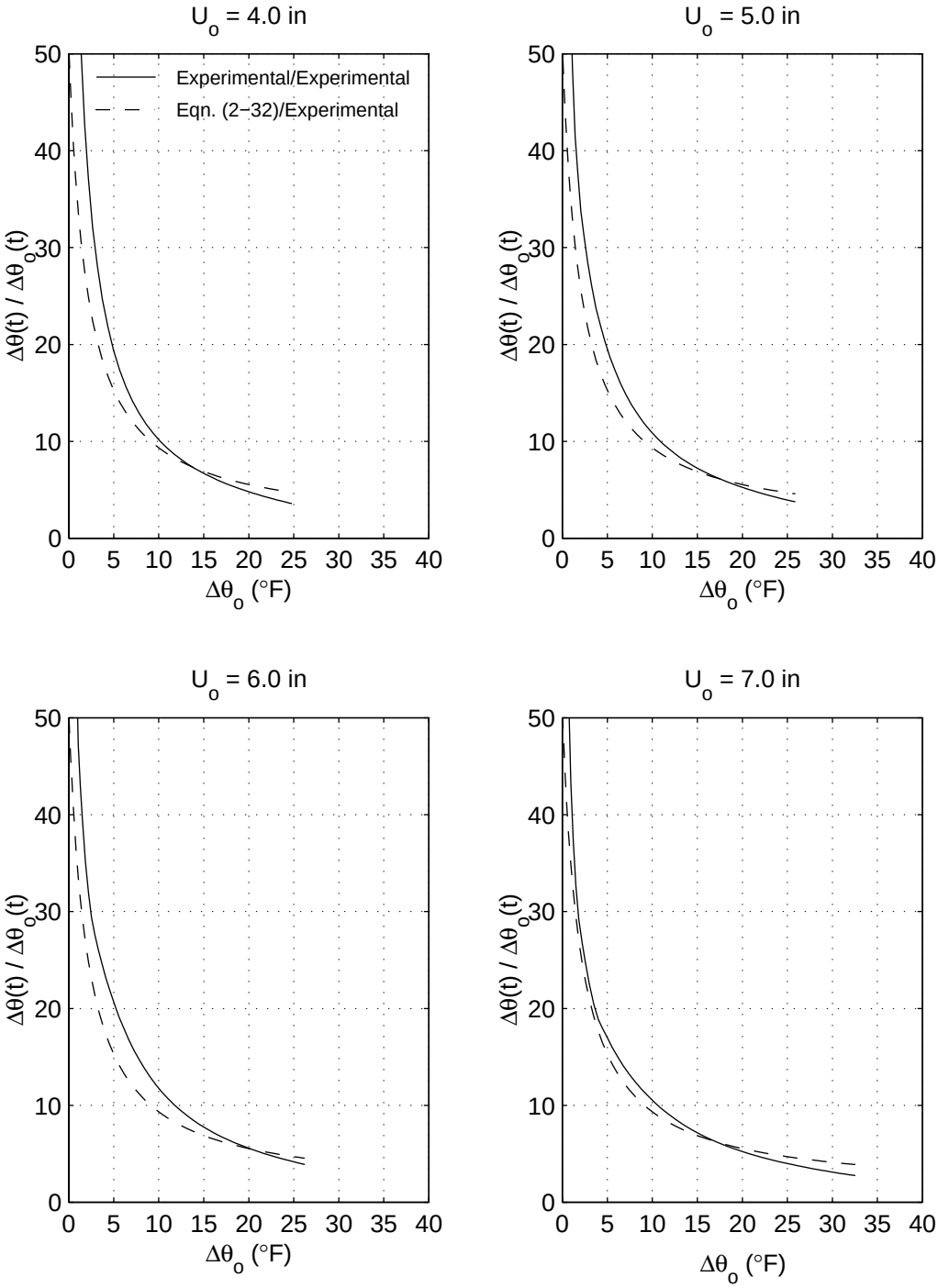

Figure 5-8. Ratio of change in internal to change in external temperature for tests conducted on the 250 kip damper with velocity amplitude Vo = 17.5 in/sec. The solid lines plot ratios of experimental data, whereas, the dashed lines plot the ratio of Eqn. (2-32) to the recorded external temperature.

Figure 5-10 plots the variation of the peak force with input cycles (top) and internal and external temperatures (middle and bottom) for all of the tests conducted on the 3 kip damper. The figure shows that the 3 kip damper exhibits a nearly constant force output when it is loaded at high temperatures with a slight increase in force at internal temperatures in excess of 160° F.

15 kip Damper

Figure 5-11 plots recorded displacement, force, velocity and internal temperature histories for test number 4 conducted on the 15 kip damper. This plot shows a gradual increase in force for the same peak velocity as loading progresses. Figure 5-12 plots the variation of the peak force with input cycles (top) and internal and external temperatures (middle and bottom) for all of the tests conducted on the 15 kip damper. The figure shows that the force output remains nearly constant for increasing temperature. The largest variation in force is seen in the test conducted at a velocity amplitude of 12.67 in/sec which shows a slight increase of approximately 5%.

250 kip Damper - Large Amplitude Motion

Figure 5-13 plots recorded displacement, force, velocity and internal temperature histories for test number 12 ($U_o = \pm 7.0$ in, $f = 0.341$ Hz) conducted on the 250 kip damper. While the third plot from the top shows that the loading maintained its peak velocity, the peak values of the recorded force show a gradual decrease of 15 kip over a period of five cycles. A similar behavior is observed in Figure 5-14 that plots recorded time histories from test number 10 ($U_o = \pm 5.0$ in, $f = 0.477$ Hz).

Figures 5-15 through 5-18 present a summary of all tests conducted on the 250 kip damper. The figures plot the maximum cyclic force and velocity for each cycle (top two plots), as well as plotting the force against the external and internal temperature (bottom two plots) for all the tests con-

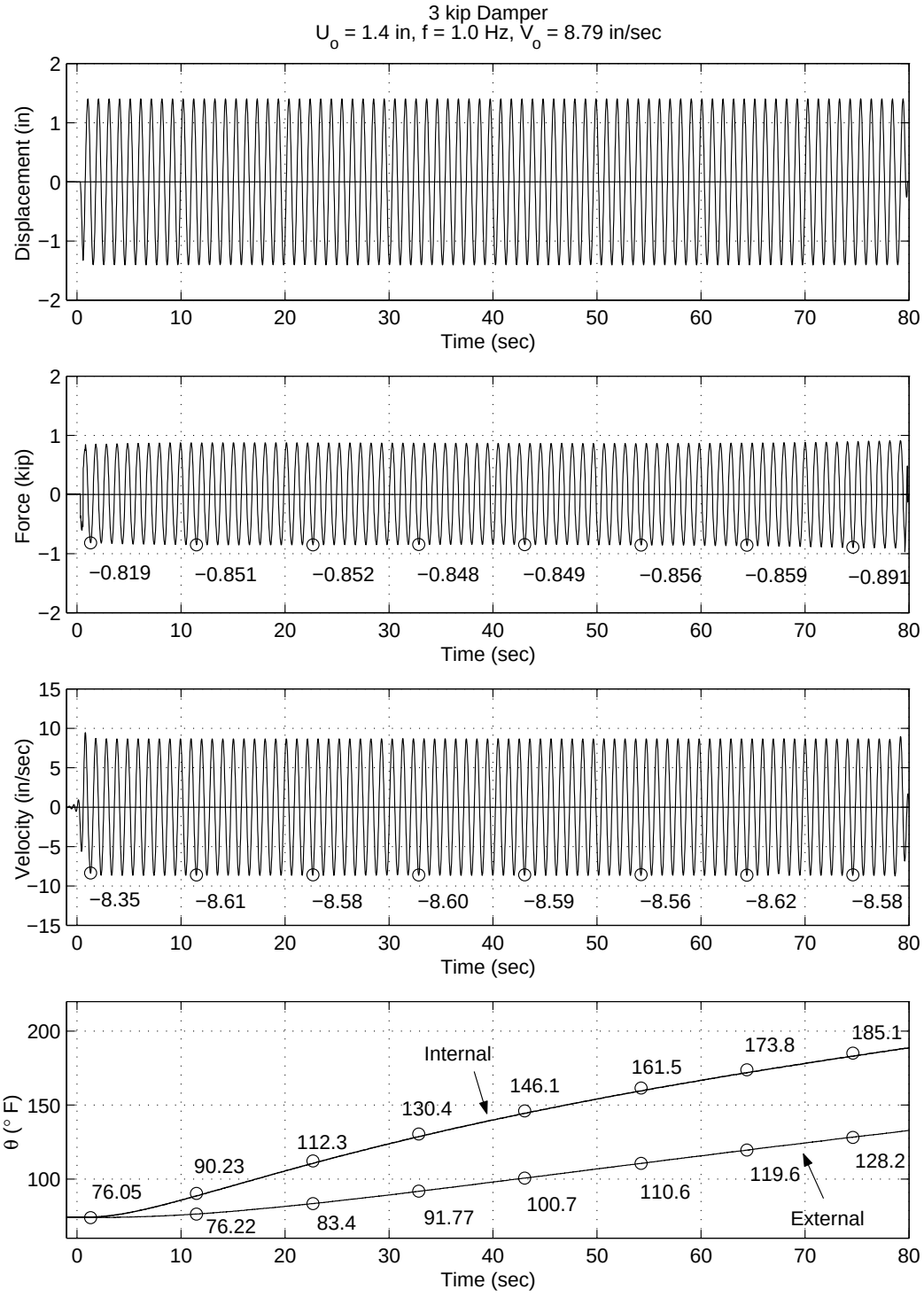

Figure 5-9. Displacement, force, velocity and temperature histories from test No. 5 on the 3 kip damper. The maximum vales are indicated at 10 cycle increments.

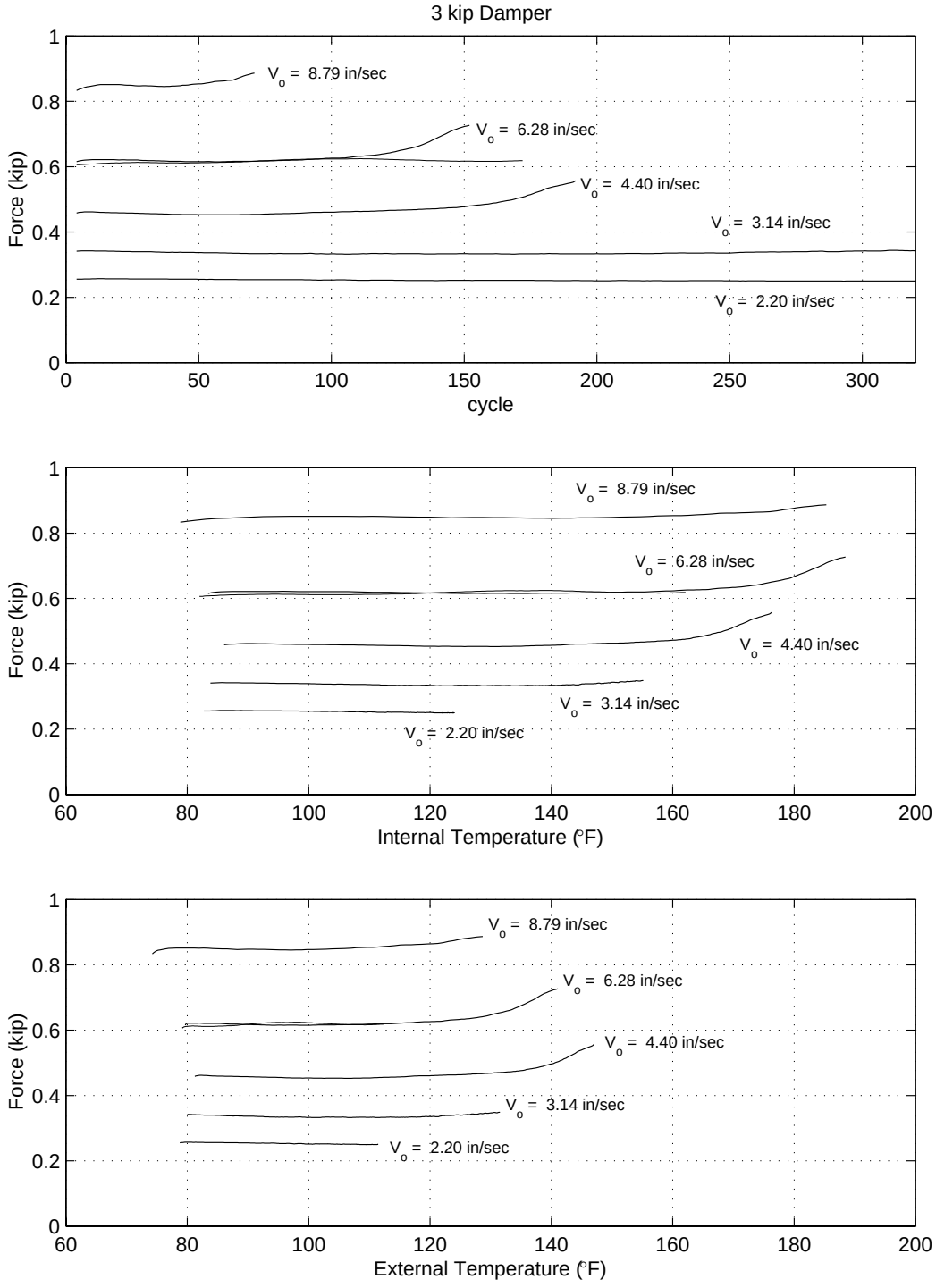

Figure 5-10. Maximum force developed in the 3 kip damper as a function of cycle (top), internal temperature (middle), and external temperature (bottom), for each test performed.

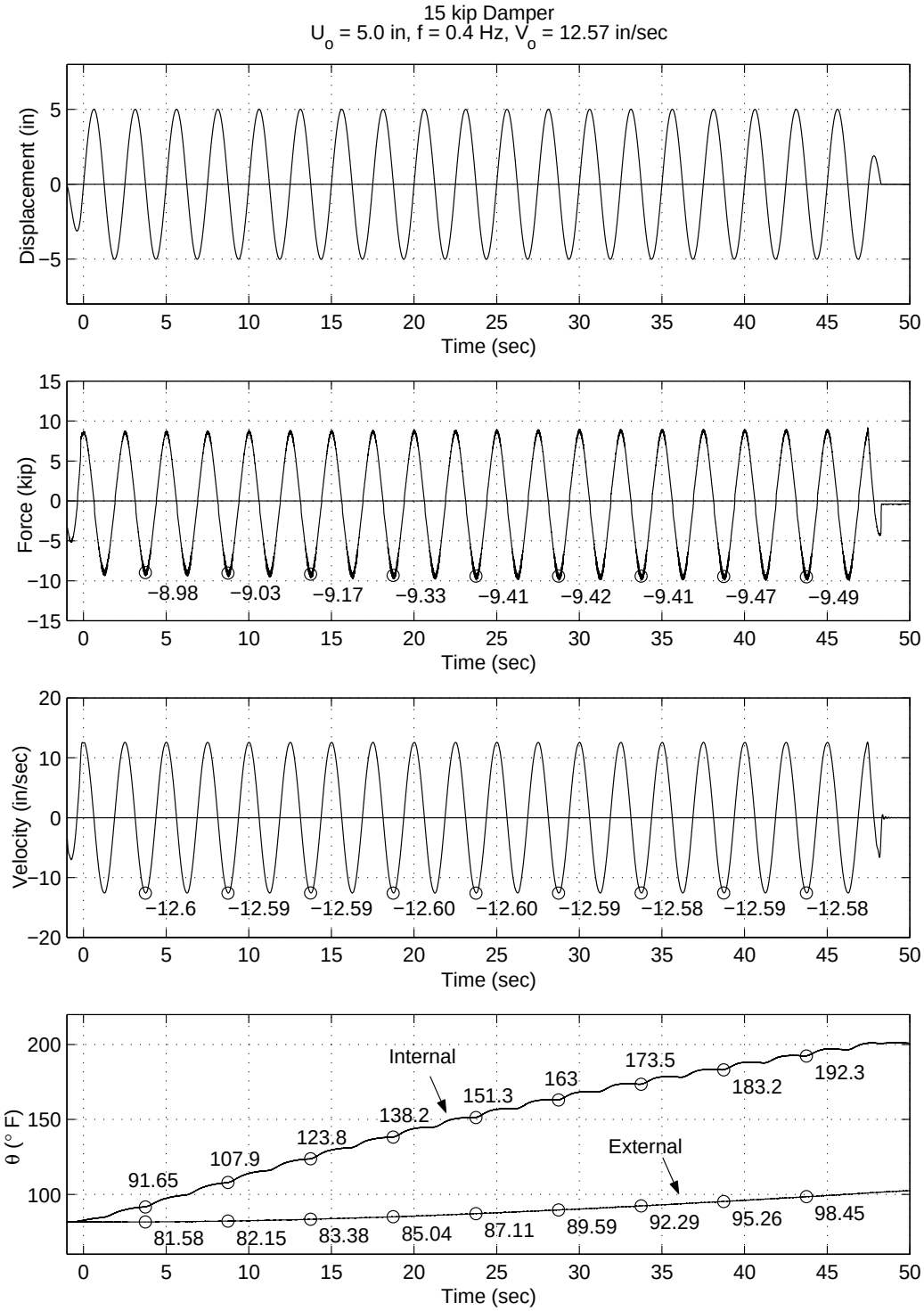

Figure 5-11. Displacement, force, velocity and temperature histories from test No. 4 on the 15 kip damper. The maximum values are indicated at 2 cycle increments.

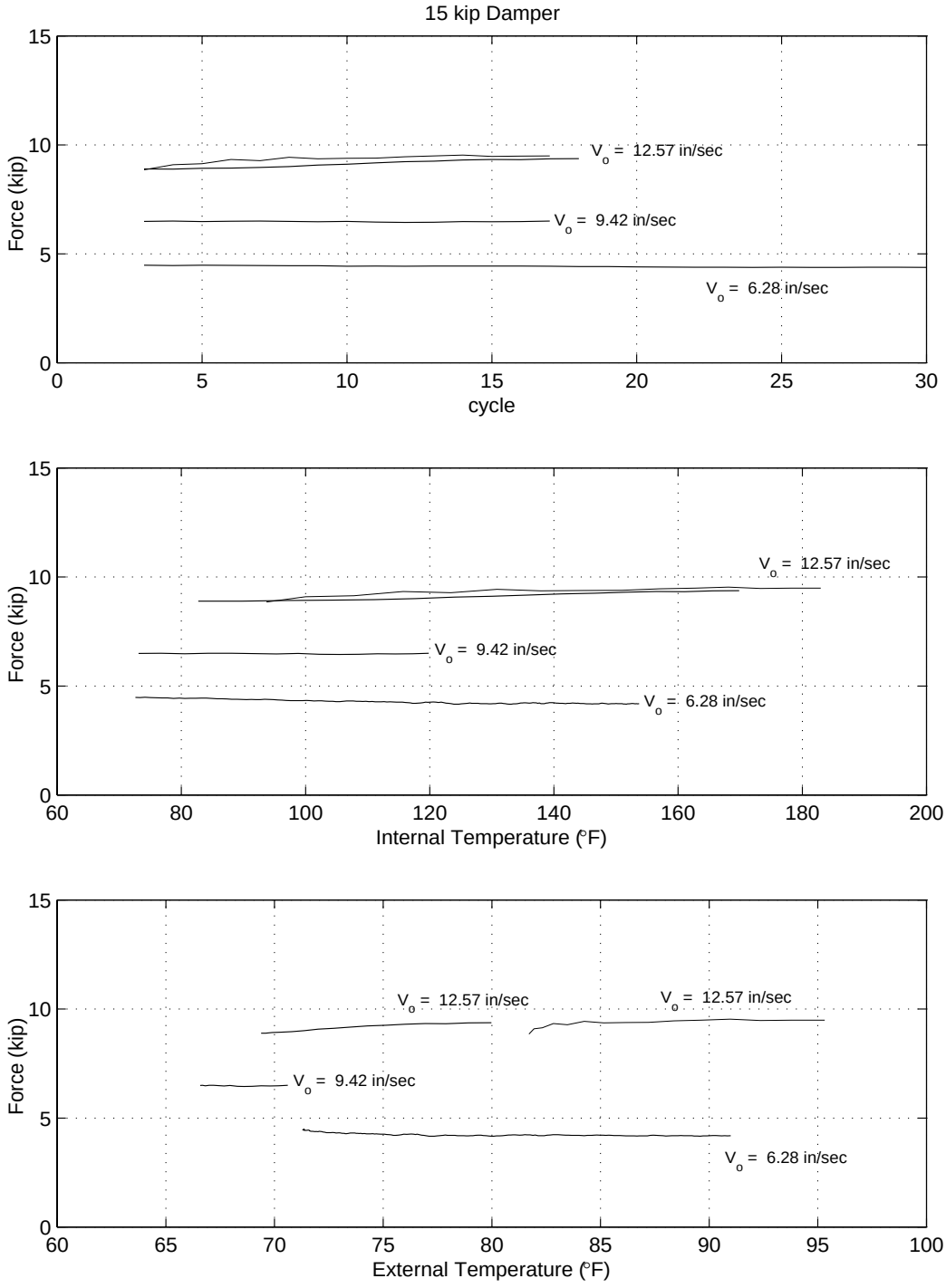

Figure 5-12. Maximum force developed in the 15 kip damper as a function of cycle (top), internal temperature (middle), and external temperature (bottom), for each test performed.

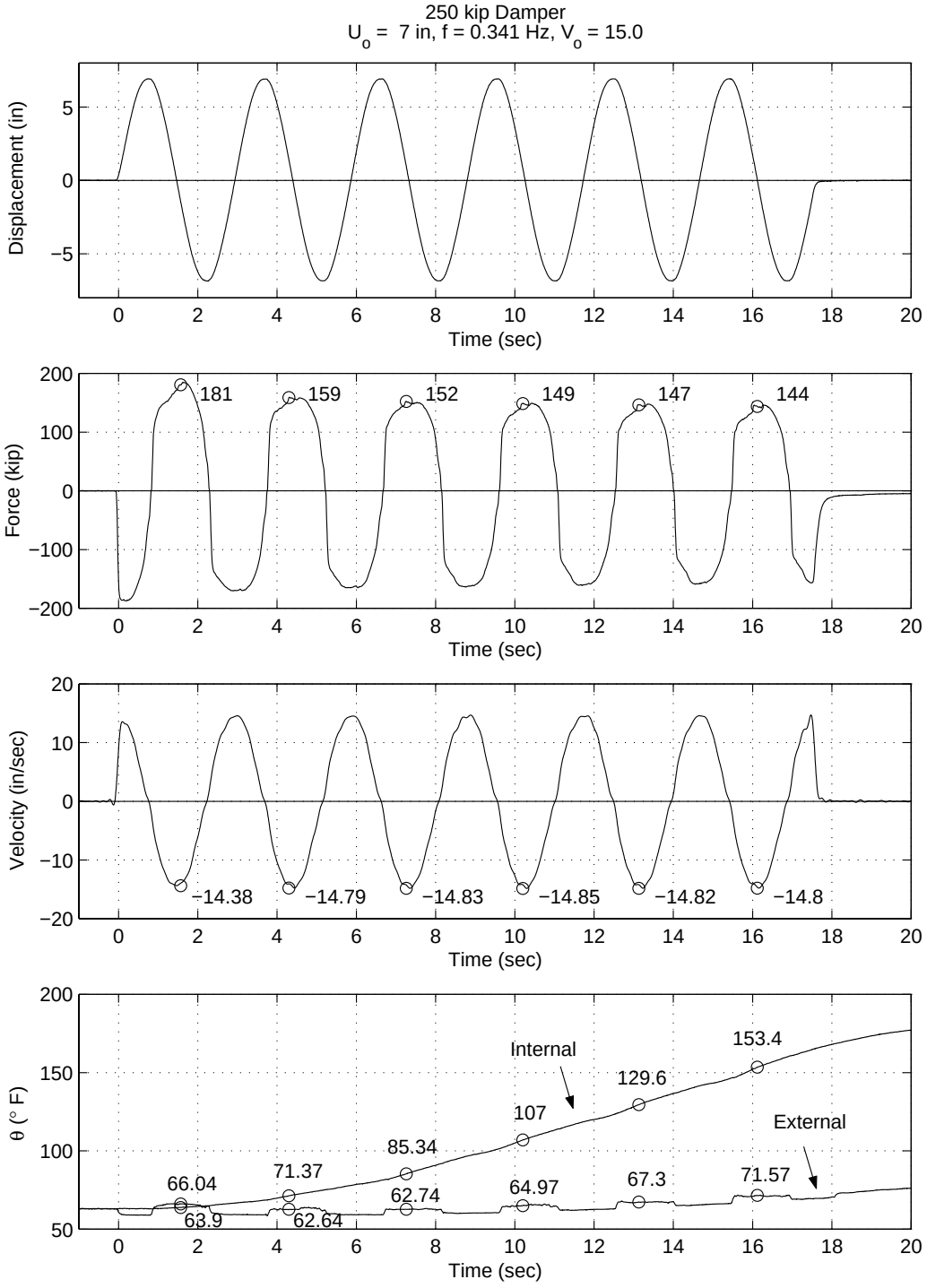

Figure 5-13. Displacement, force, velocity and temperature histories from test No. 12 on the 250 kip damper. The maximum values are indicated for each cycle.

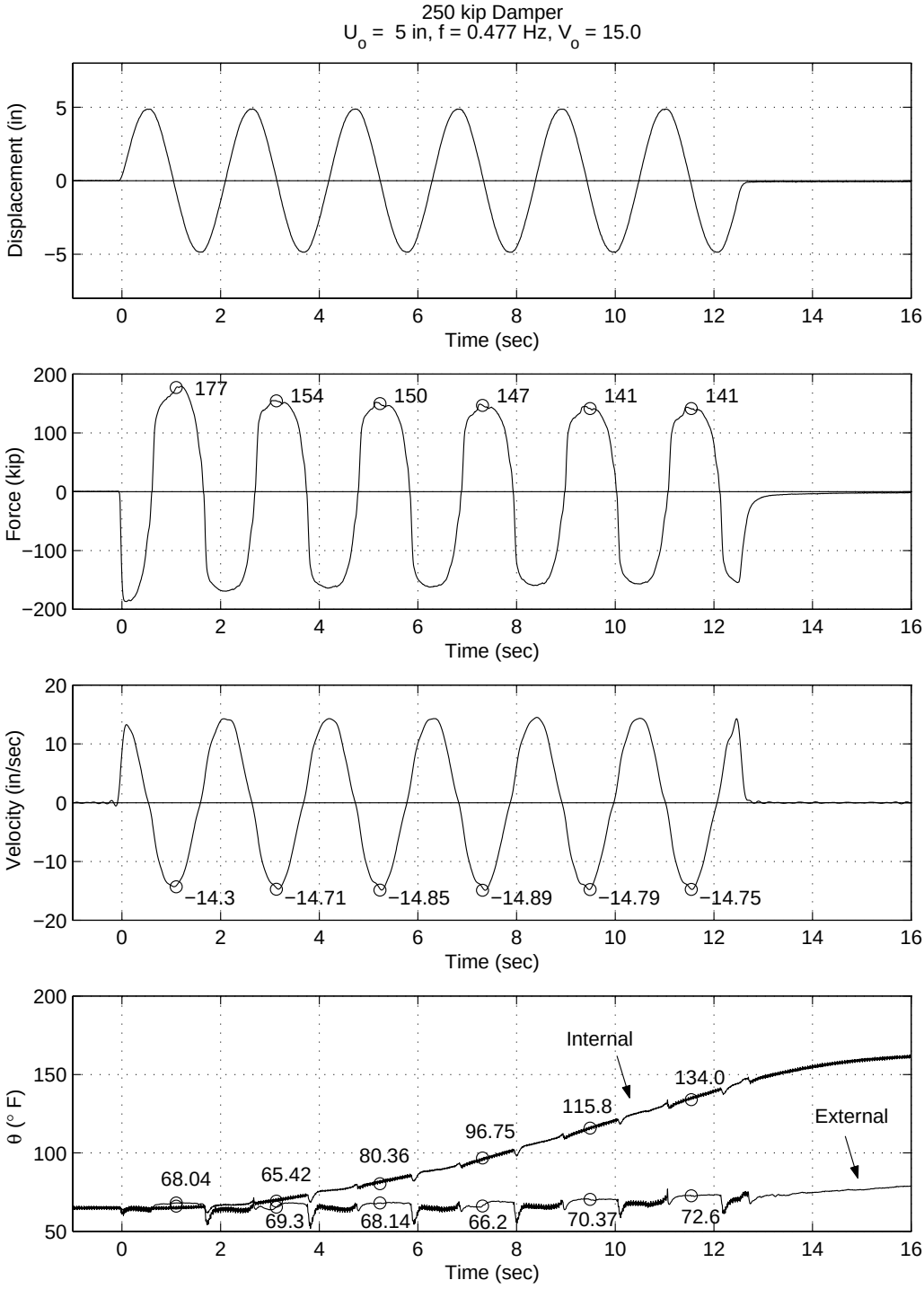

Figure 5-14. Displacement, force, velocity and temperature histories for 250 kip damper Test No. 12 on the 250 kip damper. The maximum vales for are indicated for each cycle.

ducted with velocity amplitudes V_o = 10, 12.5, 15 and 17.5 in/sec, respectively. It is seen that even though velocity remains nearly constant for all cycles, the force output in the 250 kip damper drops 6% to 12% over 6 cycles. As shown in Figures 5-13 and 5-14 (and the temperature histories in Chapter 4), this drop in force corresponds to an increase in internal oil temperature of approximately 50 to 120 ° F depending on the input velocity and amplitude. .

The information contained in Figures 5-15 through 5-18 is further summarized in Figure 5-19 which plots the average force and temperature values calculated from all tests performed at each velocity (V_o = 10, 12.5, 15, and 17.5 in/sec). The plot shows that the maximum cyclic force drops roughly 2 kips for every 10 ° F rise in internal fluid temperature through 6 cycles.

250 kip Damper - Small Amplitude Motion

Figure 5-20 presents the damper force as a function of number of loading cycles and the internal and external temperatures for the low-amplitude, long-duration (wind) testing presented in Chapter 3. As discussed in Chapter 3, the measured external and internal temperatures resulting from the low-amplitude tests are virtually the same.

For design needs it is useful to have an expression that relates the force-drop as a function of loading. Figure 5-20 (top) shows that when the force-drop is expressed as a function of number of cycles it becomes evident that even at small amplitude motions the piston velocity plays a dominant role. For a loading amplitude of 0.5 inches for example, the force-drop over 10 minutes of loading ranges from 1.6% for piston velocity of 0.63 in/sec, to 13% for a piston velocity of 2.07 in/sec. For this reason it is more attractive to present the force-drop as a function of temperature near the mid-stroke. From Figure 5-20 (middle and bottom) it is seen that the rate of decrease is similar for all three testing velocities, roughly 1 kip for every 10 ° F rise in temperature.

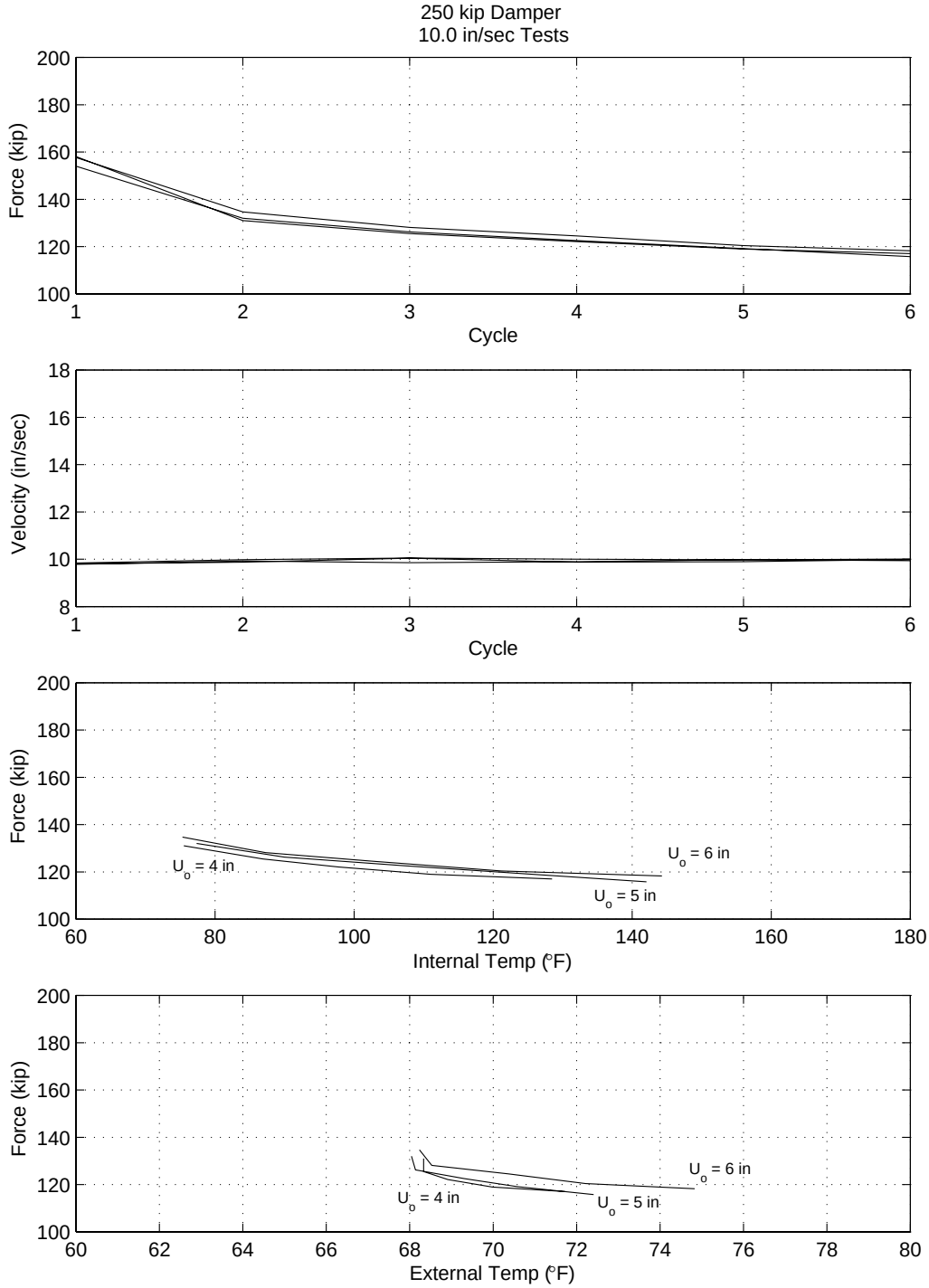

Figure 5-15. Maximum cyclic force developed in the 250 kip damper as a function of cycle and internal and external temperatures for each test performed at 10 in/sec.

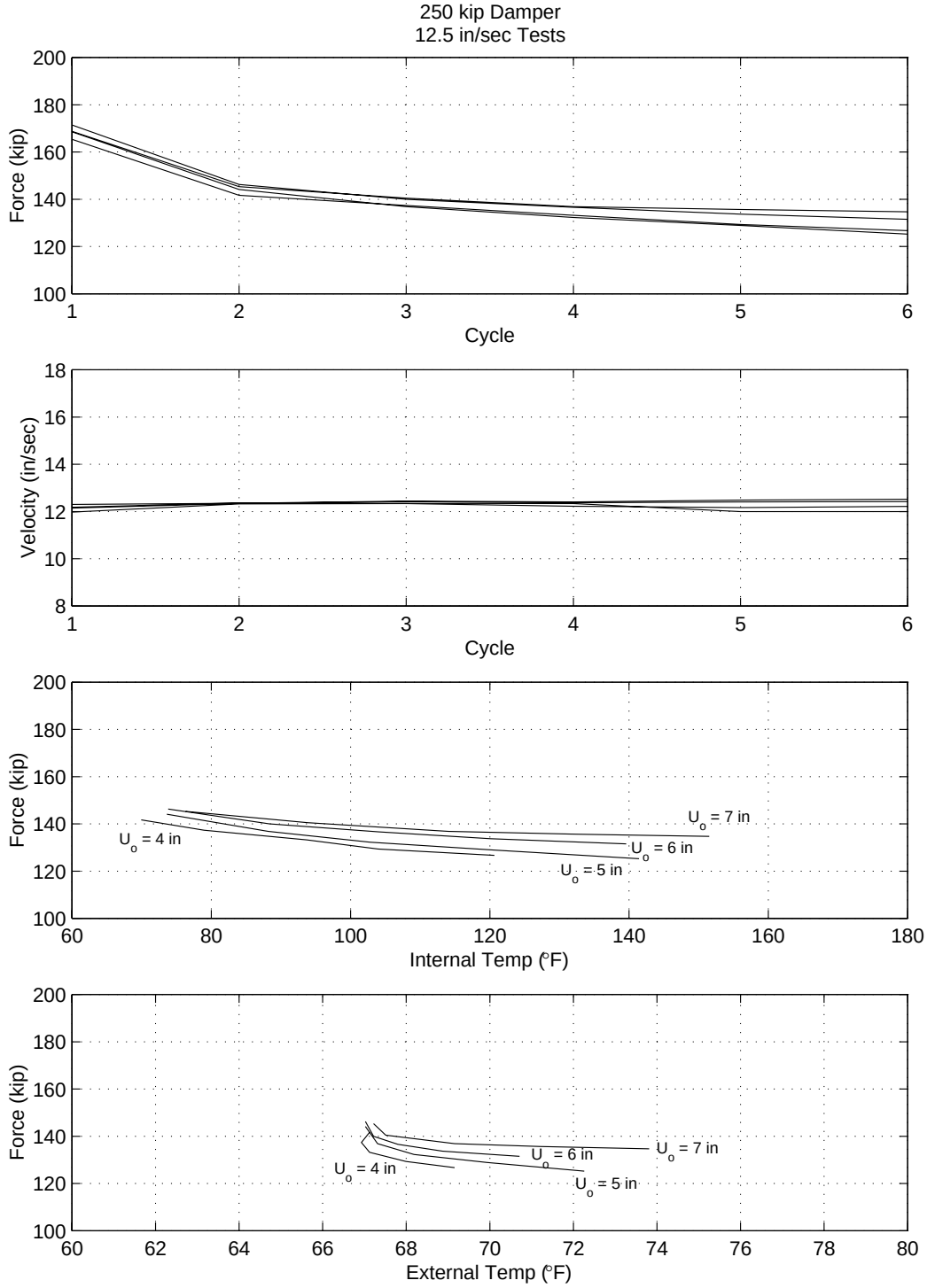

Figure 5-16. Maximum cyclic force developed in the 250 kip damper as a function of cycle and internal and external temperatures for each test performed at 12.5 in/sec.

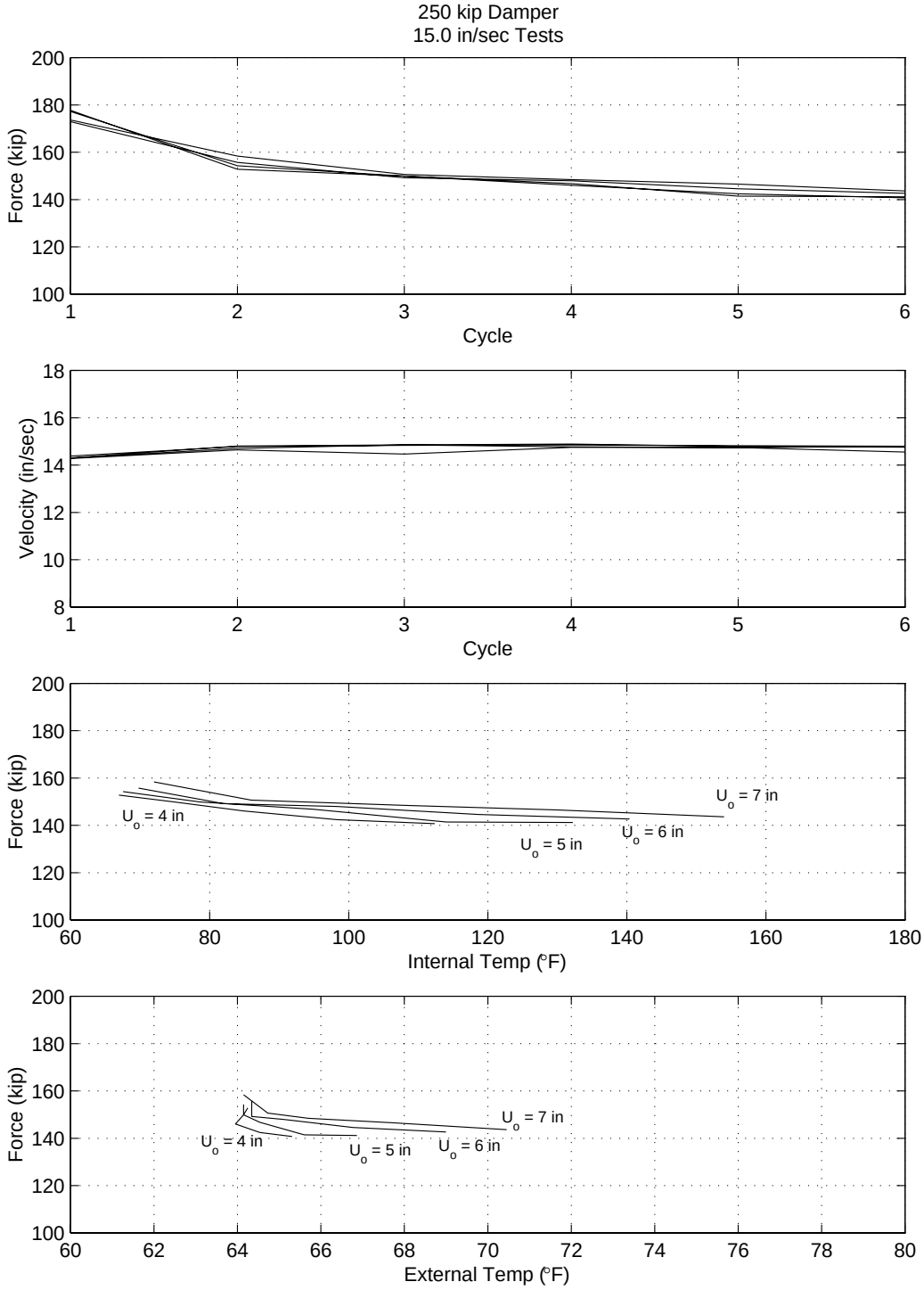

Figure 5-17. Maximum cyclic force developed in the 250 kip damper as a function of cycle and internal and external temperatures for each test performed at 15 in/sec.

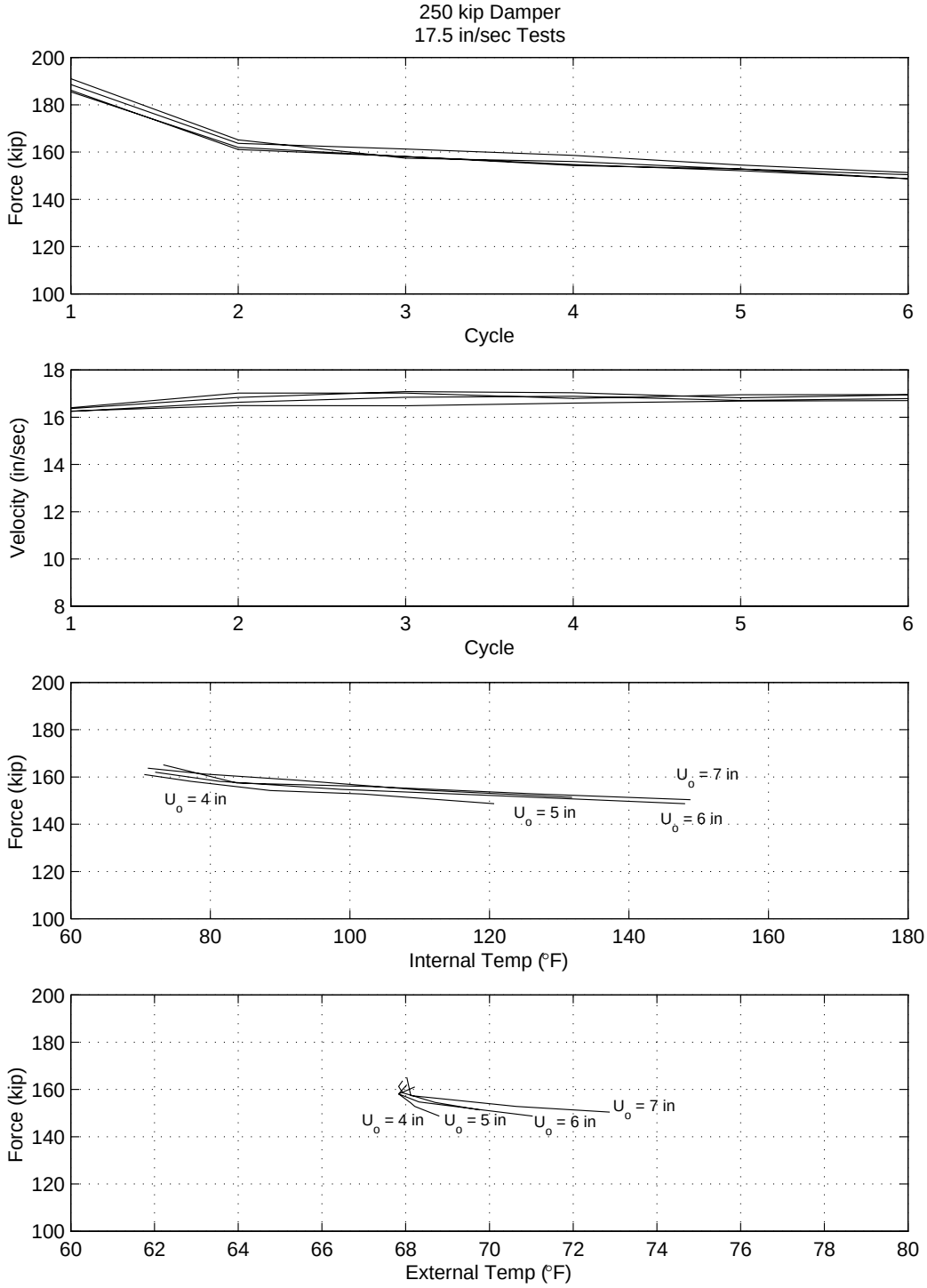

Figure 5-18. Maximum cyclic force developed in the 250 kip damper as a function of cycle and internal and external temperatures for each test performed at 17.5 in/sec.

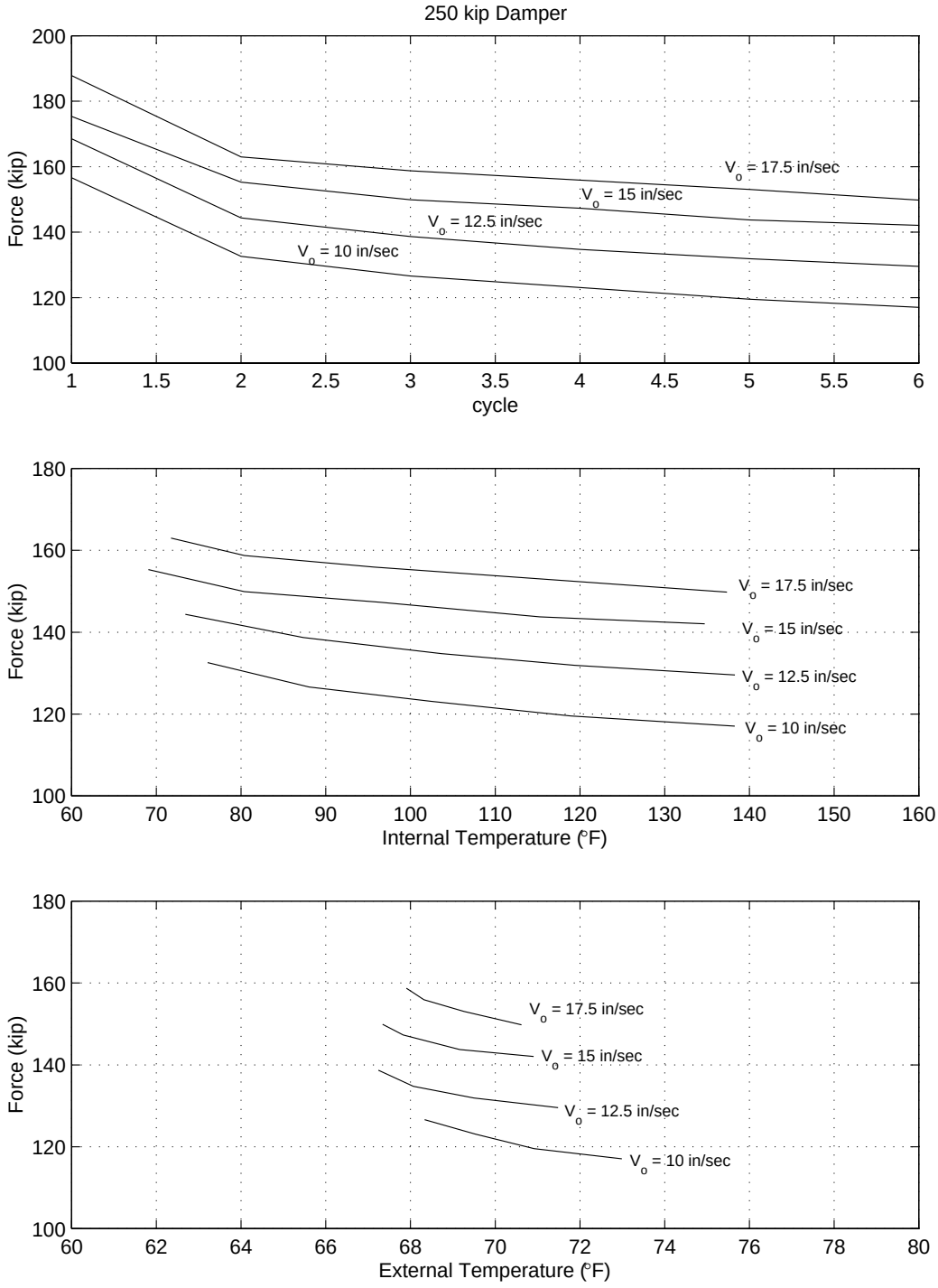

Figure 5-19. The average cyclic force developed in the 250 kip damper as a function of cycle and internal and external temperatures, for each long-stroke testing velocity. The average values are calculated from all tests performed at that velocity.

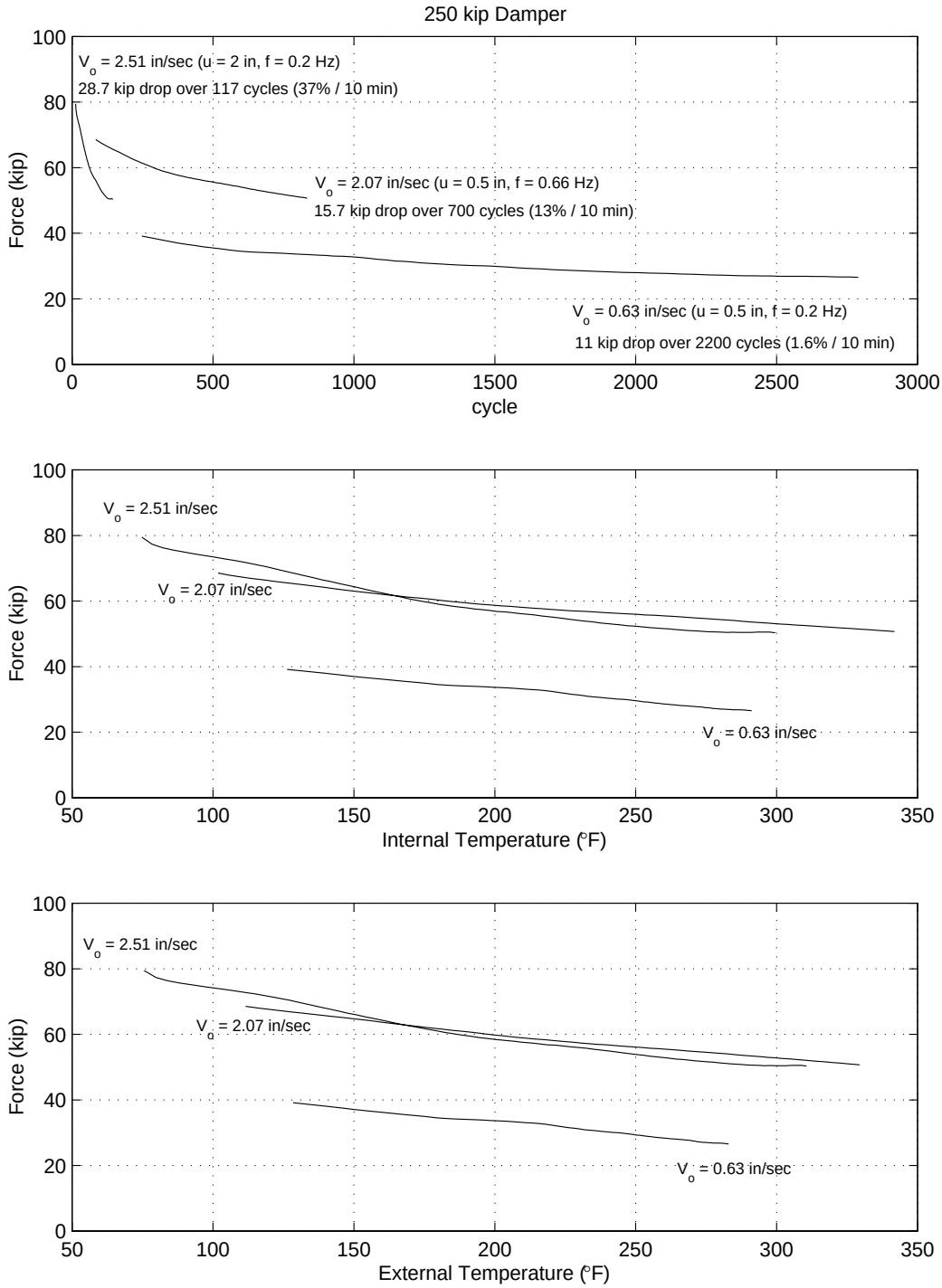

Figure 5-20. The cyclic force developed in the 250 kip damper as a function of cycle and internal and external temperatures, for each small-amplitude testing velocity.

5.4 COOLING

Figure 5-21 shows results from test number 14 conducted on the 250 kip damper. The internal and external temperatures at the mid-stroke and end-of-stroke locations are shown for 60 minutes following the end of loading. It is seen that the internal temperature at the mid-stroke decreases rapidly as the heat spreads into the outer tube and, to a lesser extent, longitudinally through the internal fluid. Figure 5-21 shows that the internal and external temperatures at mid-stroke reach roughly the same temperature within 10-15 minutes. At this point, the temperature at the mid-stroke location slowly decreases while the temperature at the end-of-stroke location slowly increases until a homogeneous temperature is reached throughout.

Similar cooling trends are seen in Figure 5-22 which shows the temperature for the seven minutes following the end of loading in test number 15. It is seen that the internal temperature at the mid-stroke location drops from 190° F to 140° F over 2 minutes. This rapid initial decrease in the internal temperature at the mid-stroke location is seen for all tests. For the four largest velocity tests conducted on the 250 kip damper, the average temperature decrease is 50° F. This decrease follows an average increase of roughly 100° F (over six cycles). It was observed that for all tests, the temperature throughout the damper dropped to within 15-20 ° F of the ambient air temperature within 5 hours.

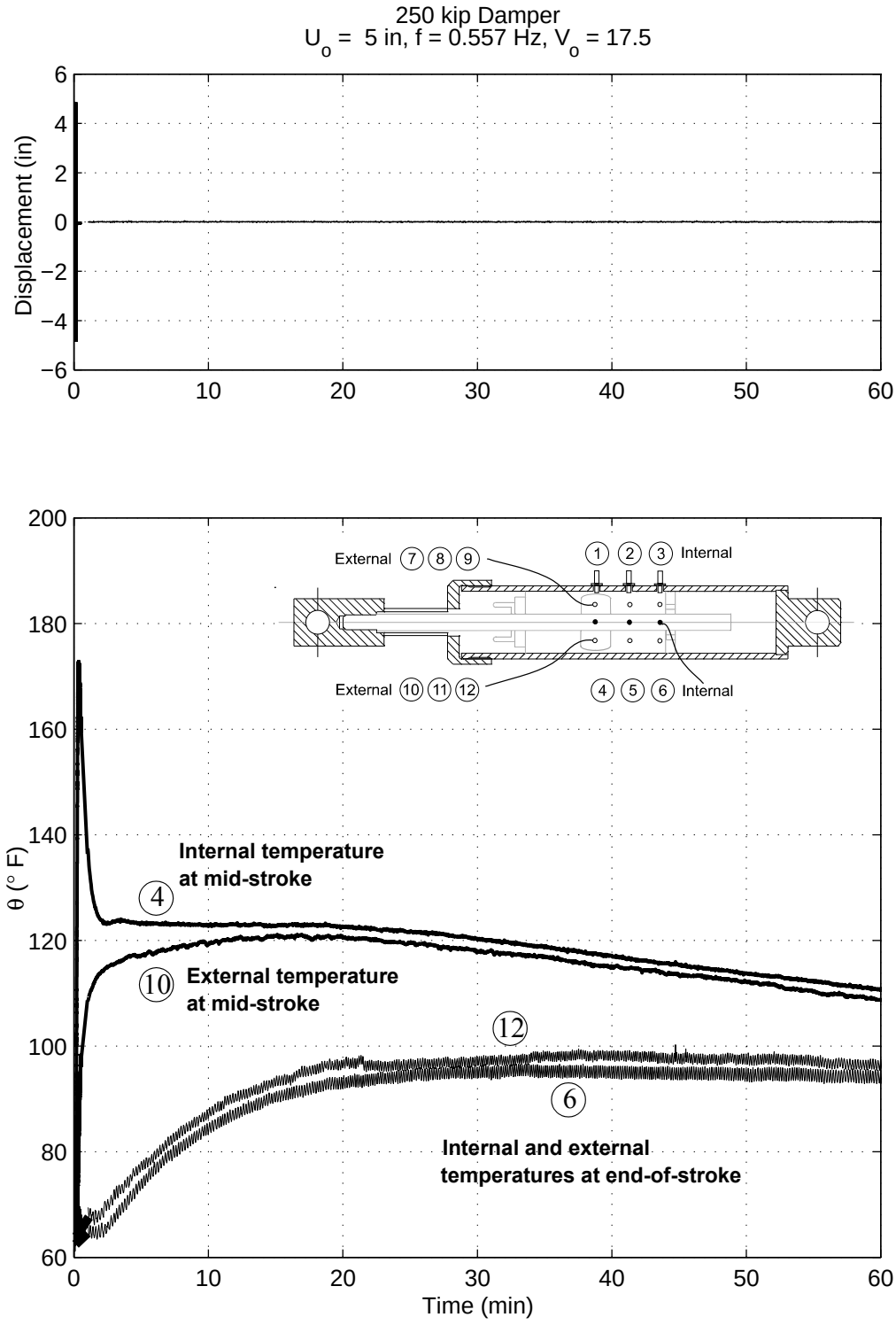

Figure 5-21. Temperature histories showing the initial rapid decrease in internal temperature at the mid-stroke location followed by the slow progression to an homogeneous temperature throughout.

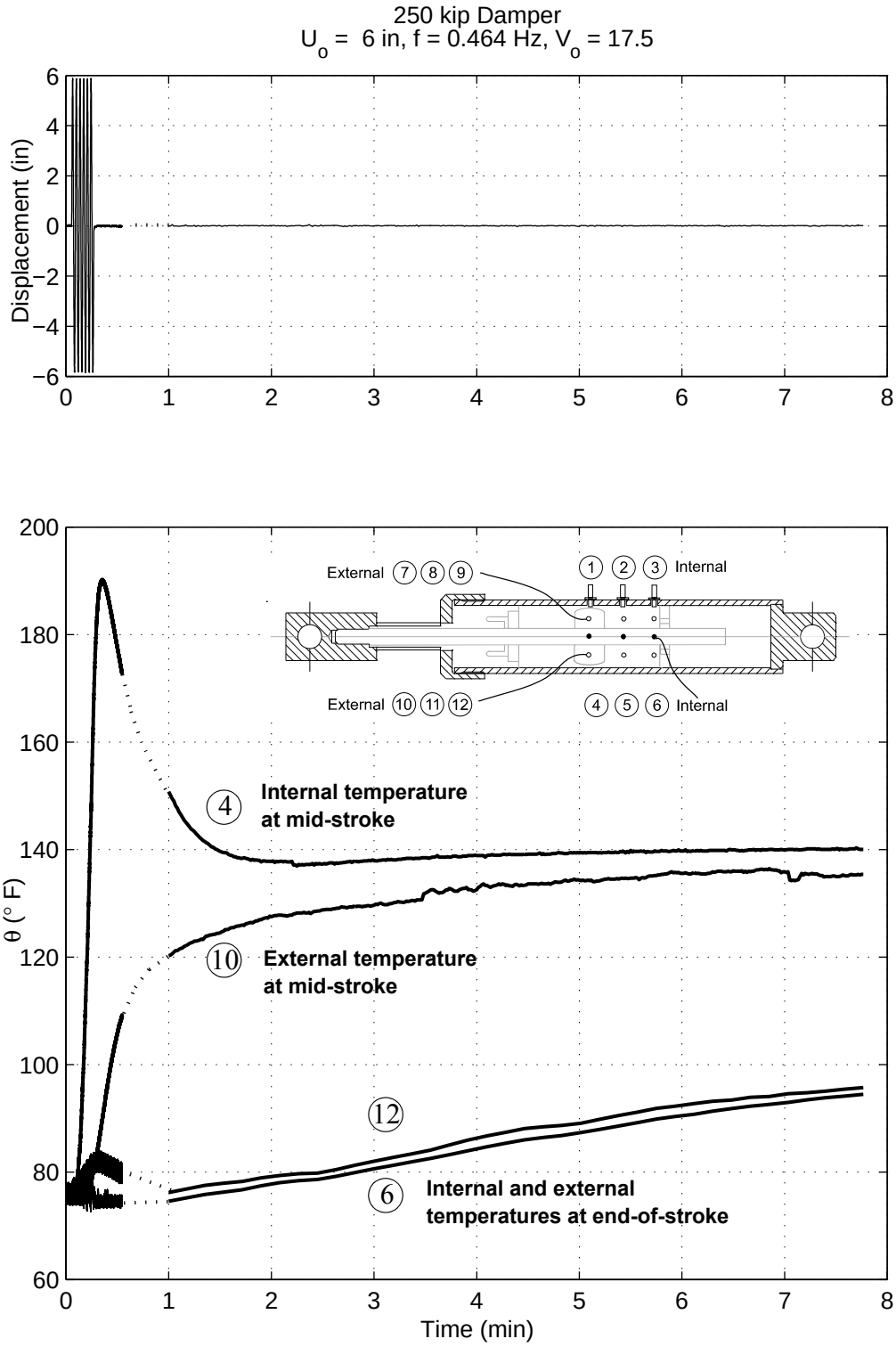

Figure 5-22. Temperature histories showing the initial rapid decrease in internal temperature at the mid-stroke location. The dashed portions indicate time with no recorded data.

6 CONCLUSIONS

This report presents an experimental investigation on the problem of viscous heating of fluid dampers during long-stroke motions. Temperature histories at various locations along the damper casing and within the silicone fluid that undergoes the shearing action have been recorded and used to validate closed form expressions which estimate the internal temperature of the damper fluid during wind and earthquake loading.

• Under small-amplitude motions (stroke is a fraction of the piston diameter) it was shown that the temperature rise is more intense in the vicinity of the piston head; while there is a significant delay at the end-stroke position. Experimental data under small amplitude motion of a 250 kip damper showed that a single closed-form expression (Equation 2-11) is capable of predicting the temperature rise at different locations of the damper with remarkable fidelity.

• Under long-stroke motions (more than two times the piston diameter) it was shown that few cycles (four to six) are sufficient to raise the temperature of the internal fluid of the damper by approximately 100° F near the center where the piston experiences the highest velocity while the temperature rise at the end-of-stroke location—the location of the internal seals—is relatively small. More specif-

ically, the temperature increase at the mid-stroke location is more than an order of magnitude greater than that at the end of the stroke (see Figure 3-38).

• The heat conduction, heat convection and radiation were combined into a global cooling law. Initially, the validity of a one parameter cooling law know as Newton's law of cooling was examined and shown to present only fair results depending on the particular damper and the loading history. Subsequently, a two parameter cooling law was proposed and resulted in a dependable model for all the dampers studied. Interestingly, for the mid-size (15 kip) and the large (250 kip) damper, the regression analysis resulted in the same model parameters for the cooling law.

• A one-dimensional macroscopic energy balance equation in association with each of the above mentioned cooling laws resulted in either a linear or a nonlinear differential equation that yields a theoretical prediction of the internal temperature of the fluid by knowing only the damper's geometrical and material characteristics and the loading history. For the 250 kip damper, which is of great interest for bridge applications, the theoretical (or analytical) solutions over-estimate the internal temperature in all cases. The over estimation in the temperature rise from the analytical expressions originates from the assumption that the energy balance equation involves a constant localized source of heat which approximates the energy input by the piston head. Large fluid dampers have massive steel piston heads that can absorb appreciable energy before the surrounding fluid heats uniformly. Accordingly, for the smaller, 3 and 15 kip dampers, the analytical solutions offer better estimates of the internal temperature rise. This study concludes that Equation (2-

32), which is derived from the two-parameter cooling law, is a dependable tool to estimate the internal temperature rise of fluid dampers under earthquake loading when the external temperature is known.

• It was observed that the force-output of the 3 and 15 kip dampers was relatively unaffected by increasing internal fluid temperature, whereas, for the large 250 kip damper, it was shown that over the course of 6 long-stroke cycles (earthquake loading), the internal temperature rise can be in excess of 100 ° F with a corresponding force drop of approximately 12% from its initial value (See Figure 5-19).

• Wind loading tests indicate that even under small stroke motions, piston velocity plays a dominant role in heating and the associated reduction in force output. For a loading amplitude of 0.5 inches for example, the force-drop over 10 minutes of loading ranges from 1.6% for a piston velocity of 0.63 in/sec, to 13% for a piston velocity of 2.07 in/sec (see Figure 5-20). For this reason it is more straight forward to characterize the force-drop as a function of temperature near the mid-stroke as the decrease is similar for all velocities tested, roughly 1 kip for every 10 ° F rise in temperature.

REFERENCES

Abramowitz, M., Stegun, I.A. (1970). *Handbook of Mathematical Functions with Formulas, Graphs, and Mathematical Tables*, Dover Publications, Inc., New York, NY.

Bird, R.B., Stewart, W.E., Lightfoot, E.N. (1960). *Transport Phenomena*, John Wiley & Sons, New York, NY.

Boley, B.A., Weiner, J.H. (1997). *Theory of Thermal Stresses*, Dover Publications, Inc, Mineola, NY, 1997.

Chang, S.-P., Makris, N., Whittaker, A.S., Thompson, A.C.T. (2000). "Experimental and Analytical Studies on the Performance of Hybrid Isolation Systems," *Earthquake Engng Struct. Dyn*., **31,** pp. 421–443

Delis, E.A., Malla, R.B., Madani, M., Thompson, K.J. (1996). "Energy Dissipation Devices in Bridges Using Hydraulic Dampers," *Building to Last, Proc. Structures Congress XIV*, Chicago, IL, **2** pp.188-196.

ENR (1995). "Hospital girds for quake," *Engrg News Record*, **11**, pp. 24-26.

Jakob, M., Hawkins, G.A. (1942). *Elements of Heat Transfer and Insulation*, John Wiley and Sons, London, U.K.

Kakac, S., Yener, Y. (1993). *Heat Conduction, Third Edition*, Taylor and Francis, Washington, DC.

Landau, L.D., Lifshitz, E.M. (1987). "Fluid Mechanics," *Course of Theoretical Physics*, Vol. 6, Pergamon Press, Oxford, UK.

Lighthil, M.J. (1989). *An Introduction to Fourier Analysis and Generalized Functions*, Cambridge University Press, Cambridge, UK.

Makris, N. (1998). "Viscous Heating of Fluid Dampers I: Small Amplitude Motions," *J. of Eng. Mech*., ASCE, Vol. **124**, No. ll. pp. 1210-1216.

Makris, N., Zhang, J. (2004). "Seismic response analysis of a highway overcrossing equipped with elastomeric bearings and fluid dampers," ASCE, **130**(6). pp. 846-860.

Miyamoto, H.K., Scholl, R.E. (1997). "Design of Steel Pyramid Using Seismic Dampers," *Building to Last, Proc. Structures Congress XV*, Portland, OR.

Papanikolas, P.K. (2002). "Deck Superstructure and Cable Stays of the Rion-Antirion Bridge," *Proc. 4th National Conference on Steel Structures*, Patras, Greece.

Schlichting, H. (1979). *Boundary-layer theory*. McGraw Hill, New York, NY.

Shackelford, J.F., Alexander, W., Park, J.S. (1994). *Materials Science and Engineering Handbook*. CRC Press, Boca Raton, FL.

Zhang, J., Makris, N., Delis, T. (2004). "Structural Characterization of Modern Highway Overcrossings—Case Study," ASCE, *J. of Struc. Eng.,* ASCE, **130**(6). pp. 830-845.